Morphological studies

Confocal microscopy: Immunofluorescent morphological observation of tubulin architecture

The newly synthesized compounds were designed to be antimitotic compounds by interfering with microtubule dynamics in actively dividing cells. Confocal microscopy was employed to observe the effects of the newly synthesized compounds on the cytoskeletal microtubule architecture of control and treated MCF-12A, MCF-7 and MDA-MB-231 cells. Morphological observations of tubulin architecture were performed after 24 h of exposure to the newly synthesized compounds.

Exponentially growing MCF-7, MDA-MB-231 and MCF-12A cells were seeded at 350 000 cells per well in 6-well plates. After 24 h attachment the medium was discarded and the cells were exposed to the GI_{50} concentrations of the newly synthesized compounds and incubated for 24 h. Alpha tubulin was marked with anti-alpha tubulin antibodies and counter stained with an anti-mouse Ig1 Alexa-Fluor 488 secondary antibody for 90 min. The nucleus was stained with 4',6-diamidino-2-phenylindole (DAPI). Stained cells were viewed with a Zeiss 510 META confocal laser microscope(Carl Zeiss (Pty) Ltd., Johannesburg, South Africa).

Qualitatively, MCF-7, MDA-MB-231 and vehicle-treated control cells presented with normal nuclearmorphology and tubulin architecture during interphase, prophase,metaphase, anaphase, and telophase (Table 3.12, Table 3.13 and Table 3.14). ESE-15-one, ESE-15-ol and ESE-16 showed similar types of interference including formation of multiple spindle poles, abrogation of spindle formation during mitosis and abnormal mitotic spindle formation during mitosis(Table 3.12, Table 3.13 and Table 3.14). These results suggest that thenewly synthesized compounds are antimitotic agents that interferewith the microtubule dynamics in actively dividing cells.

Table 3.12: MCF-7 cells stained with DAPI and Alexa-488 anti-tubulin after 24 h exposure. Normal transition of cell cycle phases were observed in vehicle-treated cells. Metaphase chromatids as well as abnormal spindle formation in metaphase was observed in MCF-7 cells treated with ESE-15-one (130 nM), ESE-15-ol (50 nM) and ESE-16 (200 nM).

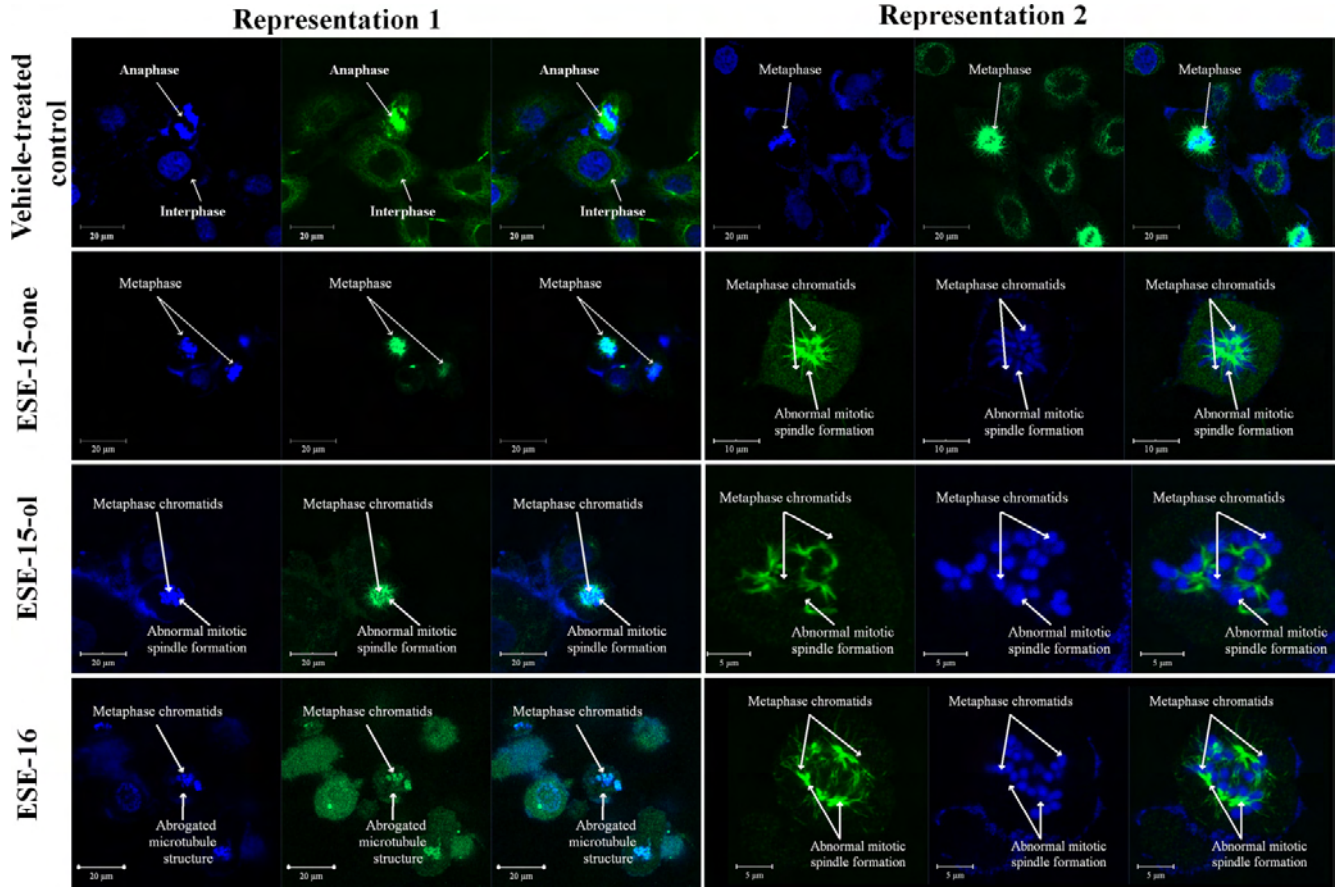

Table 3.13: MDA-MB-231 cells stained with DAPI and Alexa-488 anti-tubulin after 24 h exposure.Vehicle-treated cells in prophase and late stages of metaphase (met-anaphase) were observed. Metaphase chromatids, abrogated microtubule structures and abnormal mitotic spindles are observed in ESE-15-one-, ESE-15-ol- and ESE-16-treated cells.

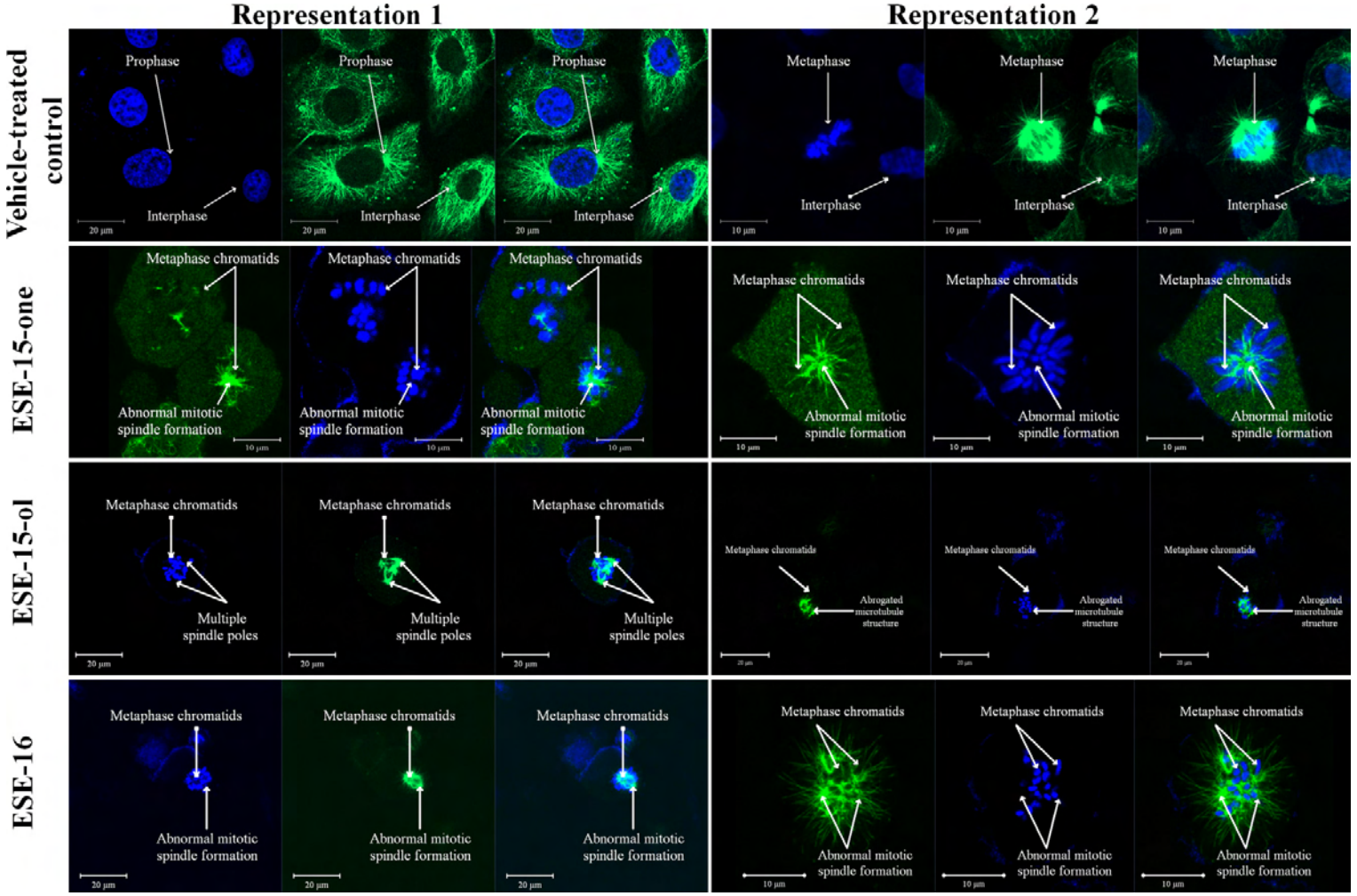

Table 3.14: MCF-12A cells stained with DAPI and Alexa-488 anti-tubulin after 24 h exposure.Vehicle-treated cells do not show any signs of interference with microtubule dynamics in actively dividing cells. Abnormal metaphase mitotic spindles are observed in ESE-15-one-, ESE-15-ol- and ESE-16-treated cells.

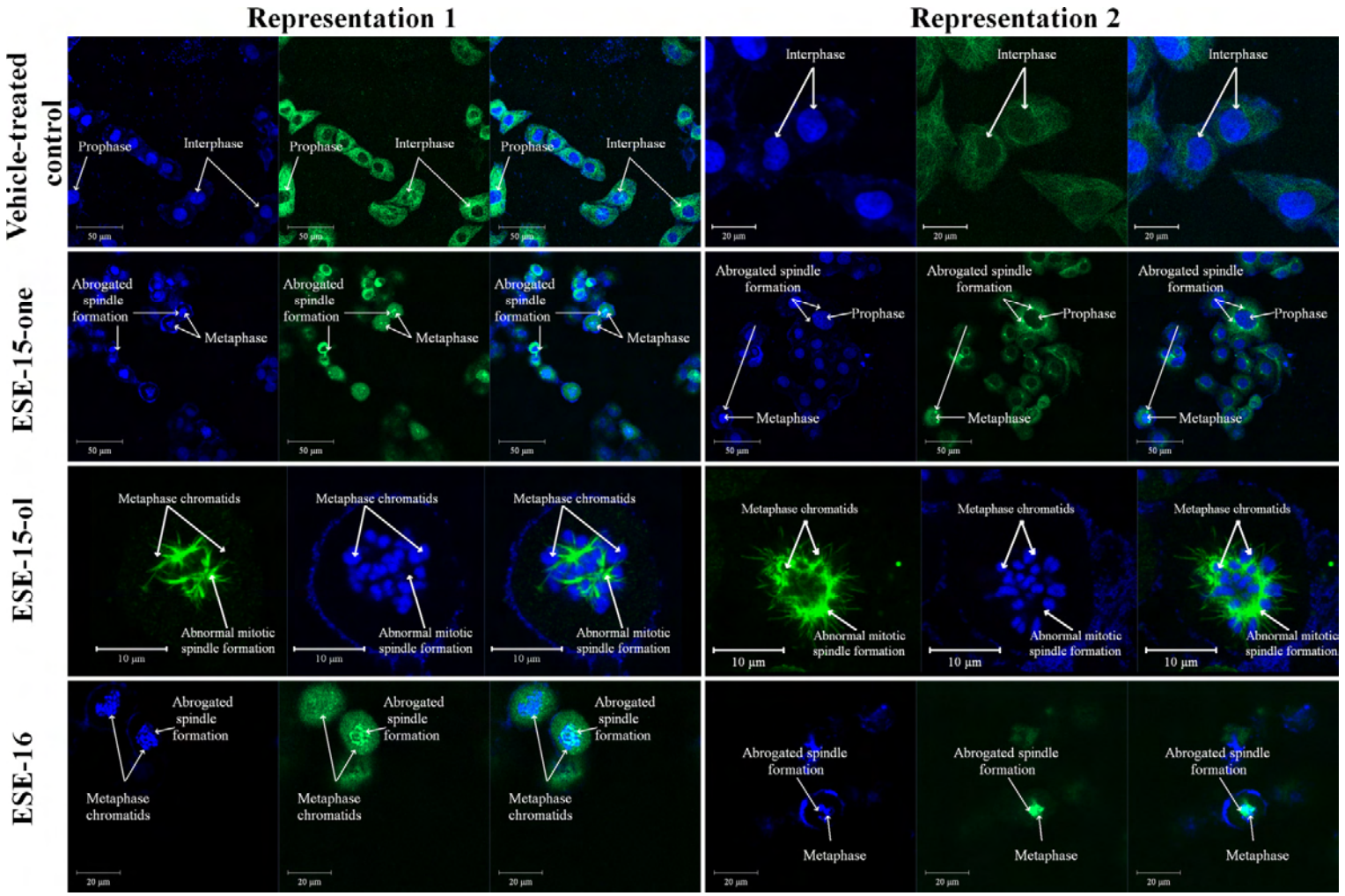

Light and Fluorescent microscopy: Polarization-optical differential interference contrast and Hoechst 33342, acridine orange and propidium iodide fluorescent staining

The effects of ESE-15-ol (50 nM) and ESE-16 (200 nM) on cell density and cell morphology were ascertained by means of PlasDIC and fluorescent microscopy using acridine orange (green) and Hoechst 33345 (blue). Acridine orange is a lysosomotropic fluorescent compound that serves as a tracer for acidic vesicular organelles including autophagic vacuoles and lysosomes (210). Cells undergoing autophagy will have an increased tendency for acridine orange staining when compared to viable cells, however acridine orange is not a specific marker for autophagy and therefore other techniques are needed to verify the appearance of increased autophagic activity. Hoechst 33342 is a fluorescent dye that can penetrate intact cell membranes of viable cells and cells undergoing apoptosis and stain the nucleus.

Qualitative observations of Hoechst 33342-stained MCF-7 (Figure 3.13 A and D), MDA-MB-231 (Figure 3.13 G and J) and MCF-12A (Figure 3.13 M and P) cells at a 100x magnification revealed a possible increase in cell density from 24 h to 48 h in vehicle-treated cells. ESE-15-ol- (Figure 3.13 B and H) and ESE-16-treated (Figure 3.13 C and I) MCF-7 and MDA-MB-231 cells appear to have a slight decrease in cell density after 24 exposure when compared to the vehicle-treated control. A decrease in cell density after 24 h exposure was not qualitatively evident in the MCF-12A cells treated with ESE-15-ol (Figure 3.13 N) or ESE-16 (Figure 3.13 O). Cell density was compromised after 48 h exposure in all tested cell lines for ESE-15-ol (Figure 3.13 E, K and Q) as well as ESE-16-treated cells (Figure 3.13 F, L and R) when compared to the vehicle-treated control. However, cell density after 48 h was less compromised in MCF-12A cells treated with ESE-15-ol and ESE-16 when compared to the MCF-7-treated cells (Figure 3.13 E, F Q and R) and MDA-MB-231-treated cells (Figure 3.13 K, L Q and R).

Cells stained with Hoechst 33342 where observed at 200x magnification with a Zeiss Filter 2 as well as PlasDIC and where overlaid to represent composite pictures of fluorescent and PlasDIC figures (Figure 3.14 and Figure 3.15). After 24 h exposure, an increase in the formation of apoptotic body formation and cells blocked in metaphase appear to be evident (qualitatively), in

ESE-15-ol- (Figure 3.14 B, E and H) and ESE-16-treated cells (Figure 3.14C, F and I) when compared to the vehicle-treated controls (Figure 3.14 A, D and G). Apoptotic body formation appears (qualitatively) to be more pronounced in MCF-7 and MDA-MB-231 cells when compared to the MCF-12A cells.

After 48 h exposure a marked reduction in cell density is observed inMCF-7 (Figure 3.15 B and C) and MDA-MB-231 (Figure 3.15 E and F) cells treated with ESE-15-ol and ESE-16 when compared to the vehicle-treated controls (Figure 3.15 A and D respectively). Cell density was also compromised in MCF-12A cells treated with ESE-15-ol (Figure 3.15 H) and ESE-16 (Figure 3.15 I) when compared to the vehicle-treated control (G). This effect was less pronounced when compared to MCF-7 and MDA-MB-231 cells treated with the compounds. An increase in the formation of apoptotic body formation and cells blocked in metaphase are also observed (qualitatively) in ESE-15-ol- (Figure 3.15 B, E and H) and ESE-16-treated (Figure 3.15 C, F and I) cells.

Cells stained with Hoechst 33342 and acridine orange were observed at 400x magnification. Cells in various stages of cell division (including prometaphase, metaphase, met-anaphase, telophase) where observed in MCF-7 (Figure 3.16 A-C, Figure 3.19 A-C), MDA-MB-231 (Figure 3.17 A-C, Figure 3.20 A-C) and MCF-12A (Figure 3.18 A-C, Figure 3.21 A-C) vehicle-treated cells after 24 h and 48 h. Cells blocked in metaphase appeared to be more prominent in ESE-15-ol- (Figure 3.16 D-F, Figure 3.17 D-F and Figure 3.18 D-F) and ESE-16-treated (Figure 3.16 G-I, Figure 3.17 G-I and Figure 3.18 G-I) MCF-7, MDA-MB-231 and MCF-12A cells after 24 h exposure. Qualitatively, an increase in acridine orange staining was observed in cells blocked in metaphase in the treated samples.

After 48 h exposure, formation of apoptotic bodies and hypercondensed chromatin was observedin ESE-15-ol- (Figure 3.19 D-F and Figure 3.20 D-F) and ESE-16-treated (Figure 3.19 G-I and Figure 3.20 G-I) MCF-7 and MDA-MB-231 cells. In MCF-12A-treated cells after 48 h exposure, cells in metaphase appeared to be more prominent in ESE-15-ol- (Figure 3.21 D-F) and ESE-16-treated cells (Figure 3.21 G-I) when compared to vehicle-treated cells (Figure 3.21 A-C).

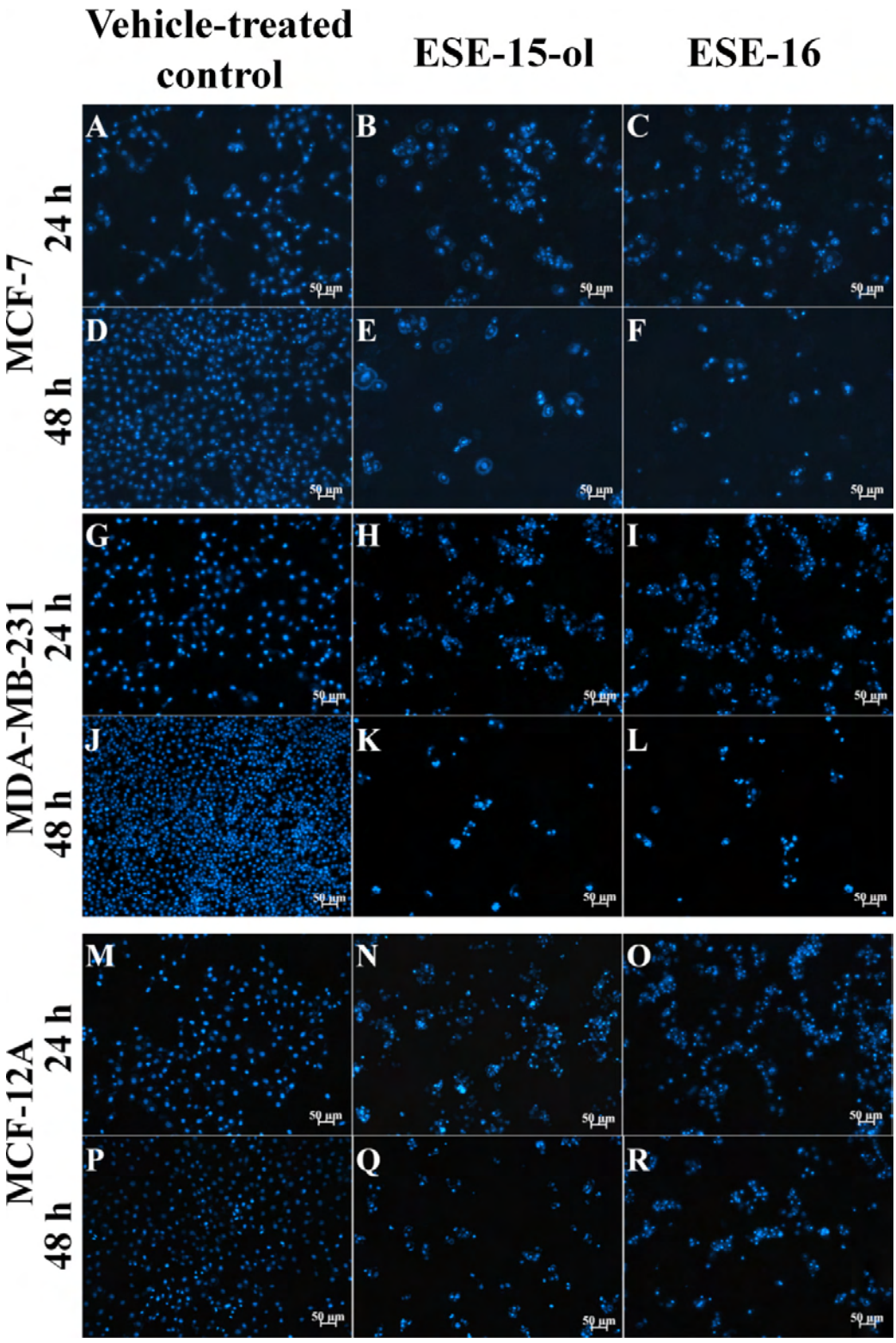

Figure 3.13:Hoechst 33342 staining of MCF-7, MDA-MB-231 and MCF-12A cells at 100x magnification.A marked decrease in cell density after 48 h exposure is observed in MCF-7 cells (A-F) and MDA-MB-231 (G-L)cells treated with ESE-15-ol and ESE-16. The effect on cell density was less pronounced in MCF-12A-treated(M-R) cells.

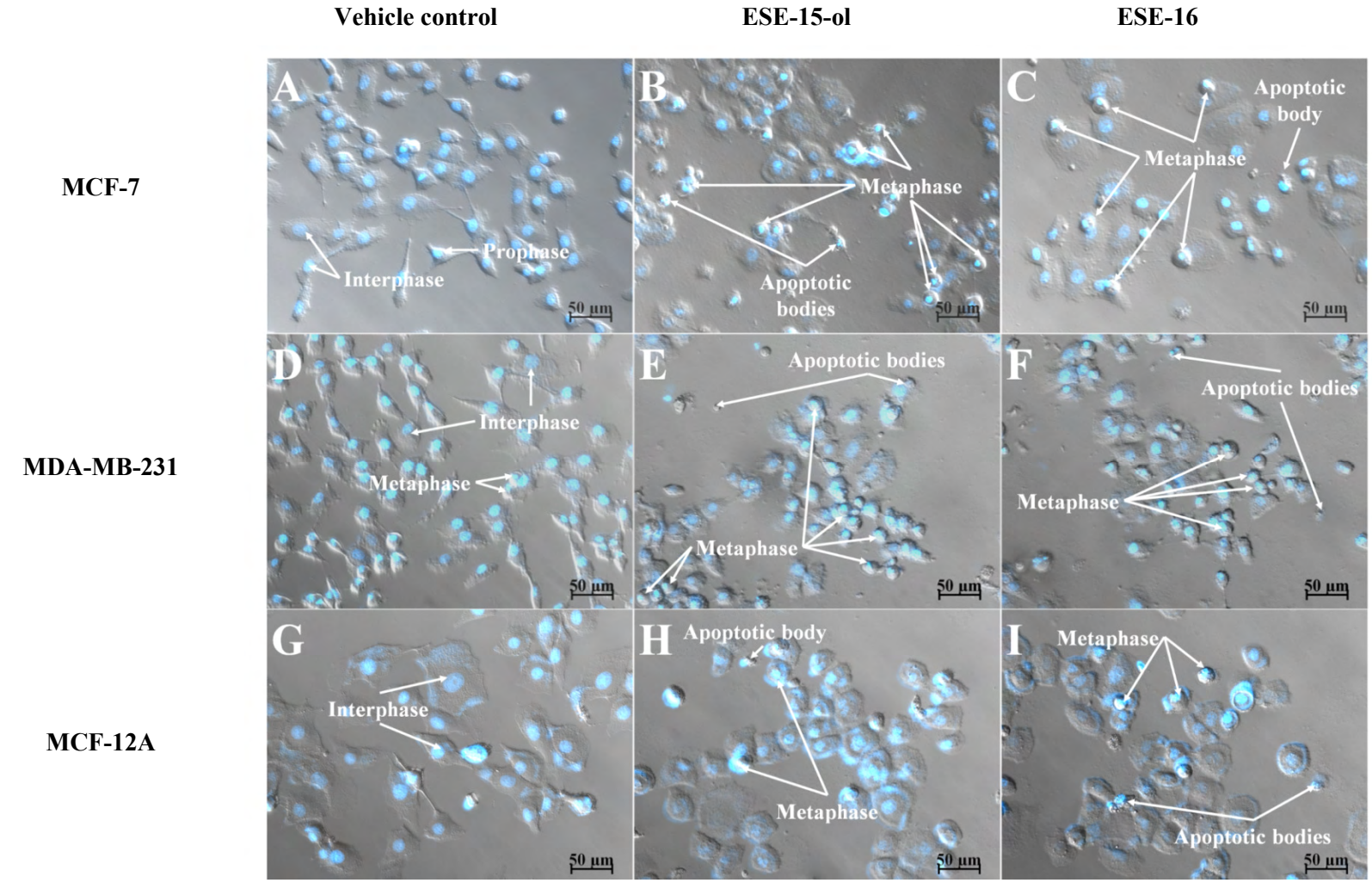

Figure 3.14: PlasDIC representations of Hoechst 33342 stained MCF-7, MDA-MB-231 and MCF-12A cells at 200x magnification after 24 h exposure.An increase in the formation of apoptotic body formation and cells blocked in metaphase are observed in ESE-15-ol- (B, E and H) and ESE-16-treated cells (C, F and I) is observed. The effect is more pronounced in MCF-7 and MDA-MB-231 cells when compared to the MCF-12A cells.

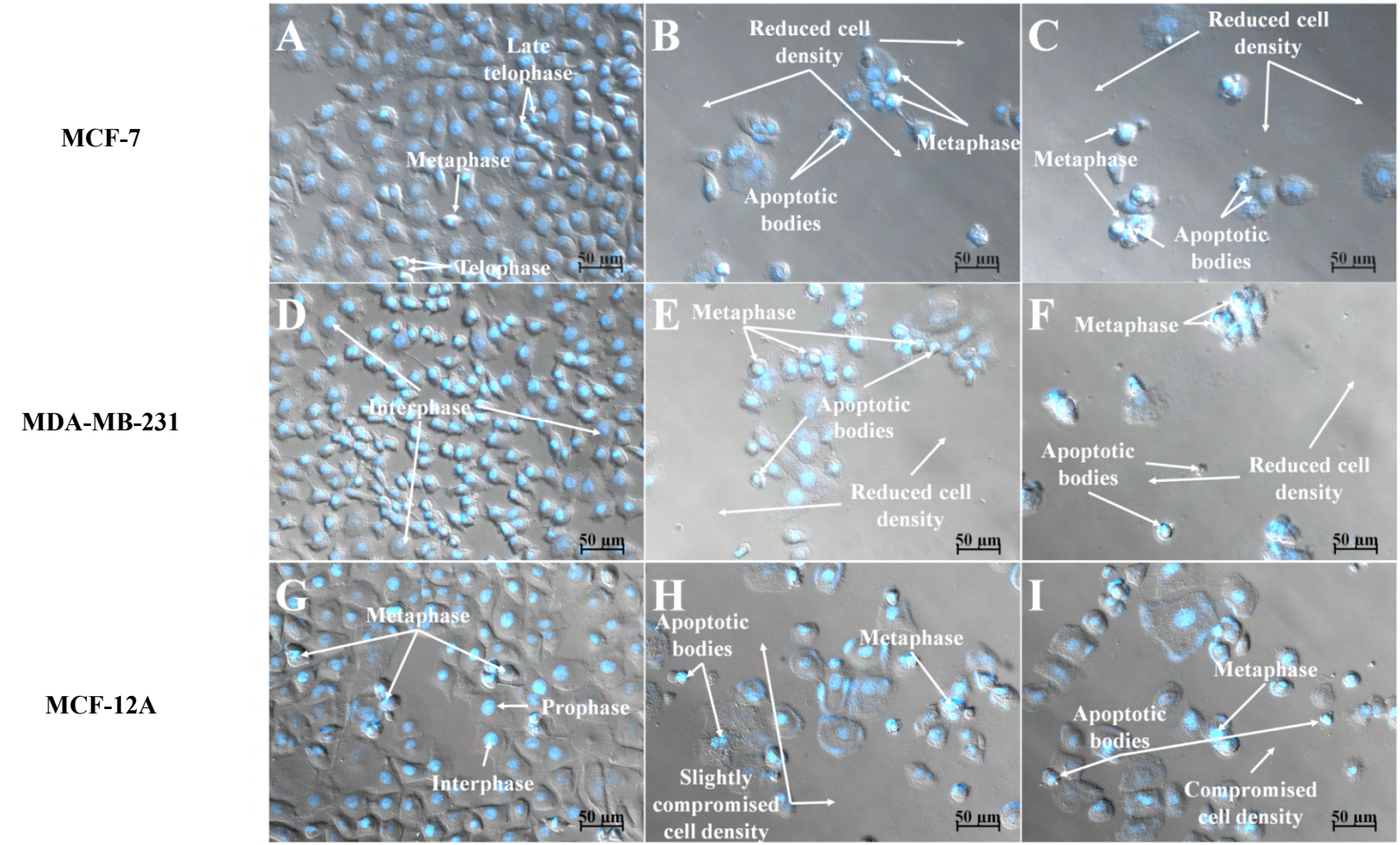

Figure 3.15: PlasDIC representations of Hoechst 33342 stained MCF-7, MDA-MB-231 and MCF-12A cells at 200x magnification after 24 h exposure.A marked reduction in cell density is observed inMCF-7 (B and C) and MDA-MB-231 (E and F) cells treated with ESE-15-ol and ESE-16 when compared to the vehicle-treated controls (A and D respectively). Cell density was also compromised in MCF-12A cells treated with ESE-15-ol (H) and ESE-16 (I) when compared to the vehicle-treated control (G), but was less pronounced when compared to MCF-7 and MDA-MB-231-treated cells. An increase in the formation of apoptotic body formation and cells blocked in metaphase are observed in ESE-15-ol- (B, E and H) and ESE-16-treated (C, F and I) cells.

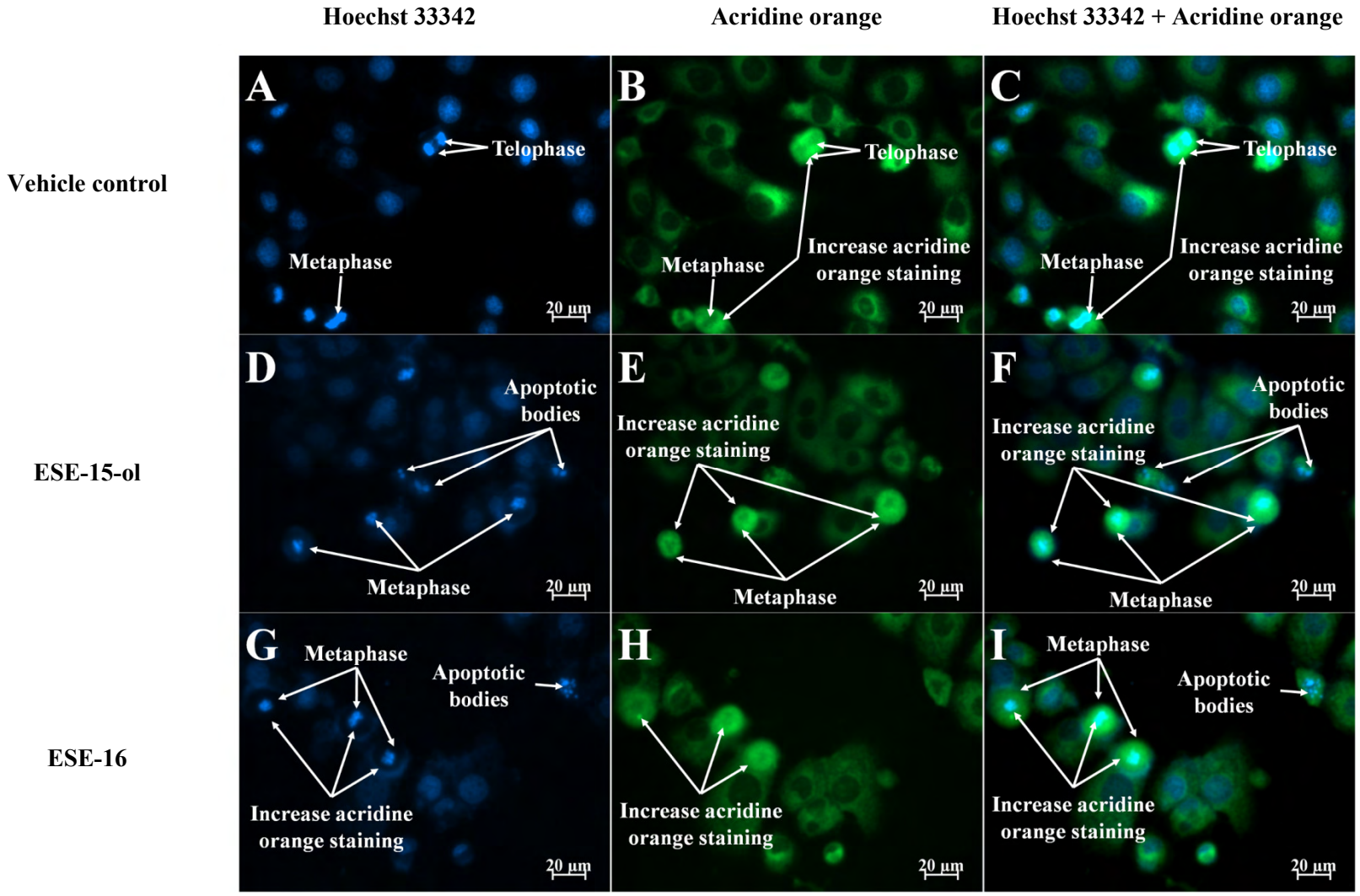

Figure 3.16: Hoechst 33342 and acridine orange-stained MCF-7cells at 400x magnification after 24 h exposure. Cells completing cell division (telophase) are observed in vehicle-treated cells (A-C) while an increase in the number of cells blocked in metaphase is observed in ESE-15-ol- (D-F) and ESE-16-treated cells (G-I). Acridine orange staining appears to be more concentrated in actively dividing cells in both treated and untreated cells.

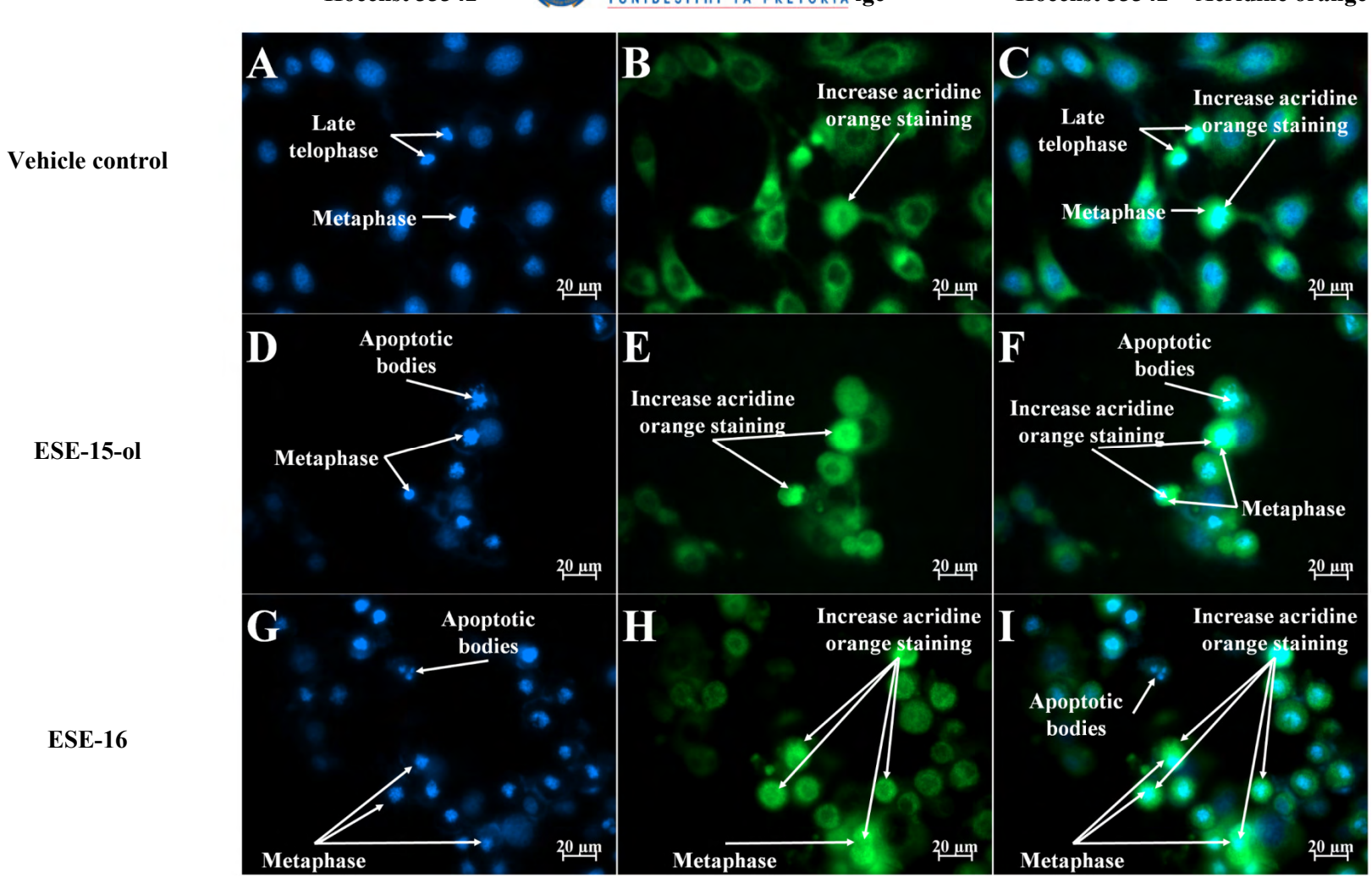

Figure 3.17: Hoechst 33342 and acridine orange-stainedMDA-MB-231 cells at 400x magnification after 24 h exposure. Vehicle-treated cells (A-C) various stages of the cell cycle (late telophase and metaphase) are observed. ESE-15-ol- (D-F) and ESE-16-treated cells (G-I) have an increased number of cells blocked in metaphase. Cell blocked in metaphase have an increase in acridine orange staining.

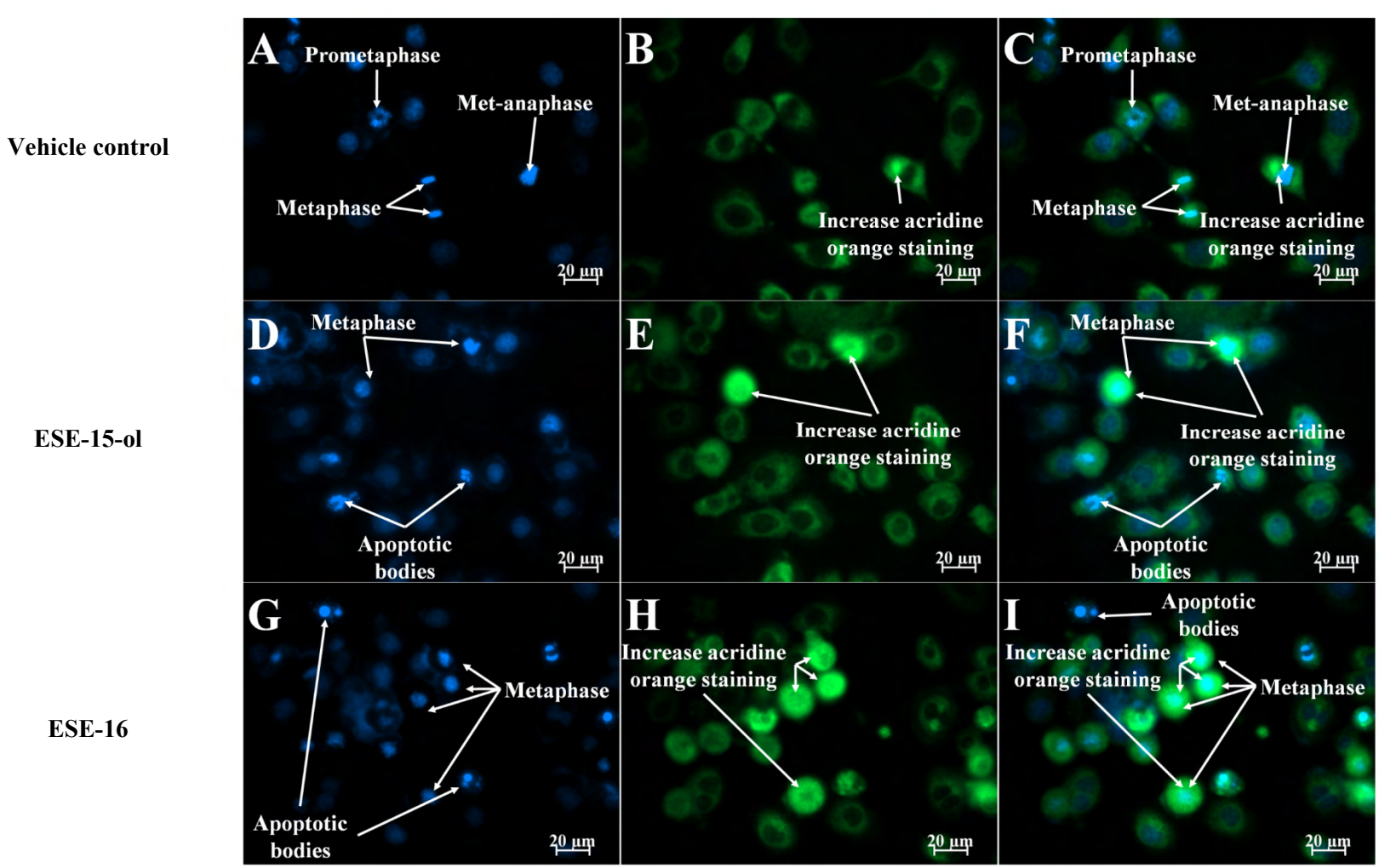

Figure 3.18: Hoechst 33342 and acridine orange-stained MCF-12A cells at 400x magnification after 24 h exposure.Vehicle-treated cells (A-C) various stages of the cell cycle (prometaphase, met-anaphase and metaphase) are observed. ESE-15-ol- (D-F) and ESE-16-treated cells (G-I) have an increased number of cells blocked in metaphase. Acridine orange staining is increased in cells blocked in metaphase.

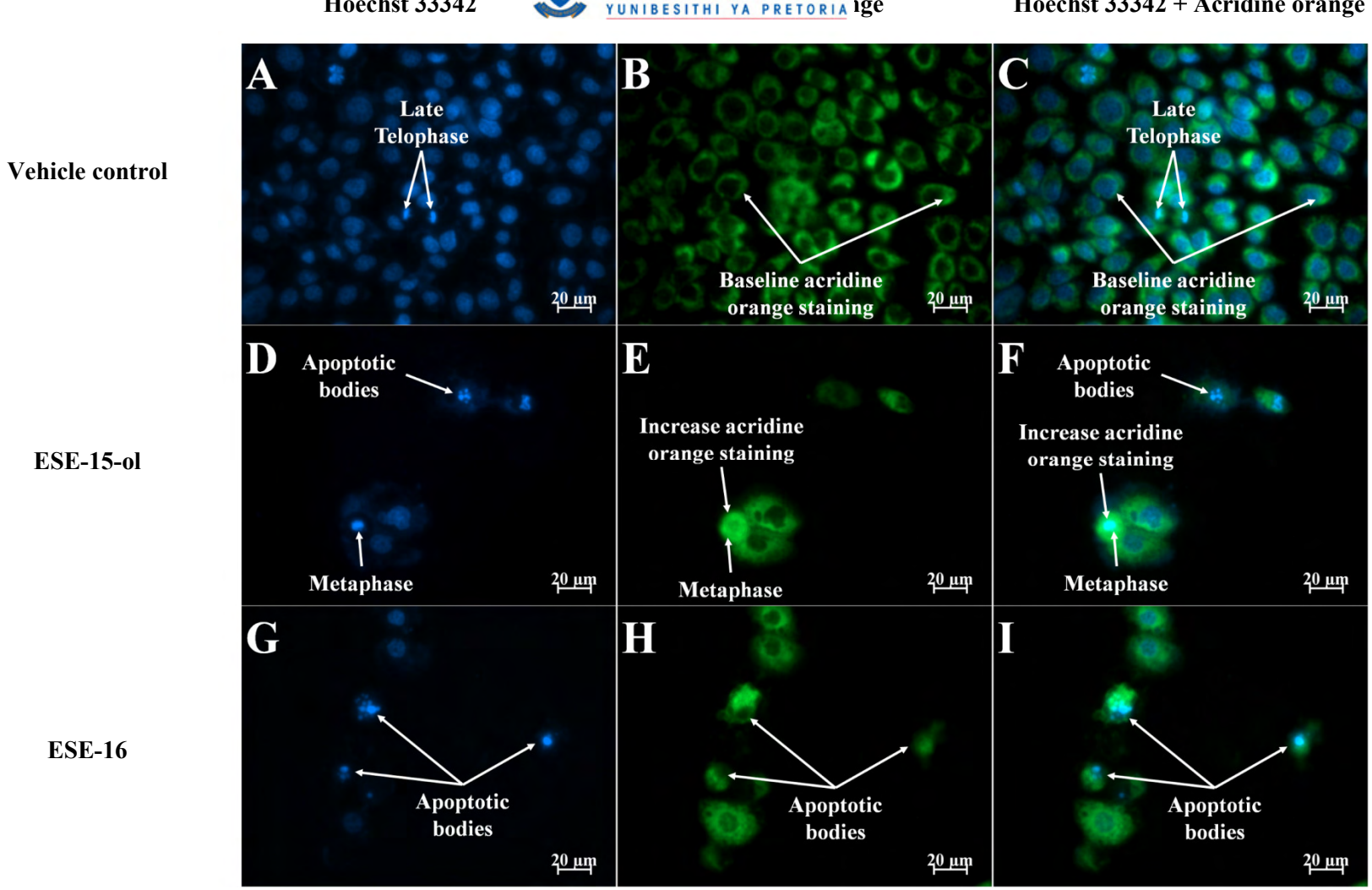

Figure 3.19: Hoechst 33342 and acridine orange-stained MCF-7 cells at 400x magnification after 48 h exposure.Vehicle-treated cells (A-C) various stages of the cell cycle (late telophase) are observed. Formation of apoptotic bodies are observed in ESE-15-ol- (D-F) and ESE-16-treated cells (G-I).

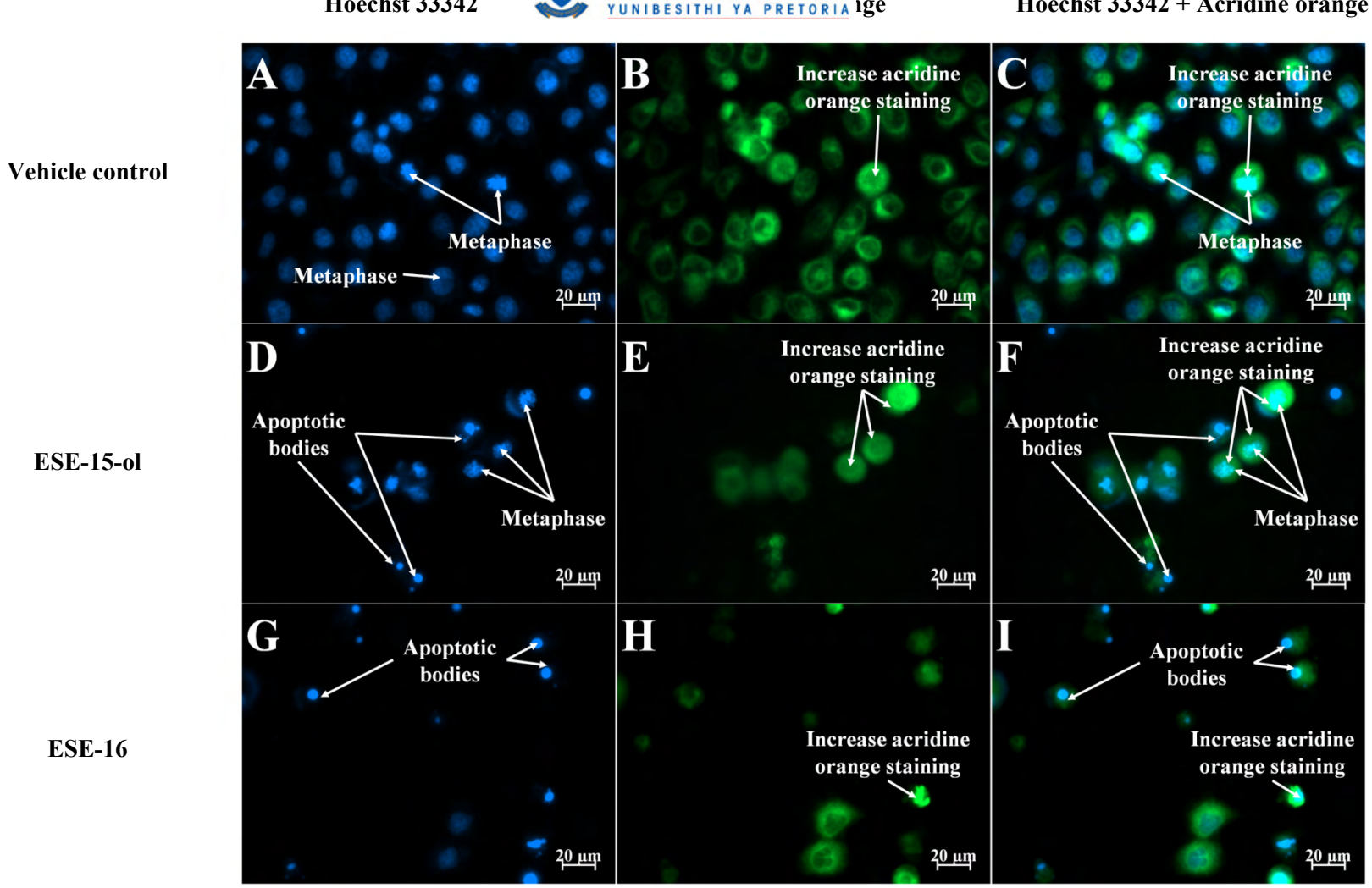

Figure 3.20: Hoechst 33342 and acridine orange-stainedMDA-MB-231 cells at 400x magnification after 48 h exposure.An increase in the formation of apoptotic bodies are observed in ESE-15-ol- (D-F) and ESE-16-treated cells (G-I) when compared to vehicle-treated cells (A-C).

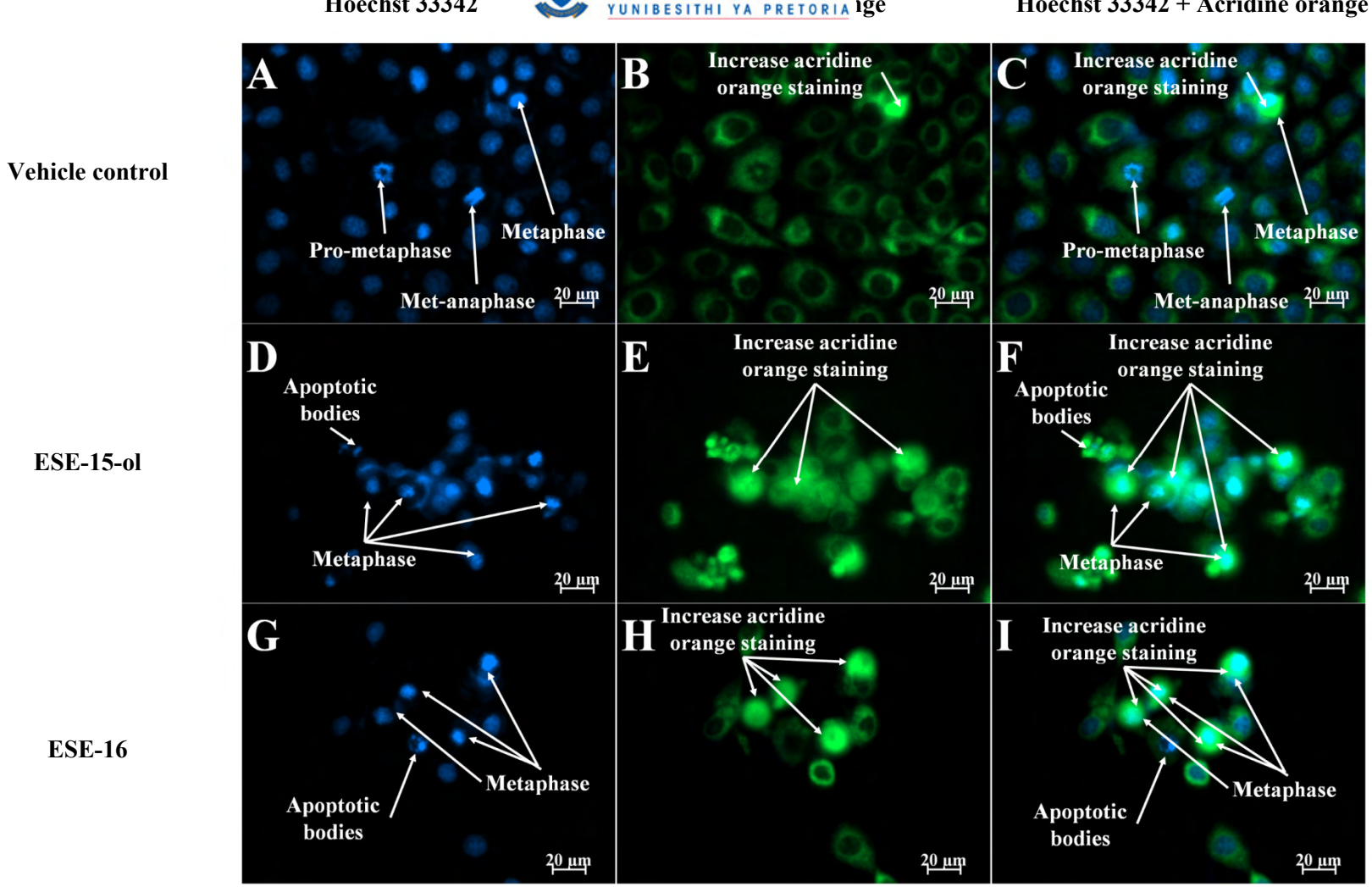

Figure 3.21: Hoechst 33342 and acridine orange-stained MCF-12A cells at 400x magnification after 48 h exposure.An increase in the number of cells in metaphase is observed in ESE-15-ol-(D-F) and ESE-16-treated (G-I) cells when compared to vehicle-treated cells (A-C).

Transmission electron microscopy: Morphological examination of intracellular ultrastructure.

The effects of ESE-15-ol (50 nM) and ESE-16 (200 nM) exposure for 24 h and 48 h on ultrastructutal changes in MCF-7, MDA-MB-231 and MCF-12A cells were monitored with TEM. TEM is a useful technique to determine the ultrastructure of intracellular components of exposed and control cells. TEM is also a reliable method for verifying autophagy (210). When autophagy occur the number and size of vacuoles increase and many of them contain myelin figures or are filled with lipids which appear as pale gray inclusions in the cytoplasm under electron microscopy (278). The nucleus of a cell undergoing autophagic cell death can become pyknotic and identifiable as such by light and fluorescence microscopy. Nuclear condensation may occur due to autophagic activity, however, it is not as common or as remarkable as that of apoptosis (278).

Vehicle-treated control MCF-7, MDA-MB-231 and MCF-12A cells after 24 h and 48 h presented with normal nuclear and cytoplasmic morphology (Figure 3.22 A and E, Figure 3.23A and E, Figure 3.24A and E). In actinomycin D-treated MCF-7, MDA-MB-231 and MCF-12A cells hypercondensed chromatin and the formation of stress vacuoles were observed (Figure 3.22 B and F, Figure 3.23B and F, Figure 3.24B and F).After 24 h exposure to ESE-15-ol (50 nM) and ESE-16 (200 nM), metaphase chromatid formation was observed in MCF-7, MDA-MB-231 and MCF-12A cells (Figure 3.22 C and D, Figure 3.23C and D, Figure 3.24C and D). This was also the case in MCF-12A cells treated with ESE-15-ol and ESE-16 after 48 h exposure (Figure 3.24G and H).

Intracellular vacuoles containing light and dark grey inclusions were observed in MCF-7 and MDA-MB-231 cells exposed to ESE-15-ol and ESE-16 after 48 h exposure (Figure 3.22 G and H, Figure 3.23G and H). Together these results support the view that autophagy is active in MCF-7 and MDA-MB-231 cells treated with ESE-15-ol and ESE-16, especially after 48 h of exposure to the compounds.

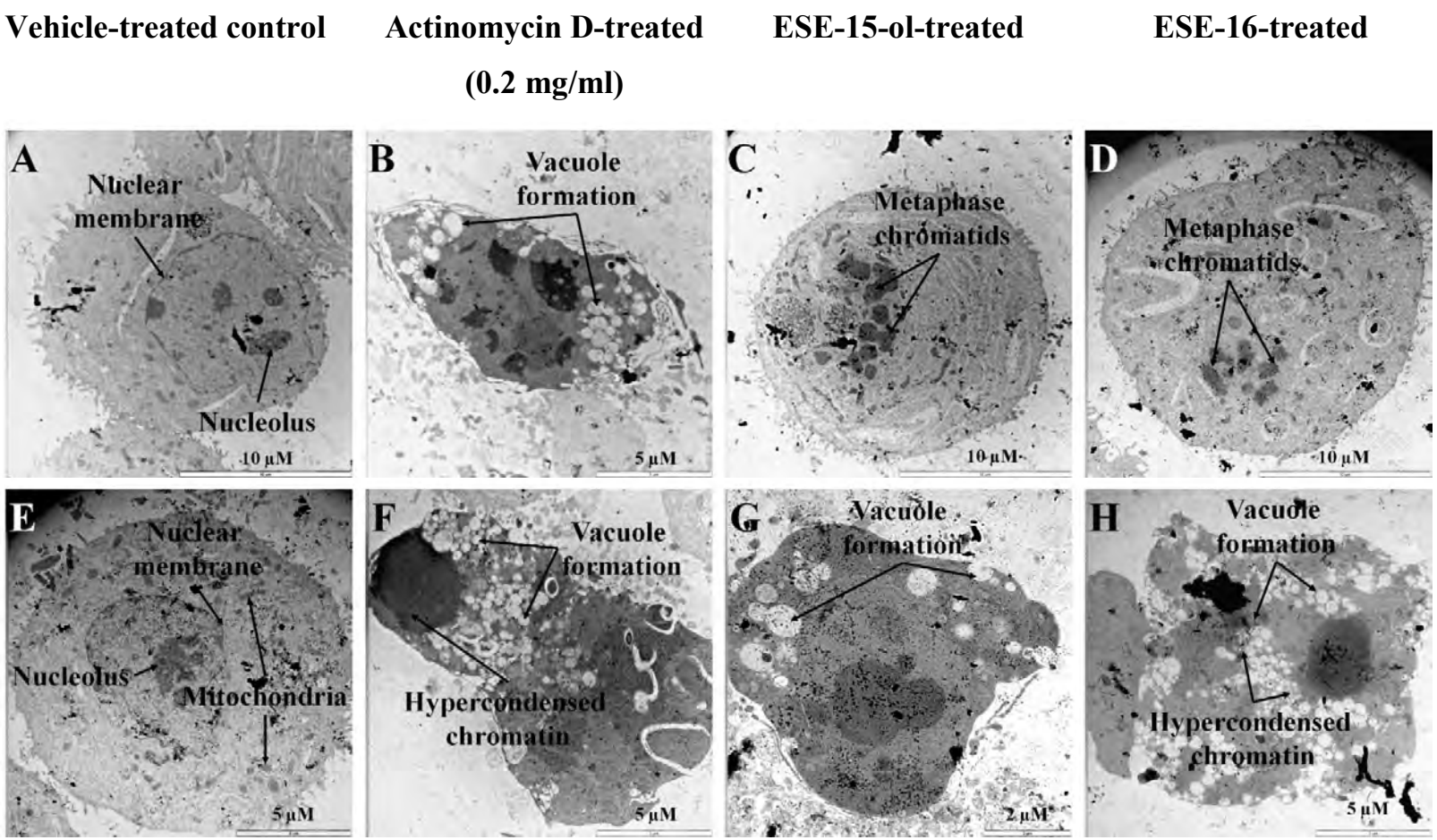

Figure 3.22: Transmission electron micrographs of MCF-7 cells. Vehicle-treated control cells after 24 h (A) and 48 h (E) presented with normal nuclear and cytoplasmic morphology. Hypercondensed chromatin was observed in Actinomycin D-treated cells (B and F). After 24 h exposure, metaphase chromatid formation was more prevalent in ESE-15-ol- (C) and ESE-16-treated (D) cells. The formation of vacuoles with small pale grey inclusions were observed in ESE-15-ol- (G) and ESE-16-treated (H) cells after 48 h of exposure.

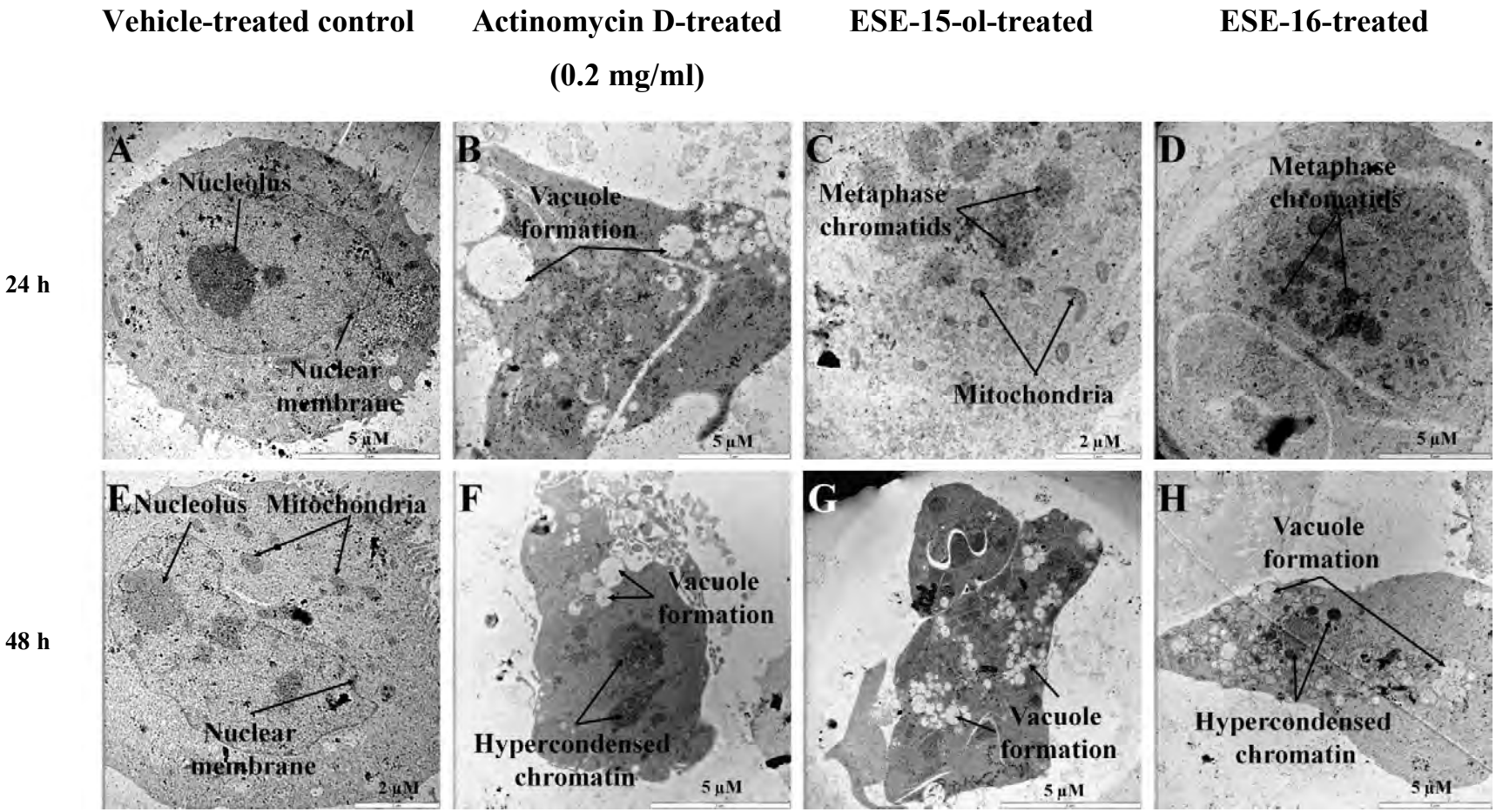

Figure 3.23: Transmission electron micrographs of MDA-MB-231 cells. Vehicle-treated control cells after 24 h (A) and 48 h (E) presented with normal nuclear and cytoplasmic morphology. Hypercondensed chromatin and stress vacuoles were observed in Actinomycin D-treated cells (B and F). After 24 h exposure, metaphase chromatid formation was more prevalent in ESE-15-ol- (C) and ESE-16-treated (D) cells. The formation of vacuoles with small pale grey inclusions as well as hypercondensed chromatin were was observed in ESE-15-ol- (G) and ESE-16-treated (H) cells after 48 h of exposure.

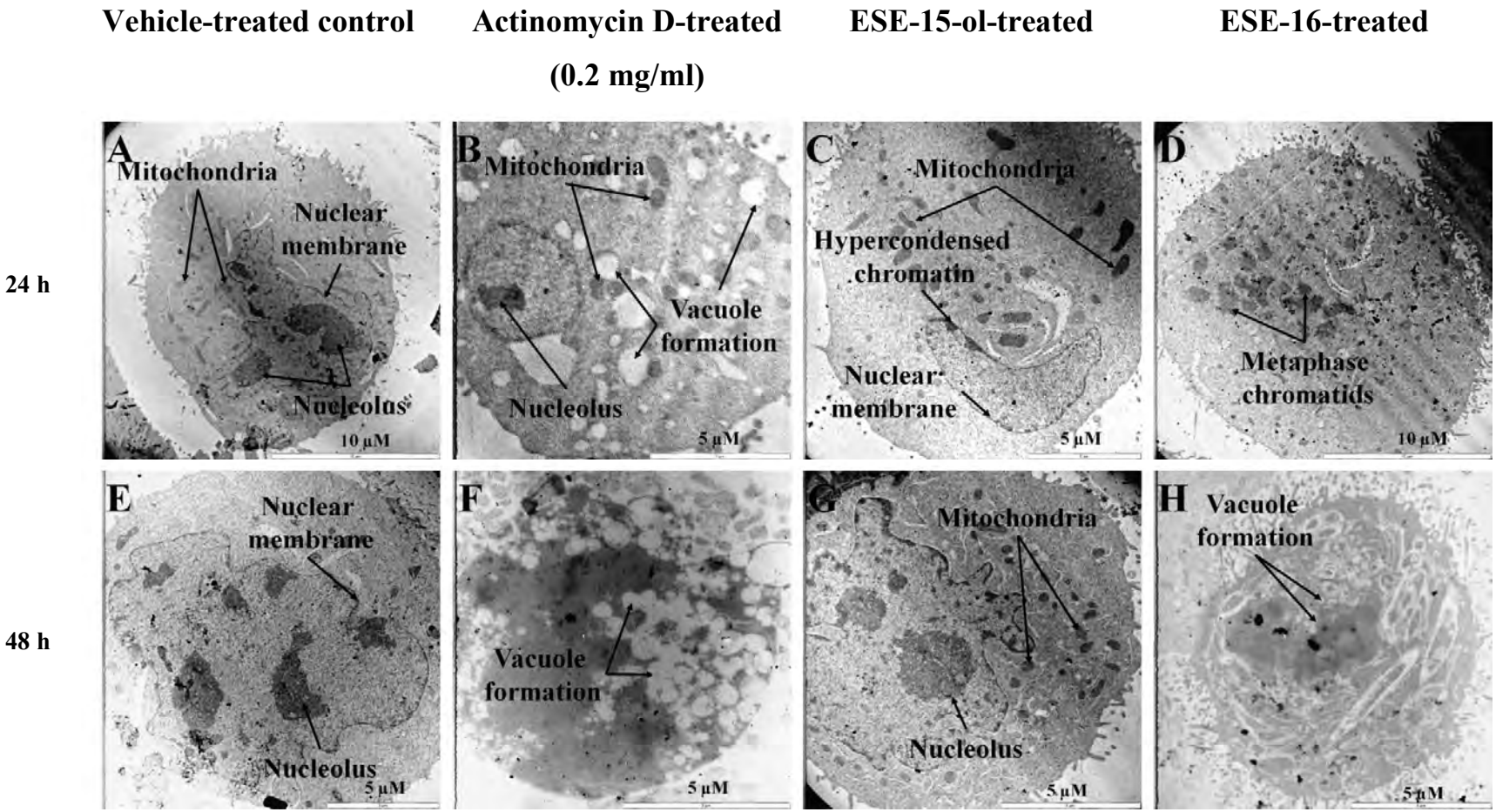

Figure 3.24: Transmission electron micrographs of MCF-12A cells. Normal nuclear and cytoplasmic morphology was observed in vehicle-treated control cells after 24 h (A) and 48 h (E). Stress vacuoles were observed in Actinomycin D-treated cells (B and F). Metaphase chromatid formation was more prevalent in ESE-15-ol- (C) and ESE-16-treated (D) cells after 24 h exposure.

Cell cycle progression

DNA content of cells was measured as an indication of cells in the various stages of the cell cycle. This was carried out to determine the effect that ESE-15-ol(50 nM) and ESE-16(200 nM) have on cell cycle progression (Figure 3.25, Figure 3.26 and Figure 3.27). In ESE-15-ol-treated and ESE-16-treated cells a gradual increase in the number of cells in the G_2/M phase was observed, reaching a maximum at different stages for each cell line.

For ESE-15-ol, the maximum number of cells in the G_2/M phase for MCF-7 (58.7% ±7.4) (Figure 3.28 C, Figure 3.30 A and Table 3.15) and MDA-MB-231 (58.4% ±6.4) (Figure 3.28 C, Figure 3.30 B and Table 3.16) cells was at 24 h. For the MCF-12A cells it was at 12 h (36.6% ±6.5) (Figure 3.28 C, Figure 3.30 C and Table 3.17). In ESE-16-treated cells the maximum number of cells in the G_2/M phase for MCF-7 (66.7% ±3.5) (Figure 3.28 D, Figure 3.30 A and Table 3.15) was at 18 h. For MDA-MB-231 (61.1% ±3.8) (Figure 3.28 D, Figure 3.30 B and Table 3.16) cells it was 24 h and for the MCF-12A cells it was at 12 h (46.3% ±7.4) (Figure 3.28 D, Figure 3.30 C and Table 3.17). This indicates the maximum number of cells in the sub-G_2/M fraction for MCF-12A-treated cells was not as high as MCF-7 and MDA-MB-231-treated cells, suggesting that the anti-mitotic effects of the compounds are more pronounced in the MCF-7 and MDA-MB-231 cells.

For both ESE-15-ol- and ESE-16-treated MCF-7 and MDA-MB-231 cells this was accompanied with a gradual increase in the number of cells in the sub-G_1 fraction and a gradual decrease in the number of cells in the G_1 phase (Figure 3.28 A-D, Figure 3.29 A and B, Figure 3.30 A and B, Table 3.15 and Table 3.16). Together these results suggest that the MCF-7 and MDA-MB-231 cells that are blocked in metaphase due to exposure to ESE-15-ol and ESE-16 proceed towards cell death rather than completing cell division.

For both ESE-15-ol- and ESE-16-treated MCF-12A cells there was also an accompanied gradual increase over time of cells in the sub-G_1 fraction and was statistically significantly less after 48 h exposure when compared to MCF-7 and MDA-MB-231-treated cells (Figure 3.28 A-D, Figure

3.29 C, Figure 3.30 A and B). However, unlike MCF-7 and MDA-MB-231 cells, the number of cells in the G_1 phase did not decrease, instead it remained steady (Table 3.17). This, together with the observation of a lower maximum number of cells in the sub-G_2/M fraction ofMCF-12A-treated cells when compared to MCF-7 and MDA-MB-231-treatedcells, suggest that MCF-12A cells are less sensitive to the growth inhibitory and cell death-inducing effects of ESE-15-ol and ESE-16.

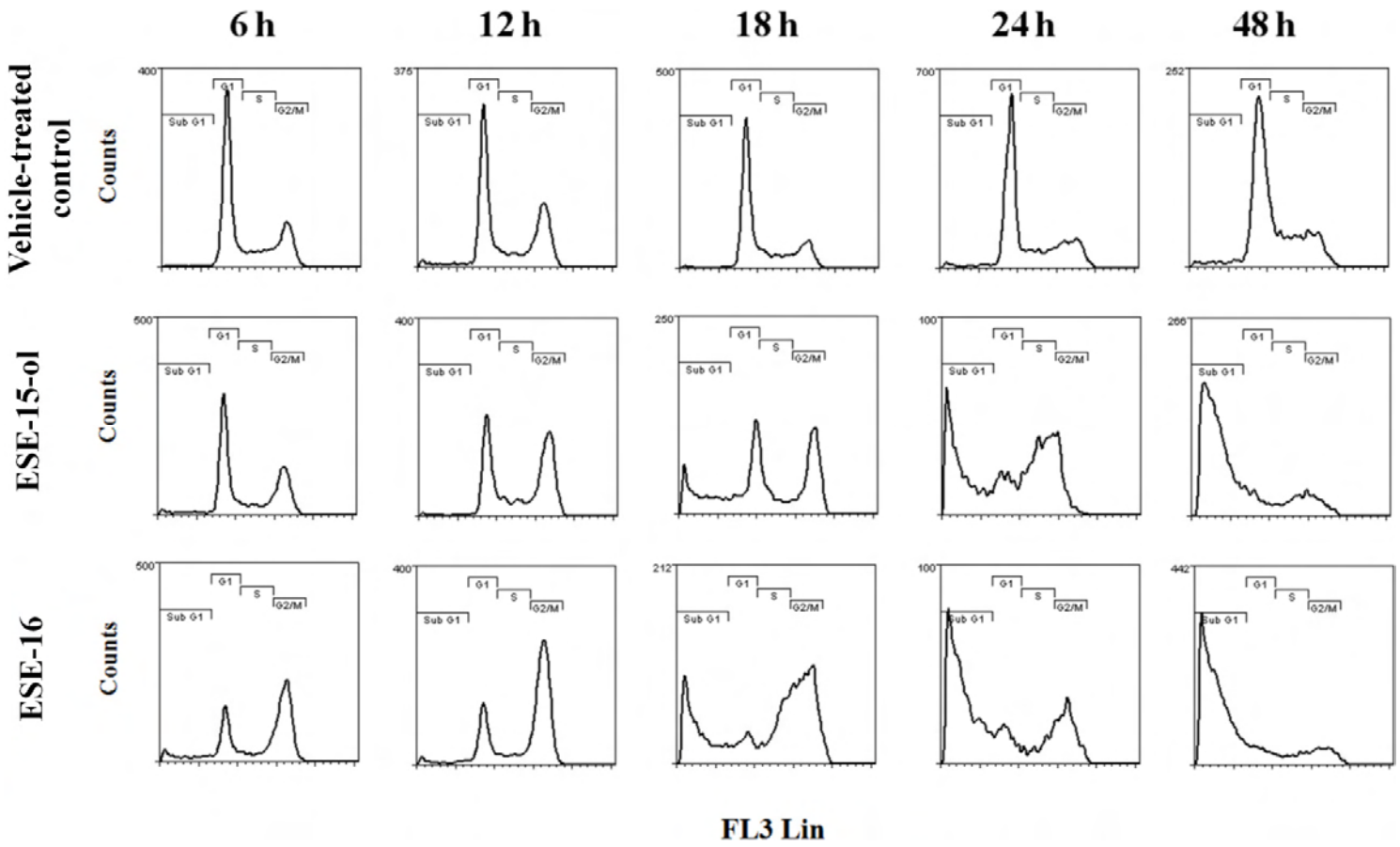

Figure 3.25: Cell cycle histograms of vehicle-treated, ESE-15-ol- and ESE-16-treated MCF-7 cells after 6 h, 12 h, 18 h, 24 h and 48 h exposure.A gradual increase in the G_2/M fraction was observed until 24 h for ESE-15-ol-treated cells and until 18 h for ESE-16-treated cells. After these intervals there appears to be a decrease in the G_2/M fraction with an accompanied increase in the sub-G_1, indicating increased cell death.

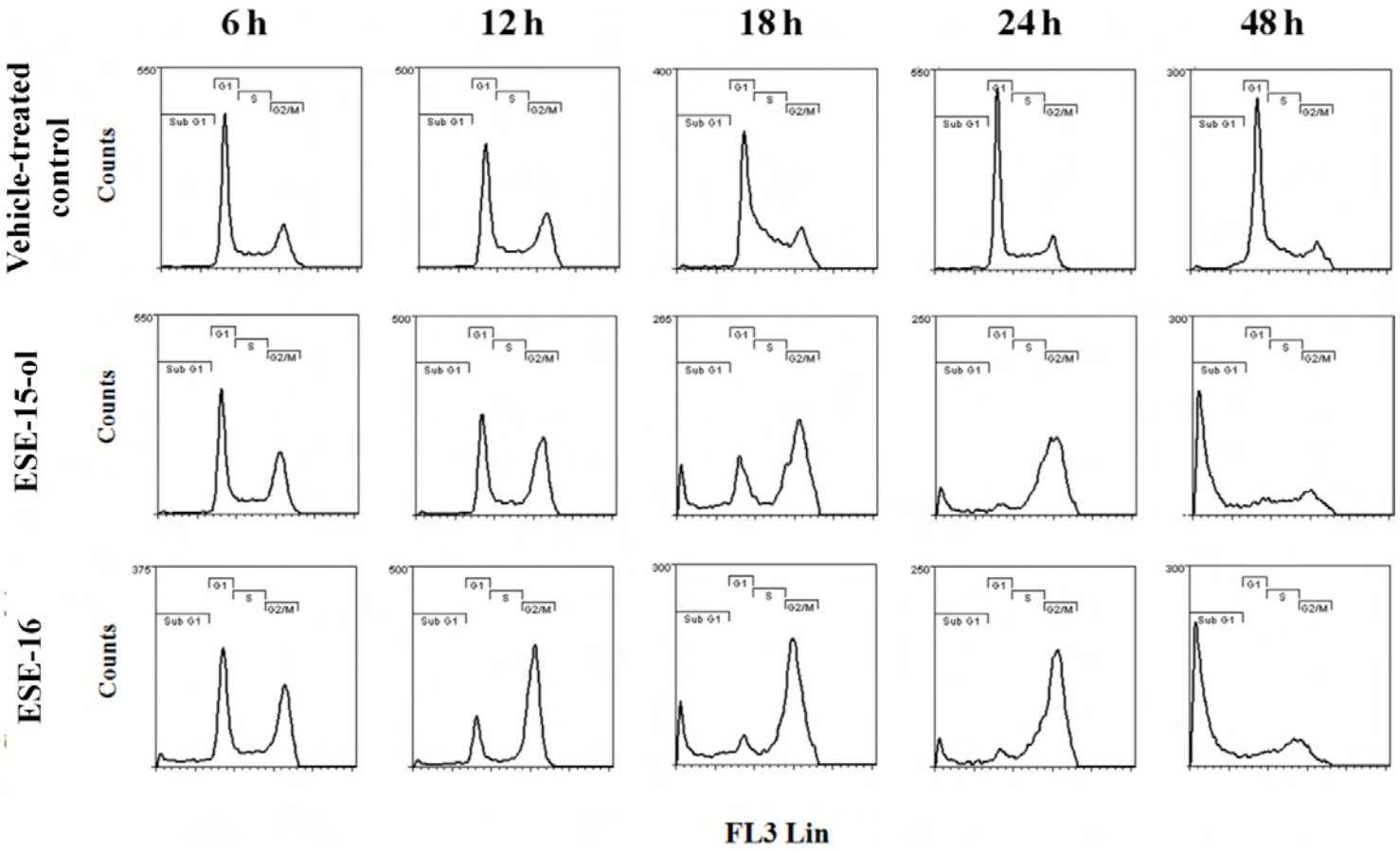

Figure 3.26: Cell cycle histograms of vehicle-treated, ESE-15-ol- and ESE-16-treated MDA-MB-231 cells after 6 h, 12 h, 18 h, 24 h and 48 h exposure.A gradual increase in the G_2/M fraction was observed until 24 h for ESE-15-ol- and ESE-16-treated. After these intervals there appears to be a decrease in the G_2/M fraction with an accompanied increase in the sub-G_1, indicating increased cell death.

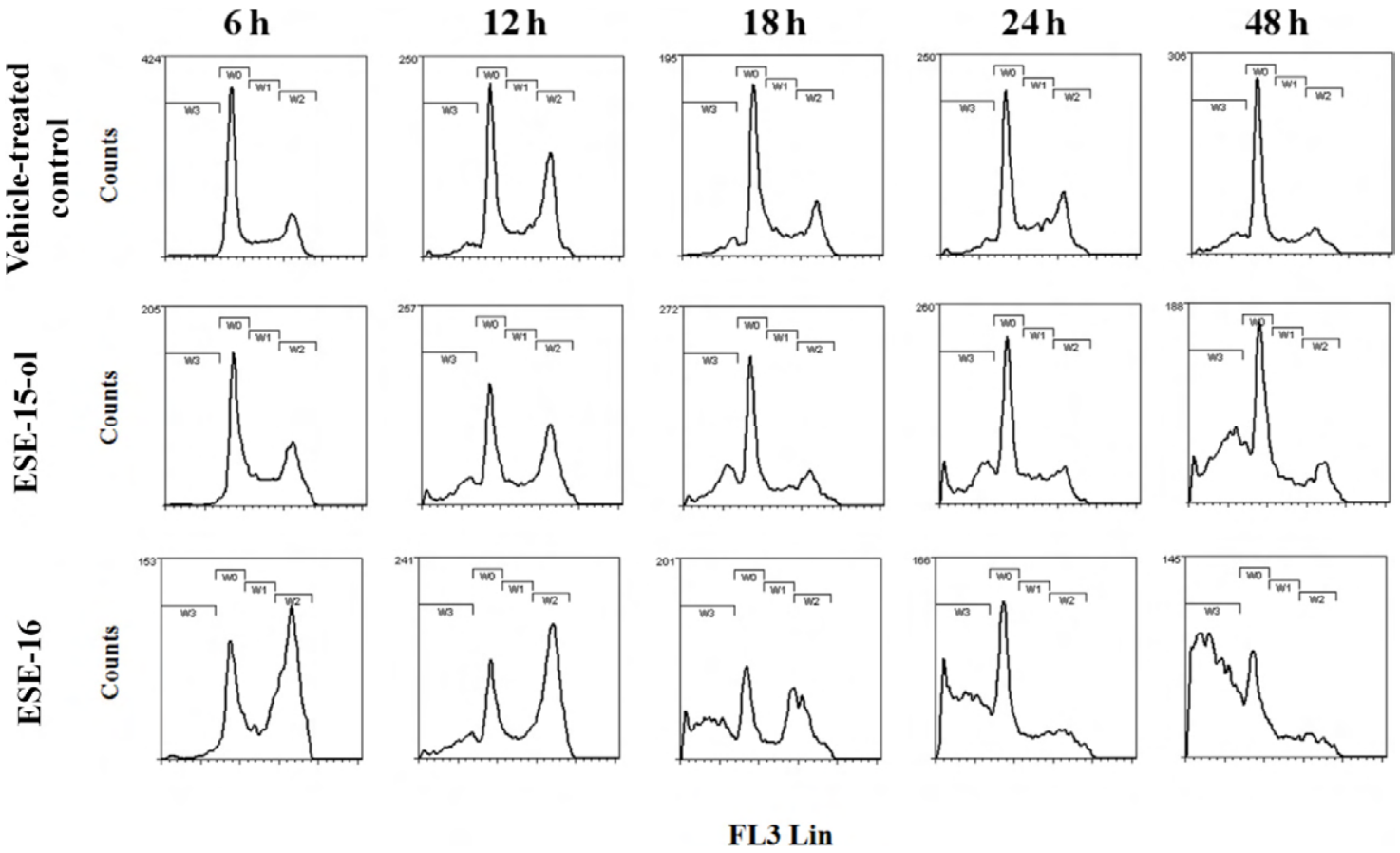

Figure 3.27: Cell cycle histograms of vehicle-treated, ESE-15-ol- and ESE-16-treated MCF-12A cells after 6 h, 12 h, 18 h, 24 h and 48 h exposure.A gradual increase in the sub-G_1 fraction is observed over time in ESE-15-ol- and ESE-16-treated MCF-12A cells, indicating increased cell death.A gradual increase in the G_2/M fraction was observed until 12 h for ESE-15-ol- and ESE-16-treated. After these intervals there appears to be a decrease in the G_2/M fraction with an accompanied increase in the sub-G_1.

Table 3.15: Measurement of DNA content in MCF-7 cells after 6 h, 12 h, 18 h, 24 h and 48 h exposure to vehicle-treated control, ESE-15-ol and ESE-16.

MCF-7 cells		**6 h**		**12 h**		**18 h**		**24 h**		**48 h**	
		Average	**STDEV**	**Average**	**STDEV**	**Average**	**STDEV**	**Average**	**STDEV**	**Average**	**STDEV**
Vehicle-treated control	**G_1**	**55.0**	0.8	**43.1**	3.8	**59.6**	2.6	**61.1**	3.4	**66.0**	1.3
	S	**17.0**	0.3	**18.9**	0.5	**17.7**	1.0	**18.0**	2.1	**13.0**	1.8
	G_2/M	**26.6**	1.1	**37.5**	3.5	**21.3**	3.3	**19.5**	2.0	**19.4**	1.2
	Sub G_1	**1.8**	0.3	**0.8**	0.1	**1.6**	0.6	**1.5**	0.8	**2.1**	0.9
ESE-15-ol	**G_1**	**46.9**	0.9	**37.3**	2.1	**15.5**	6.4	**7.8**	2.2	**9.4**	5.7
	S	**15.1**	2.3	**14.6**	0.6	**13.1**	2.9	**20.5**	0.5	**8.0**	1.0
	G_2/M	**35.3**	0.5	**46.2**	2.7	**56.9**	5.6	**58.7**	7.4	**10.6**	2.1
	Sub G_1	**3.0**	1.5	**2.1**	0.5	**14.4**	2.1	**13.1**	4.5	**72.8**	5.2
ESE-16	**G_1**	**36.9**	3.6	**21.2**	0.9	**7.4**	2.8	**10.2**	2.1	**10.3**	5.6
	S	**11.2**	0.5	**8.6**	0.3	**10.3**	1.4	**17.6**	3.3	**13.3**	3.0
	G_2/M	**43.3**	4.7	**64.6**	0.5	**66.7**	3.5	**59.9**	7.0	**20.5**	5.7
	Sub G_1	**8.9**	1.2	**5.7**	1.1	**15.6**	2.2	**12.2**	1.7	**55.9**	8.5

Table 3.16: Measurement of DNA content in MDA-MB-231 cells after 6 h, 12 h, 18 h, 24 h and 48 h exposure to vehicle-treated control, ESE-15-ol and ESE-16.

MDA-MB-231 cells		**6 h**		**12 h**		**18 h**		**24 h**		**48 h**	
		Average	**STDEV**	**Average**	**STDEV**	**Average**	**STDEV**	**Average**	**STDEV**	**Average**	**STDEV**
Vehicle-treated control	**G_1**	**53.8**	3.1	**32.7**	4.4	**44.1**	0.5	**39.5**	3.4	**57.6**	3.4
	S	**14.9**	0.4	**26.9**	1.7	**26.2**	0.1	**25.2**	1.5	**16.3**	0.7
	G_2/M	**28.2**	0.9	**38.8**	0.8	**24.5**	2.2	**34.3**	2.6	**15.9**	1.5
	Sub G_1	**1.7**	0.2	**0.9**	0.2	**5.3**	2.3	**1.3**	0.4	**9.4**	1.1
ESE-15-ol	**G_1**	**49.9**	2.9	**38.5**	0.8	**21.8**	2.2	**7.3**	2.3	**17.6**	9.1
	S	**11.9**	1.9	**10.2**	3.7	**12.1**	1.0	**14.5**	4.6	**12.5**	5.9
	G_2/M	**34.0**	3.2	**47.8**	1.7	**53.6**	4.2	**58.4**	6.4	**10.8**	6.1
	Sub G_1	**4.5**	2.1	**3.7**	2.5	**11.5**	2.2	**19.8**	1.7	**61.4**	2.6
ESE-16	**G_1**	**34.9**	3.5	**26.0**	9.2	**9.5**	2.7	**9.9**	1.9	**16.1**	8.2
	S	**11.2**	0.6	**7.6**	1.2	**11.8**	1.0	**10.2**	0.9	**14.3**	7.5
	G_2/M	**46.8**	6.2	**60.4**	8.1	**55.8**	8.8	**61.1**	3.8	**16.4**	7.5
	Sub G_1	**7.2**	2.3	**6.2**	0.1	**18.8**	4.6	**18.8**	3.3	**61.1**	4.9

Table 3.17: Measurement of DNA content in MCF-12A cells after 6 h, 12 h, 18 h, 24 h and 48 h exposure to vehicle-treated control, ESE-15-ol and ESE-16.

MCF-12A cells		**6 h**		**12 h**		**18 h**		**24 h**		**48 h**	
		Average	**STDEV**	**Average**	**STDEV**	**Average**	**STDEV**	**Average**	**STDEV**	**Average**	**STDEV**
Vehicle-treated control	**G_1**	**53.3**	6.5	**46.2**	2.9	**46.8**	0.8	**44.7**	2.8	**60.1**	3.5
	S	**16.3**	1.6	**17.6**	0.4	**20.1**	1.5	**20.9**	1.9	**12.8**	0.0
	G_2/M	**24.0**	2.7	**31.2**	4.3	**26.3**	0.4	**26.6**	3.3	**19.1**	1.1
	Sub G_1	**5.1**	0.1	**5.0**	1.0	**6.9**	1.3	**8.0**	1.3	**7.8**	3.2
ESE-15-ol	**G_1**	**43.7**	8.7	**37.6**	4.1	**43.4**	2.5	**47.6**	3.4	**32.8**	8.0
	S	**14.5**	1.9	**12.5**	4.1	**15.7**	1.1	**14.4**	2.7	**13.4**	4.4
	G_2/M	**30.6**	7.5	**36.6**	6.5	**22.2**	1.7	**14.1**	1.1	**11.6**	1.0
	Sub G_1	**11.4**	7.0	**13.4**	6.6	**18.9**	3.2	**23.2**	1.9	**42.3**	2.5
ESE-16	**G_1**	**36.6**	7.4	**28.4**	5.5	**27.1**	1.7	**51.0**	3.5	**51.5**	7.0
	S	**14.6**	3.0	**12.5**	1.2	**13.5**	8.1	**10.1**	3.2	**9.2**	2.8
	G_2/M	**42.1**	7.6	**46.3**	5.3	**37.5**	5.0	**15.9**	0.6	**8.8**	0.6
	Sub G_1	**6.8**	3.3	**13.0**	1.8	**22.0**	5.7	**23.1**	2.7	**28.1**	1.8

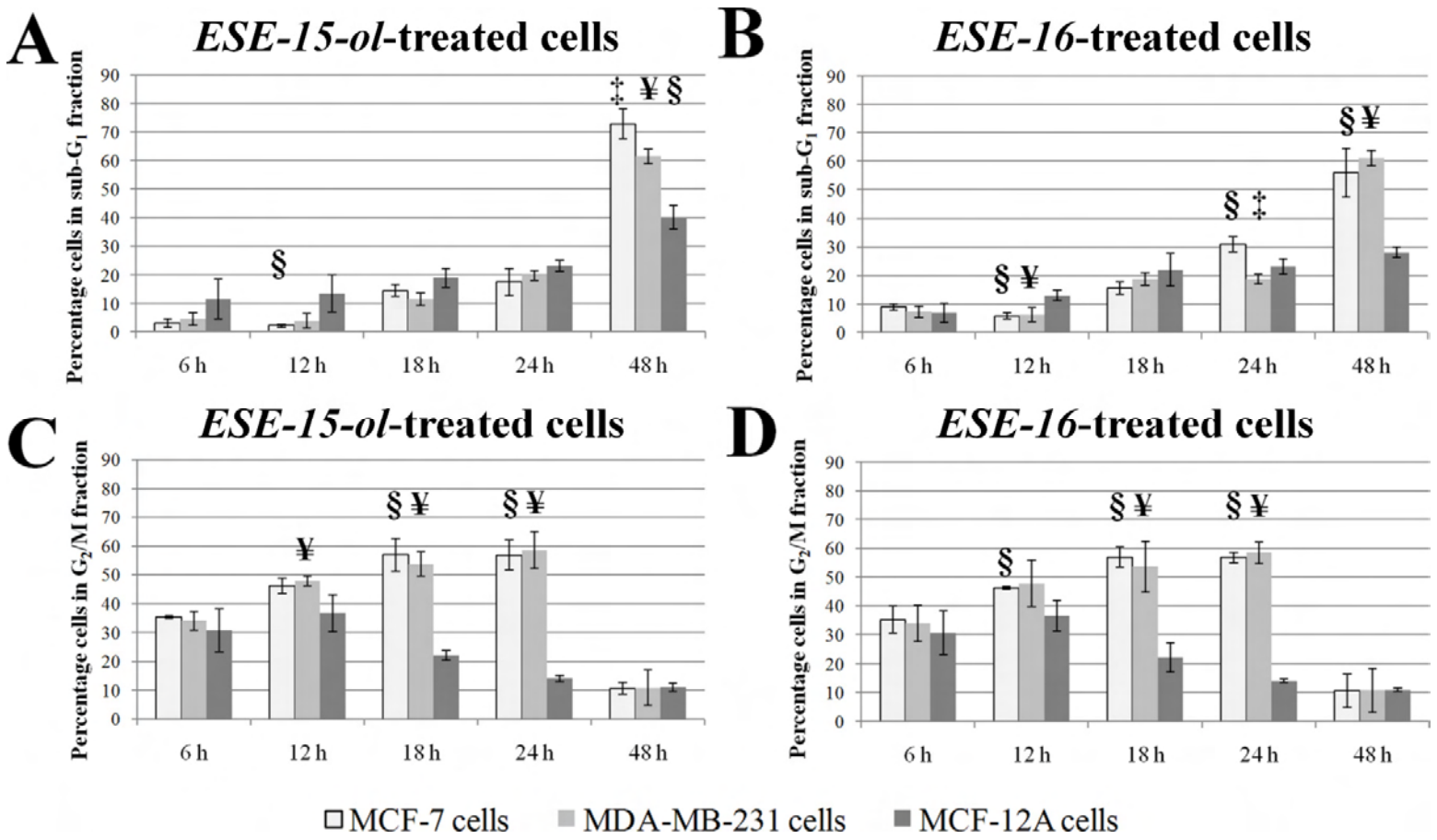

Figure 3.28: Comparisons between MCF-7, MDA-MB231 and MCF-12A cells of percentage of cells in sub G_1 and G_2/M in ESE-15-ol- and ESE-16-treated cells after 6 h, 12 h, 18 h, 24 h and 48 h exposure.

‡indicates a *P*-value < 0.05 between MCF-7 and MDA-MB-231 cells.

¥ indicates a *P*-value < 0.05 between MDA-MB-231 and MCF-12A cells.

§indicates a *P*-value < 0.05 between MCF-12A and MCF-7 cells.

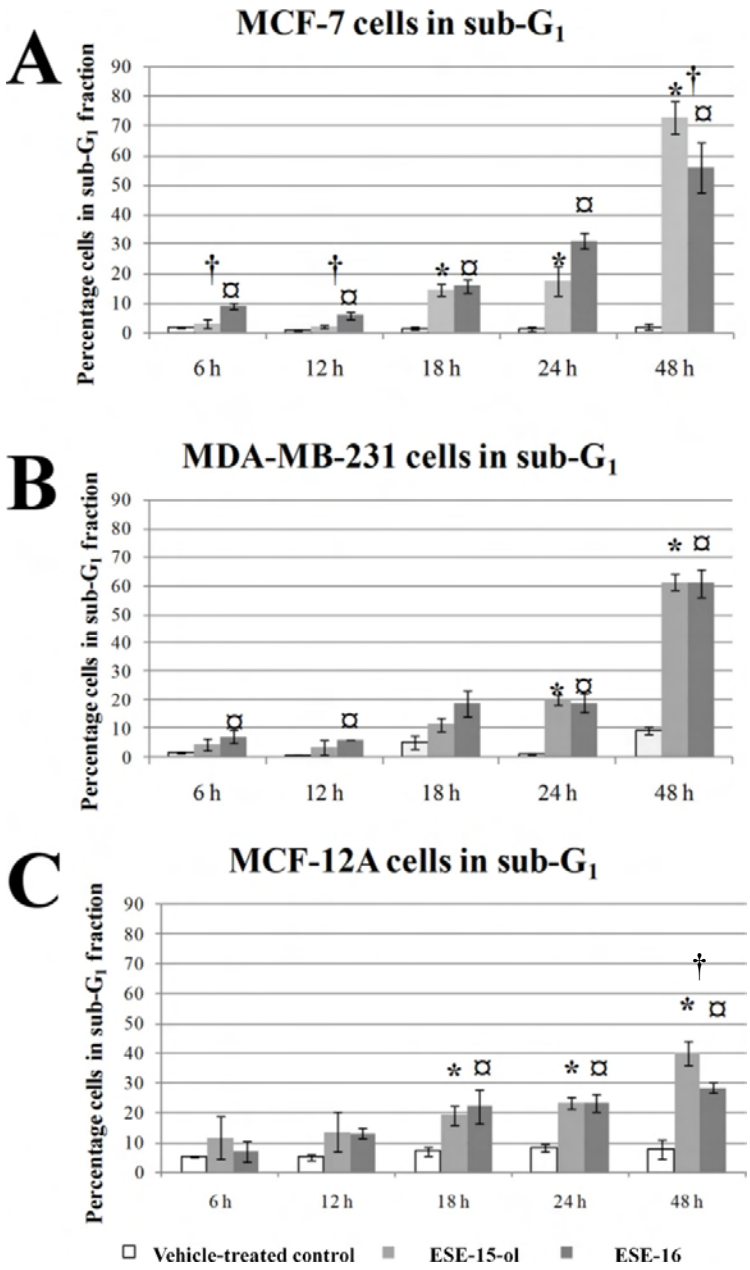

Figure 3.29: Comparisons of percentage of cells in sub G_1 phase in vehicle-treated, ESE-15-ol treated and ESE-16-treated celss for MCF-7, MDA-MB231 and MCF-12A cells after 6 h, 12 h, 18 h, 24 h and 48 h exposure.

* indicates a *P*-value < 0.05 between ESE-15-ol- and vehicle-treated cells.

¤ indicates a *P*-value < 0.05 between ESE-16- and vehicle-treated cells.

† indicates a *P*-value < 0.05 between ESE-15-ol- and ESE-16-treated cells.

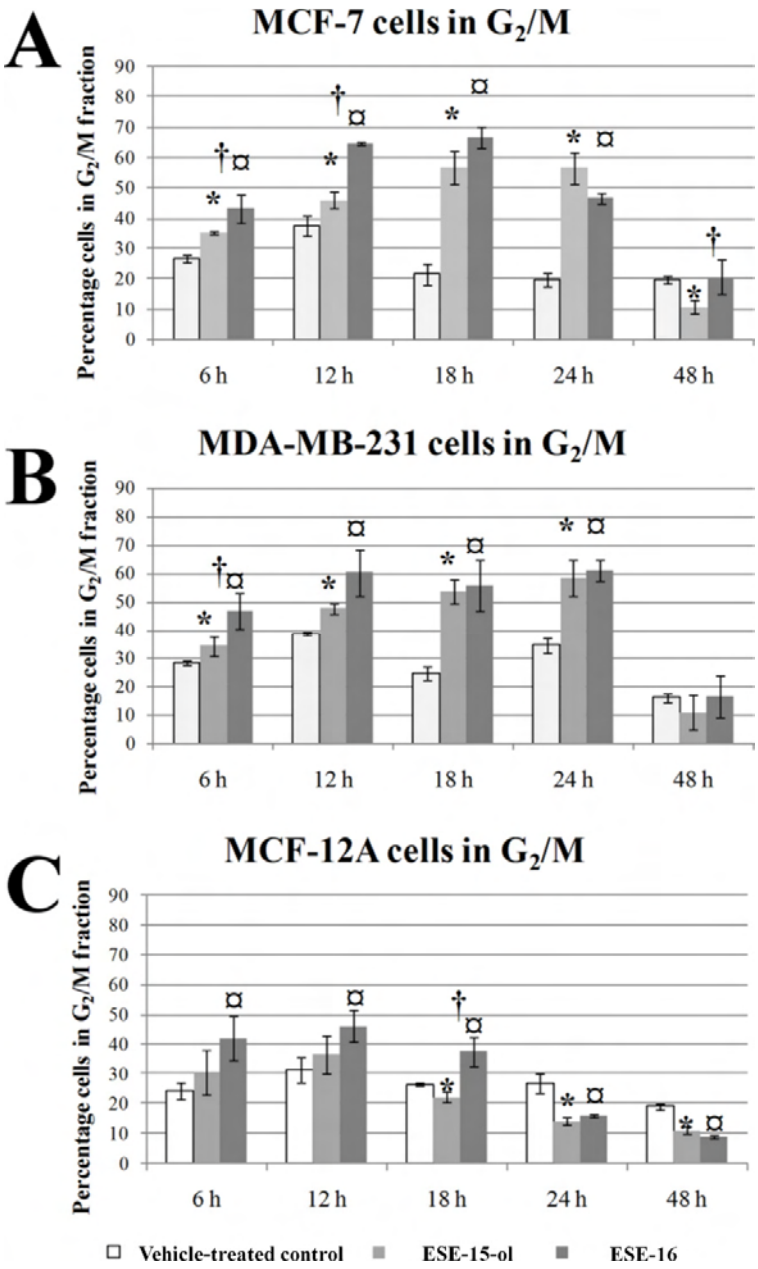

Figure 3.30: Comparisons of percentage of cells in G_2/M phase in vehicle-treated, ESE-15-ol treated and ESE-16-treated celss for MCF-7, MDA-MB231 and MCF-12A cells after 6 h, 12 h, 18 h, 24 h and 48 h exposure.

* indicates a *P*-value < 0.05 between ESE-15-ol- and vehicle-treated cells.

¤ indicates a *P*-value < 0.05 between ESE-16- and vehicle-treated cells.

† indicates a *P*-value < 0.05 between ESE-15-ol- and ESE-16-treated cells.

Cell signaling

Hydrogen peroxide and superoxideformation

In order to investigate whether increased amounts of hydrogen peroxide and superoxide are produced in ESE-16-exposed(200 nM) cells compared to the control-exposed cells, flow cytometric analyses of MCF-7, MDA-MB-231 and MCF-12A cells loaded with the H_2O_2-sensitive fluorophore DCFDA and the superoxide sensitive probe hydroethidine.

No difference in hydrogen peroxide formation was observed after 6 h and 12 h exposure to ESE-16 (Figure 3.31). Hydrogen peroxide formation statistically significantly increased in ESE-16-exposed MCF-7, MDA-MB-231 and MCF-12Acells from 18 h to 24 h when compared to the vehicle-treated cells (Figure 3.31).

Superoxide formation was statistically significantly increased from 6 h and continued to increase in ESE-16-treated MDA-MB-231cells when compared to the vehicle-treated control (Figure 3.32). For MCF-7 cells superoxide formation increased from 12 h onwards in ESE-16-treated cells when compared to the vehicle-treated control (Figure 3.32). For MCF-12A cells superoxide formation increased at 18 h and 24 h in ESE-16-treated cells when compared to the vehicle-treated control (Figure 3.32). At 24 h, an increase superoxide formation was more pronounced in ESE-16-treated MDA-MB-231 cells when compared to MCF-7 and MCF-12A cells treated with ESE-16 (Figure 3.32).

The data therefore suggest that ESE-16 is able to induce cellular changes that result on the increased formation of both hydrogen peroxide and superoxide.

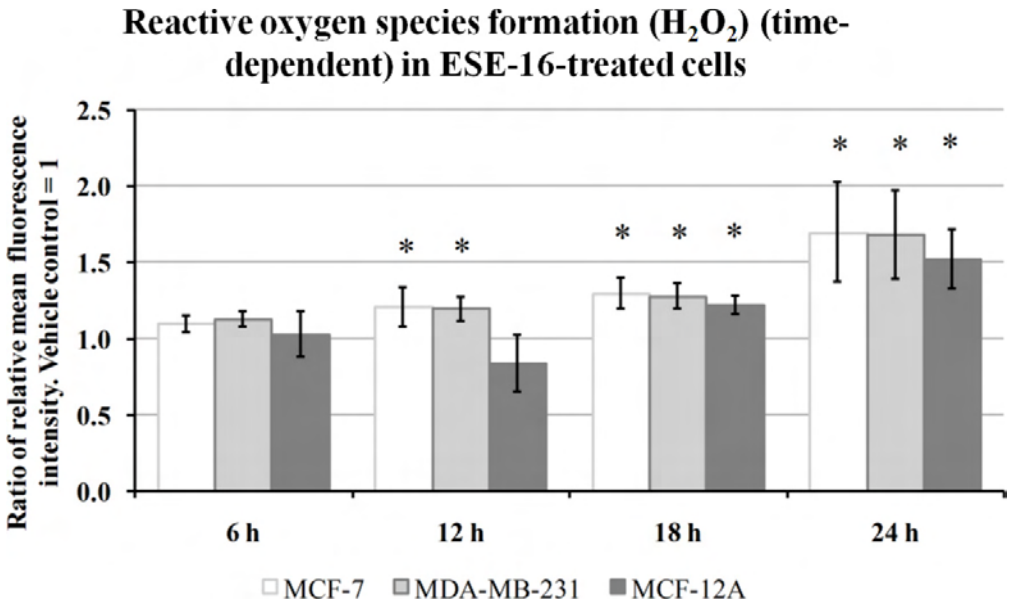

Figure 3.31: Relative mean fluorescence intensity of DCF in cells exposed to ESE-16 (200 nM) (FLG1).
* indicates a *P*-value < 0.05 between ESE-16- and vehicle-treated cells

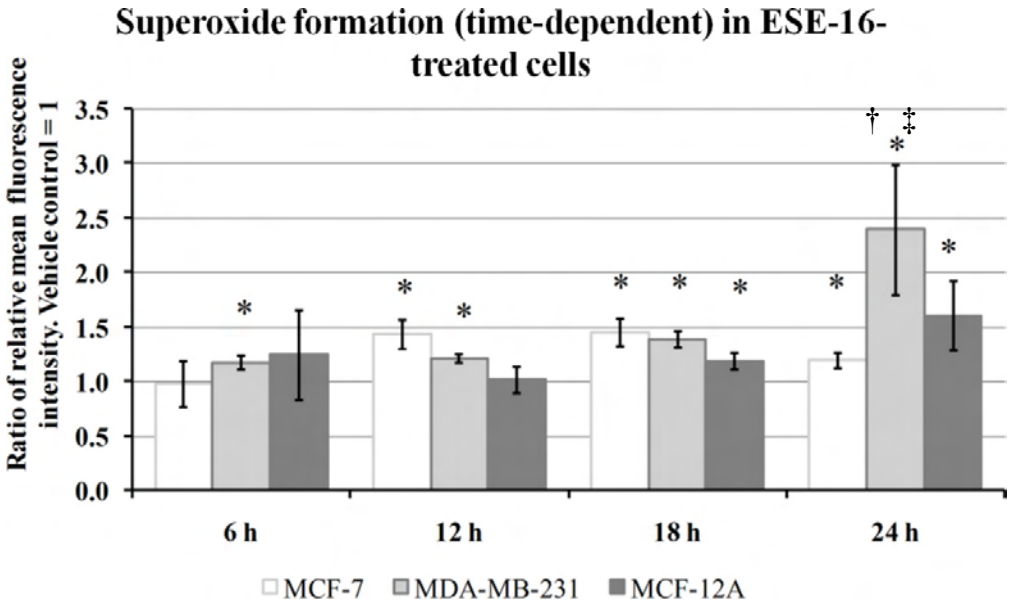

Figure 3.32:Relative mean fluorescence intensity of hydroethidinein cells exposed to ESE-16 (200 nM) (FLG3).

* indicates a *P*-value < 0.05 between ESE-16- and vehicle-treated cells

† indicates a *P*-value < 0.05 between compound MCF-7 and MDA-MB-231 cells

‡ indicates a *P*-value < 0.05 between compound MDA-MB-231 andMCF-12A cells

Apoptosis induction

Translocation of the membrane PS from the inner to the outer leaflet of the plasma membrane is normally one of the earliest indications of apoptosis. Annexin V is a 35-36 kDa, Ca^{2+}-dependent, phospholipid binding protein with a high affinity for PS. A fluorescein isothiocyanate conjugated Annexin V was used to measure the translocation PS from the inner membrane to the outer membrane as an indication of apoptosis in ESE-16-treated (200 nM) MCF-7, MCF-12A and MDA-MB-231 cells.

A gradual increase in PS externalization was observed in ESE-16-treated MCF-7 and MDA-MB-231 cells (Figure 3.33). Also, a statistically significant increase in PS externalization was observed from 6 h onwards in ESE-16-treated MCF-7 and MDA-MB-231 cells when compared to the vehicle-treated control (Figure 3.33). For MCF-12A cells, PS externalization was statistically significantly more after 48 h exposure to ESE-16 when compared to the vehicle-treated control (Figure 3.33). After 24 h and 48 h exposure to ESE-16, PS externalization was statistically significantly more in MCF-7 and MDA-MB-231 cells when compared to MCF-12A cells (Figure 3.33). These results indicate that ESE-16 is able to induce apoptosis in all the tested cell lines and that it is more pronounced in MCF-7 and MDA-MB-231 cells.

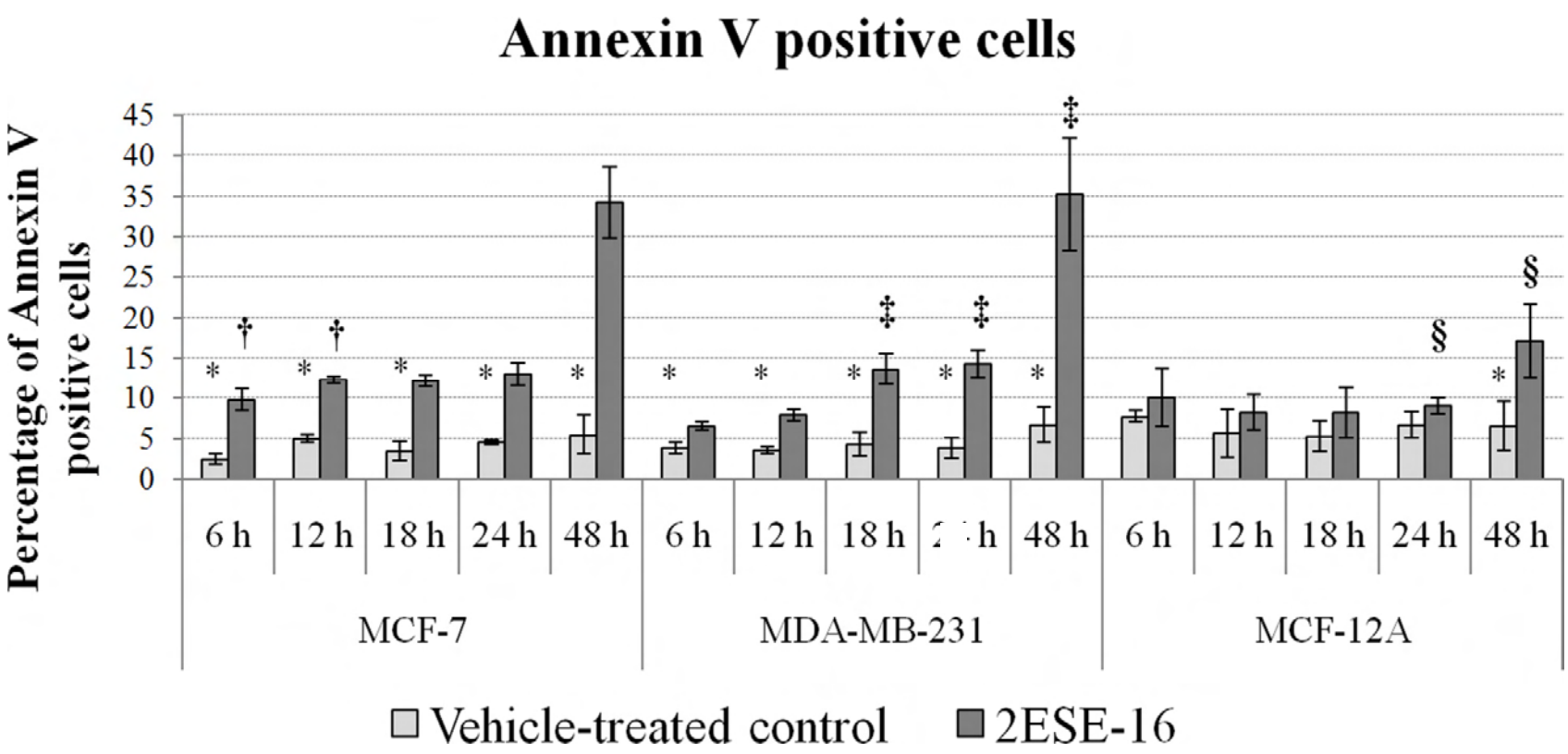

Figure 3.33: Measurement of phosphatidylserine externalization in MCF-7, MDA-MB-231 and MCF-12A cells.

*indicates a *P*-value < 0.05 between vehicle-treated cells and ESE-16-treated cells

†indicates a *P*-value < 0.05 between MCF-7 and MDA-MB-231 cells exposed to 200 nM of ESE-16.

‡ indicates a *P*-value < 0.05 between MDA-MB-231 and MCF-12A cells exposed to 200 nM of ESE-16.

§indicates a *P*-value < 0.05 between MCF-12A and MCF-7 cells exposed to 200 nM of ESE-16.

Mitochondrial membrane potential alterations

Mitochondrial membrane potential was analyzed using MitoCapture™ via flow cytometry. In apoptotic cells the reagent cannot aggregate in the mitochondria due to the altered membrane potential, and remains monomeric and in the cytoplasm generating a green fluorescence(212).MCF-7, MDA-MB-231 and MCF-12A cells were exposed to 50 nM of ESE-15-ol and tested for any changes in mitochondrial membrane potential.

In ESE-15-ol-treated cells, there was a statistically significant increase of green fluorescence across all the cell lines after 24 h exposure (Figure 6). This suggests that apoptosis is one possible form of cell death being induced by ESE-15-ol and reinforces the data from the Annexin V study.

Increased reactive species formation is able to induce the activation of mitogen-activated protein kinase 14 (p38α) and JNK which in turn play a role in inducing apoptosis as well as mitochondrial membrane depolarization (97). The effects of inhibiting the p38α and JNK1/2/3 kinases in inducing mitochondrial membrane were investigated in ESE-16-treated cells. SB239063 (15 µM) and SP600125 (25µM) were used to inhibit the p38α and JNK1/2/3 kinases respectively by incubating them with ESE-16 for 24 h. When treating MCF-7, MDA-MB-231 and MCF-12A cells with only the inhibitors, no apparent differences in mitochondrial membrane potential was observed when compared to the vehicle-treated controls (Figure 3.35). In ESE-16-treated (200 nM) cells, there was a statistically significant increase in green fluorescence across all the cell lines after 24 h exposure, thereby indicating that mitochondrial membrane depolarization was induced in ESE-16-treated cells (Figure 3.35). The JNK inhibitor had no effect in inhibiting or increasing this effect in MDA-MB-231 cells and MCF-12A cells. In MCF-7 cells, however, the JNK inhibitor was able to reduce mitochondrial membrane depolarization in MCF-7 cells treated with ESE-16 (Figure 3.35).

The p38α inhibitor had no effect in inhibiting or inducing mitochondrial membrane depolarization in MCF-7 cells (Figure 3.35). However, the p38α inhibitor was able to

reducemitochondrial membrane depolarization in MDA-MB-231 cells and MCF-12A cells treated with ESE-16 (Figure 3.35). While the respective inhibitors where unable to completely ablate the effects of ESE-16 on mitochondrial membrane potential, the data does suggest that JNK and p38α proteins play different roles in MCF-7, MDA-MB-231 and MCF-12A in inducing mitochondrial membrane depolarization in response to ESE-16 exposure.

Time-dependent studies on mitochondrial membranes were also carried out from 6 h to 48 h in MCF-7, MDA-MB-231 and MCF-12A cells exposed to ESE-16 (Figure 3.36). A gradual increase in mitochondrial membrane depolarization was observed in ESE-16-treated cells when compared to the vehicle-treated control (Figure 3.36). The effect was statistically significant after 18 h in all cell lines. After 24 h and 48 h, the effect was more pronounced in the MCF-7 and MDA-MB-231 cells when compared to the MCF-12A cells (Figure 3.36).

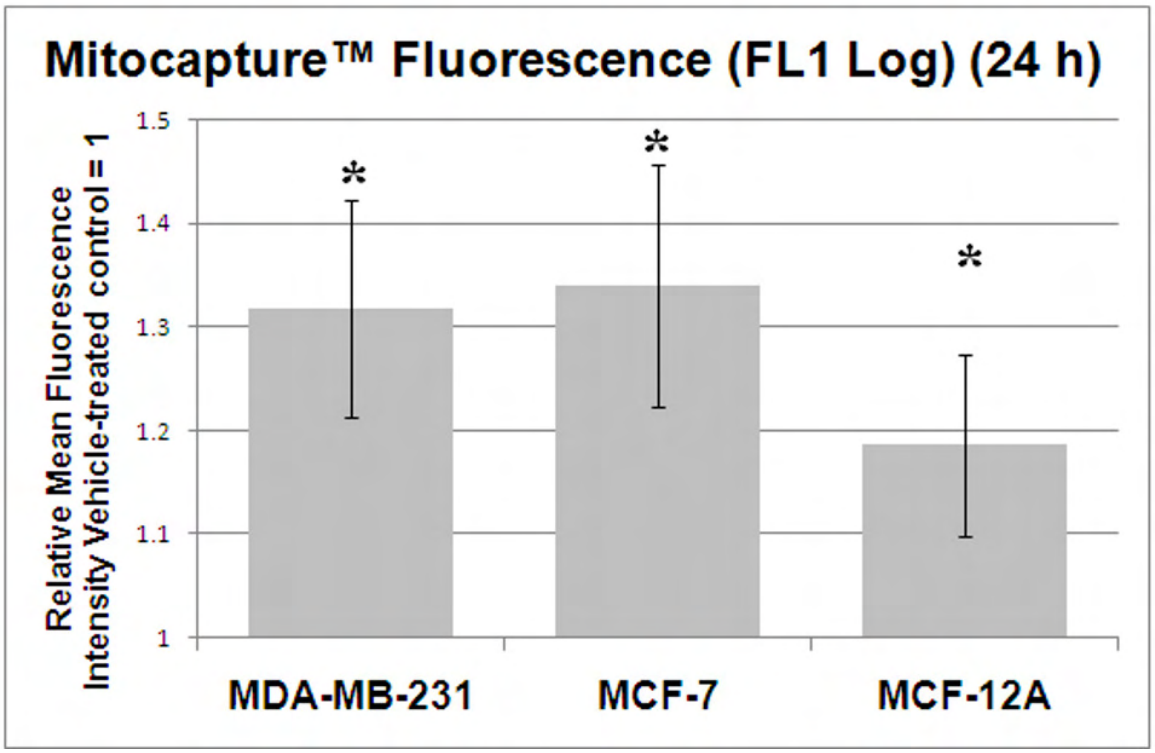

Figure 3.34: Relative fluorescence intensity for Mitocapture™(FL1 log) for ESE-15-ol-treated cells after 24 h exposure. An increase in FL1 log indicates an increase in mitochondrial membrane depolarization and potential apoptosis. A statistically significant increase in mitochondrial membrane depolarization in the ESE-15-ol-treated cells compared to the vehicle-treated cells was observed across all three cell lines.

*indicates a *P*-value < 0.05 between vehicle-treated cells and ESE-16-treated cells

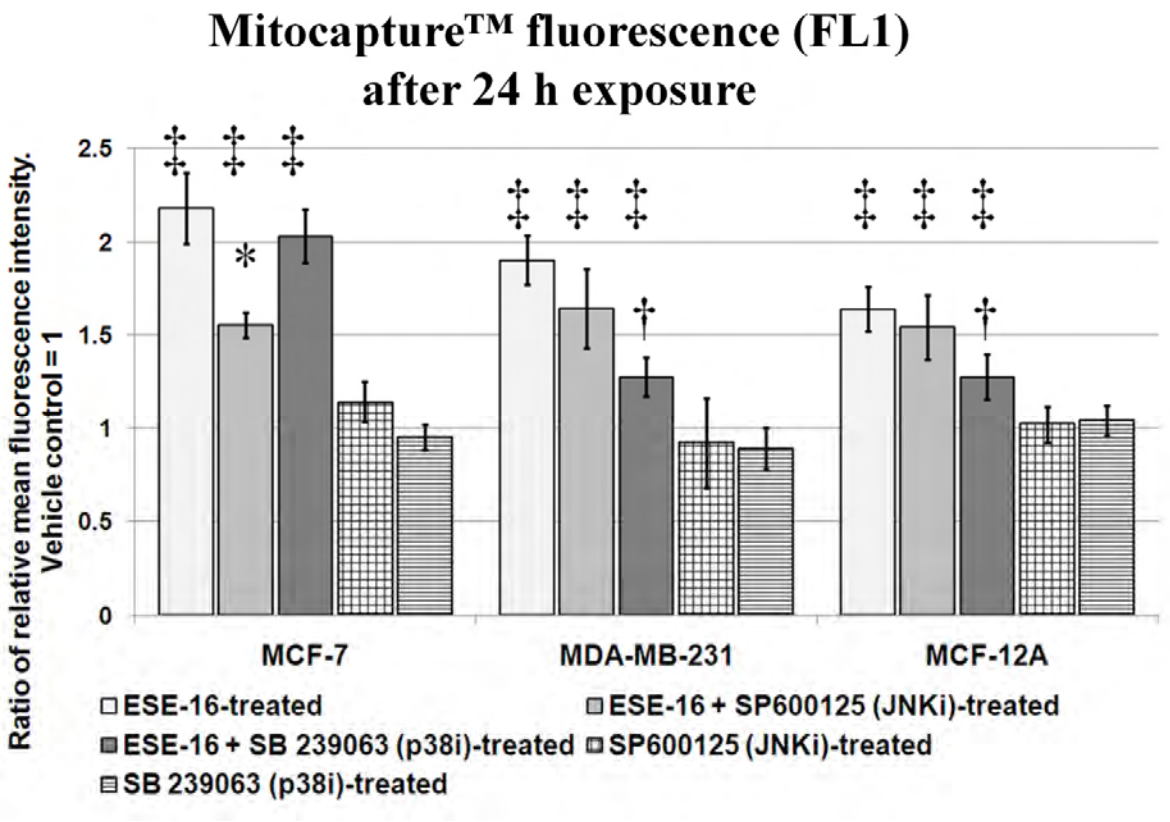

Figure 3.35: Relative fluorescence intensity for Mitocapture™(FL1 log) for ESE-16-treated cells after 24 h exposure.

*indicates a *P*-value < 0.05 between ESE-16-treated cells and cells treated with ESE-16 and the JNK inhibitor

†indicates a *P*-value < 0.05 between ESE-16-treated cells and cells treated with ESE-16 and the p38α inhibitor

‡ indicates a *P*-value < 0.05 between treated cells and untreated (vehicle-tread) cells

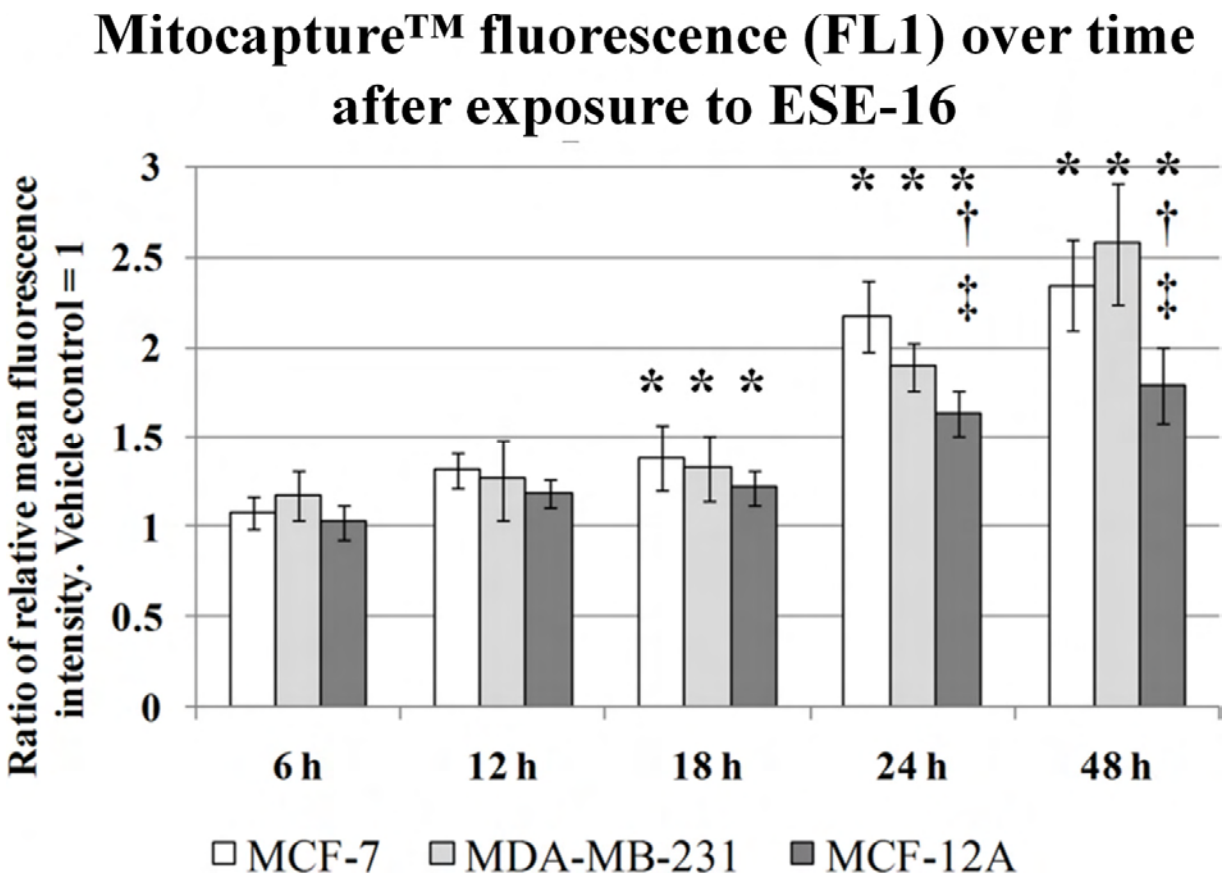

Figure 3.36: Comparison of differences in mitochondrial membrane depolarization in MCF-7, MDA-MB-231 and MCF-12A cells exposed to ESE-16 over time (6 h – 48 h).

*indicates a *P*-value < 0.05 between vehicle-treated cells and ESE-16-treated cells

†indicates a *P*-value < 0.05 between MCF-7 and MCF-12A cells exposed to 200 nM of ESE-16.

‡ indicates a *P*-value < 0.05 between MDA-MB-231 and MCF-12A cells exposed to 200 nM of ESE-16.

Autophagic activity

By staining cells with FITC-conjugated microtubule-associated proteins 1A/1B light chain 3B membrane protein (LC3) antibodywe were able to quantify the intracellular expression of LC3. LC3 expression and serves an index of autophagosome formation and thus autphagic activity (145). Tamoxifen (2.5 µM) was used as a positive control for autophagy induction in breast cancer cells (279). ESE-16-treated (200 nM) MCF-7, MDA-MB-231 and MCF-12A cells after 24 exposure did show statistically significant increases in LC3 expression when compared to the vehicle-treated control (Figure 3.37). This suggests that autophagic induction is increased due to ESE-16 and appears to support the results from TEM microscopy.

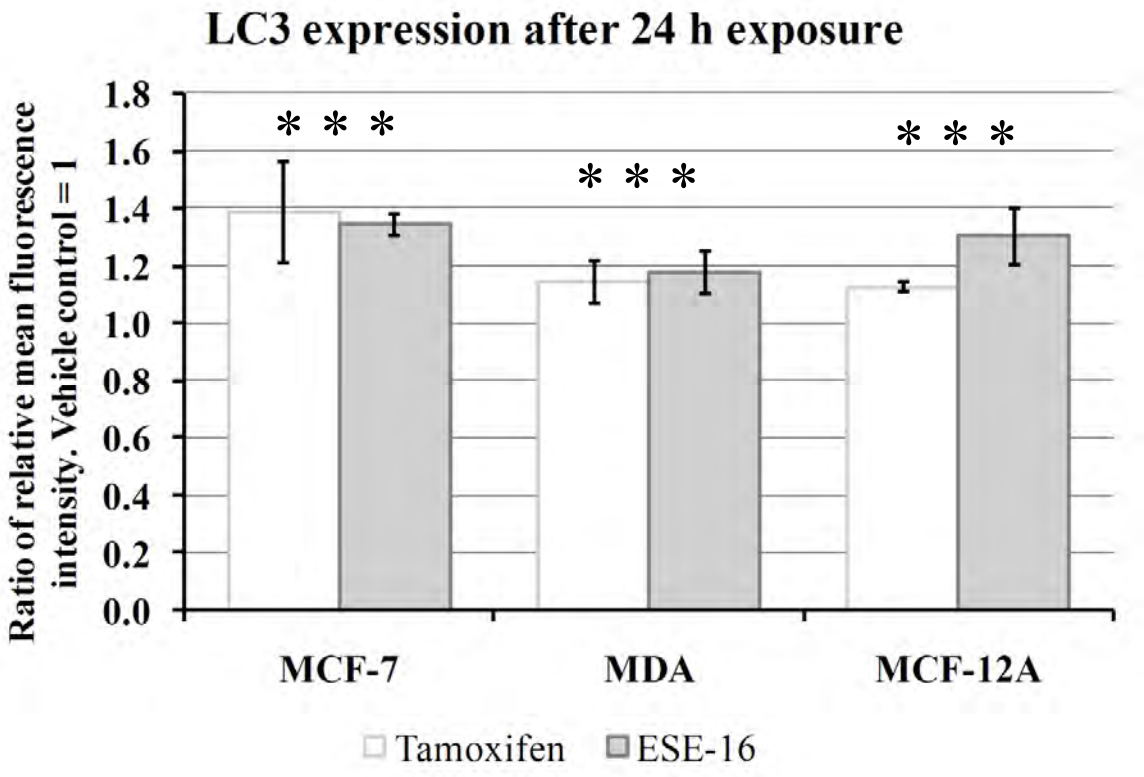

Figure 3.37: LC-3 expression in MCF-7, MDA-MB-231 and MCF-12A cells after 24 exposure.

*indicates a *P*-value < 0.05 between vehicle-treated cells and Tamoxifen- or ESE-16-treated cells

Gene expression analysis

Complimentary RNA microarray

Agilent's Human 1A Oligonucleotide Microarray was employed to collect information about gene expression changes associated with ESE-15-one-, ESE-15-ol- and ESE-16-treated cells. MDA-MB-231 cells were exposed to ESE-15-one (140nM), ESE-15-ol (50 nM) and ESE-16 (200 nM) for 24 h. MCF-7 and MCF-12A cells were exposed to 200 nM of ESE-16for 24 h. Global LOESS normalized MA-plots using the fitted M-values after normalization are represented by Figure 3.38.

For ESE-16-treated cells, 1414, 1295 and 1136 genes were considered to be statistically significantly differentially expressed in MCF-7,MDA-MB-231 and MCF-12A ell respectively. 509 gene were considered to be significantly differentially expressed in ESE-15-one-treated MDA-MB-231 cells and 369 genes were considered significantly differentially expressed in ESE-15-ol-treated MDA-MB-231 cells (Figure 3.39).

180 genes were differentially expressed in MCF-7, MDA-MB-231 and MCF-12A cells exposed to ESE-16 (Figure 3.39 A). Of these genes, 68 were differentially expressed in MDA-MB-231 exposed to ESE-15-one and ESE-15-ol (Figure 3.39 B, Table 3.18). 179 genes were differentially expressed in MDA-MB-231 cells exposed to ESE-15-one, ESE-15-ol and ESE-16 (Figure 3.39 C).

Genes that were considered statistically significantly differentially expressed (adjusted P-value < 0.05) in treated cells were mapped to genes associated with cell growth, apoptosis, autophagy, cell cycle and DNA repair, oxidative stress, phosphatases, kinases, epigenetics-related and chromatin modifications, structural, regulation of transcription and translation, Ras-related, extracellular matrix and heat-shock protein related (

Table 3.19).

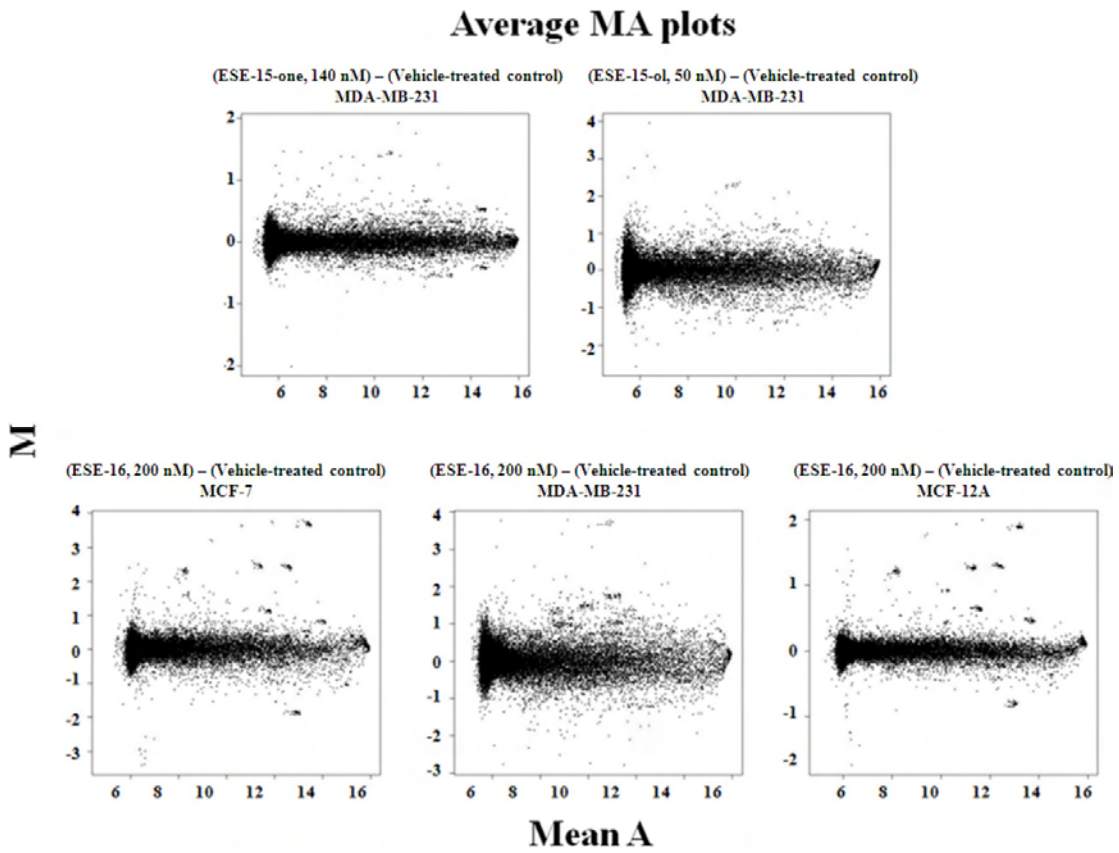

Figure 3.38: M/A plots of Loess normalized data.

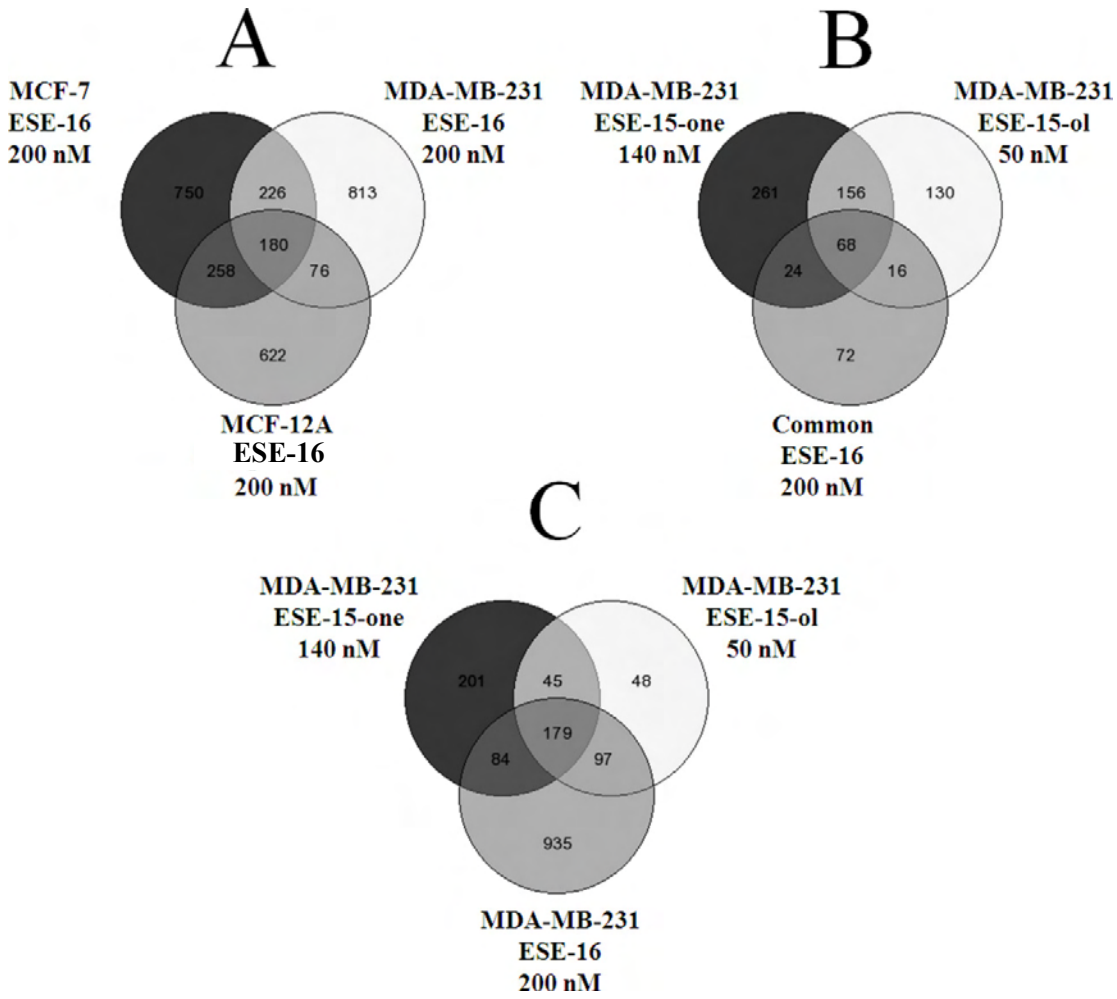

Figure 3.39: GeneVenn diagram showing common genes affected in MCF-7, MDA-MB-231 and MCF12A cells.

Table 3.18: Common differentially expressed genes in MCF-7, MDA-MB-231 and MCF12A cells exposed to ESE-15-one (140 nM), ESE-15-ol (50 nM), and ESE-16 (200 nM) for 24 h.

Refseq RNA	Gene name	Description	log M (Diff expressed)				
			ESE-15-one	ESE-15-ol	ESE-16	ESE-16	ESE-16
			MDA-MB-231 140 nM	MDA-MB-231 50 nM	MCF-7 200 nM	MDA-MB-231 200 nM	MCF-12A 200 nM
Cell growth, apoptosis, autophagy							
NM_014417	BBC3/PUMA	BCL2 binding component 3	1.68	1.54	1.66	1.7	1.81
NM_001731	BTG1	B-cell translocation gene 1 anti-proliferative	1.01	1.27	1.32	0.78	0.45
NM_004417	DUSP1	Dual specificity phosphatase 1	1.16	1.29	1.97	2.05	1.33
NM_033285	TP53INP1	Tumor protein p53 inducible nuclear protein 1	1.16	0.74	1.18	0.74	0.99
NM_145008	YPEL4	Yippee-like 4	1.71	1.71	1.5	2.27	1.12
AF100640	MB2	Metastasis related protein	3.61	2.08	0.98	3.68	1.65
NM_006533	MIA	Melanoma inhibitory activity	0.94	0.97	0.43	0.66	0.62
NM_201444	DGKA	Diacylglycerol kinase alpha 80kda	0.66	0.77	0.67	0.52	0.44
NM_001002914	KCTD11	Potassium channel tetramerisation domain containing 11	0.55	0.72	0.64	0.70	0.40
Cell cycle and DNA repair							
NM_001007793	BUB3	Budding uninhibited by benzimidazoles 3 homolog	-1.01	-1.27	-1.32	-0.78	-0.45
NM_001786	CDC2	Cell division cycle 2 G1 to S and G2 to M	-1.30	-1.43	-0.91	-1.24	-0.84
NM_030928	CDT1	Chromatin licensing and DNA replication factor 1	-0.88	-0.88	-0.52	-0.96	-0.56
NM_005573	LMNB1	Lamin B1	-0.88	-1.6	-0.98	-1.64	-1.02
NM_006739	MCM5	MCM5 minichromosome maintenance deficient 5 cell division cycle 46	-0.86	-0.77	-0.57	-0.89	-0.55
NM_004153	ORC1L	Origin recognition complex subunit 1-like	-1.45	-0.91	-0.86	-1.23	-0.99
NM_002592	PCNA	Proliferating cell nuclear antigen	-1.11	-1.05	-0.51	-1.1	-0.51
NM_006622	PLK2	Polo-like kinase 2	0.95	0.96	0.96	1.23	0.99
NM_020675	SPBC25	Spindle pole body component 25 homolog	-0.92	-1.09	-0.75	-0.69	-0.55
NM_006879	MDM2	Mdm2 transformed 3T3 cell double minute	1.77	1.53	1.23	1.85	1.13
CLTCL1	RIIAD1	Clathrin, heavy chain-like 1	0.79	0.84	0.63	0.86	0.61
Oxidative stress related							

NM_002133	HMOX1	Heme oxygenase 1	0.59	0.74	0.77	1.15	0.95
NM_175839	SMOX	Spermine oxidase	0.63	0.82	0.34	0.91	0.29
Epigenetics-related and chromatin modifications							
NM_001379	DNMT1	DNA methyl transferase 1	-0.8	-0.58	-0.45	-0.58	-0.64
NM_003642	HAT1	Histone acetyltransferase 1	-0.68	-0.88	-0.4	-1.12	-0.36
BQ683489	HIST1H2BD	Histone cluster 1 h2bd	-0.86	-1.3	-1.29	-1.98	-0.59
NM_003537	HIST1H3B	Histone cluster 1 H3b	-0.86	-1.39	-1.19	-1.56	-0.97
NM_003534	HIST1H3G	Histone cluster 1 H3g	-0.85	-1.3	-0.67	-1.61	-0.48
NM_175065	HIST2H2AB	Histone cluster 2 h2ab	-0.79	-0.78	-0.37	-1.02	-0.45
NM_003517	HIST2H2AC	Histone cluster 2 h2ac	-1.06	-1.47	-1.62	-1.68	-0.94
NM_001025303	HIST2H3PS2	Histone cluster 2 H3 pseudogene 2	-1.01	-1.44	-0.95	-1.78	-0.59
DB010344	HIST3H2BB	Histone cluster 3 h2bb	-0.82	-1.35	-1.57	-2.16	-0.75
Structural							
XR_018167	LOC647690	Tubulin, alpha 1	-0.77	-0.57	-1.10	-0.61	-1.03
NM_006306	SMC1A	Structural maintenance of chromosomes 1A	-0.90	-0.99	-0.66	-0.65	-0.60
NM_079836	TUBA2	Tubulin, alpha 2 (TUBA2), transcript variant 2	-0.66	-0.57	-1.11	-0.56	-1.11
NM_006088	TUBB2C	Tubulin beta 2C	-1.07	-0.78	-1.32	-0.80	-1.09
ENST00000355609	IFFO2	Intermediate filament family orphan 2	0.82	0.97	0.94	0.93	0.57
Regulation of Transcription							
NM_002128	HMGB1	High-mobility group box 1	-0.55	-0.68	-0.67	-0.7	-0.75
NM_000600	IL6	Interleukin 6	2.44	2.34	1.68	3.66	1.93
NM_016269	LEF1	Lymphoid enhancer-binding factor 1	0.72	0.57	0.66	0.93	0.54
NM_003168	SUPT4H1	Suppressor of Ty 4 homolog 1	0.98	0.99	0.81	0.94	0.83
NM_003246	THBS1	Thrombospondin 1	0.53	1.02	0.47	1.14	0.5
X66087	MYBL1	V-Myb myeloblastosis viral oncogene homolog (avian)-like 1	-1.13	-0.97	-0.7	-1.03	-0.94
NM_172164	NASP	Nuclear autoantigenic sperm protein	-0.81	-0.75	-0.46	-0.64	-0.44
NM_021005	NR2F2	Nuclear receptor subfamily 2 group F member 2	-0.67	-0.97	-0.91	-1.33	-0.77
NM_006191	PA2G4	Proliferation-associated 2G4 38kda	-0.72	-0.7	-0.53	-0.6	-0.54
NM_153695	ZNF367	Zinc finger protein 367	-0.88	-1.29	-0.83	-1.12	-0.72
BC011243	ZNF587	Zinc finger protein 587	-1.01	-0.95	-0.62	-0.84	-0.53
NM_006509	RELB	v-Rel reticuloendotheliosis viral oncogene homolog B	0.79	0.68	0.77	1.06	0.74

Metabolism							
AF132203	AF132203	Stearoyl-coa desaturase (delta-9-desaturase)	-0.97	-1.69	-0.74	-2.22	-0.87
NR_003262	FDPSL2A	Farnesyl diphosphate synthase-like 2	-1.13	-1.08	-0.49	-1.14	-0.67
XR_018717	FDPSL4	Farnesyl diphosphate synthetase-like 4	-1.05	-1.14	-0.49	-1.38	-0.74
NM_001386	DPYSL2	Dihydropyrimidinase-like 2	-0.71	-0.69	-0.92	-0.70	-1.25
NM_017712	PGPEP1	Pyroglutamyl-peptidase I	0.64	0.69	0.49	0.83	0.54
NM_006623	PHGDH	Phosphoglycerate dehydrogenase	-0.83	-0.83	-0.70	-0.84	-0.51
NM_014298	QPRT	Quinolinate phosphoribosyltransferase	-1.05	-0.95	-0.54	-1.25	-0.49
NM_001034	RRM2	Ribonucleotide reductase M2 polypeptide	-1.13	-0.91	-0.52	-0.94	-0.58
NM_001025390	AMPD3	Adenosine monophosphate deaminase, transcript variant 3	0.91	1.20	1.35	1.51	0.44
NM_019885	CYP26B1	Cytochrome P450, family 26, subfamily B, polypeptide 1	0.78	1.02	1.06	1.58	1.78
NM_002130	HMGCS1	3-Hydroxy-3-methylglutaryl-Coenzyme A synthase 1	-1.54	-1.57	-0.97	-1.95	-0.96
Transmembrane							
NM_153342	TMEM150	Transmembrane protein 150	0.83	1.19	0.59	1.32	0.98
NM_001040455	SIDT2	SID1 transmembrane family, member 2	0.98	1.13	0.80	1.40	0.42
NM_005780	LHFP	Lipoma HMGIC fusion partner	0.72	0.82	0.59	1.20	0.64
Extracellular matrix							
NM_003255	TIMP2	TIMP metallopeptidase inhibitor 2	1.05	1.16	1.38	1.18	0.40
Other							
AB014766	DERP12	Dermal papilla derived protein 12	2.39	1.58	1.37	3.76	1.42
AK055372	LINC00461	Long intergenic non-protein coding RNA 461	-0.93	-0.80	-0.53	-0.97	-0.41
NM_147129	ALS2CL	ALS2 C-terminal like	0.74	0.77	0.54	0.37	0.82
XR_019062	LOC643513	Importin alpha-2 subunit	-1.08	-0.93	-0.87	-1.02	-0.77
NM_022978	SERF1B	Small EDRK-rich factor 1B (centromeric)	1.07	0.87	0.64	0.95	0.65
NM_013282	UHRF1	Ubiquitin-like containing PHD and RING finger domains 1	-1.11	-1.39	-0.99	-1.59	-1.06

Table 3.19: Differentially expressed genes mapped to functional cellular pathways in MCF-7, MDA-MB-231 and MCF12A cells exposed to ESE-15-one (140 nM), ESE-15-ol (50 nM), and ESE-16 (200 nM) for 24 h.

Refseq RNA	Gene name	Description	log M (Diff expressed)				
			ESE-15-one	ESE-15-ol	ESE-16	ESE-16	ESE-16
			MDA-MB-231 140 nM	MDA-MB-231 50 nM	MCF-7 200 nM	MDA-MB-231 200 nM	MCF-12A 200 nM
Cell growth, apoptosis, autophagy							
AF100640	AF100640	Metastasis related protein	3.60	2.06	0.98		1.65
NM_147129	ALS2CL	ALS2 C-terminal like	0.74	0.77	0.54	0.82	0.37
NM_138764	BAX	BCL2-associated X protein transcript variant epsilon					0.49
NM_014417	BBC3/PUMA	BCL2 binding component 3	1.68	1.54	1.66	1.70	1.81
NM_138621	BCL2L11	BCL2-like 11				0.61	
NM_015367	BCL2L13	BCL2-like 13 nuclear gene encoding mitochondrial protein					0.42
NM_020993	BCL7A	B-cell CLL/lymphoma 7A transcript variant 1					-0.41
NM_007295	BRCA1	Breast cancer 1	-0.82	-0.76	-0.50		
NM_001018055	BRCC3	BRCA1/BRCA2-containing complex subunit 3 transcript variant 2			-0.50		-0.41
NM_001731	BTG1	B-cell translocation gene 1 anti-proliferative	1.01	1.27	1.32	0.78	0.45
NM_170589	CASC5	Cancer susceptibility candidate 5	-0.88				-0.52
NM_001814	CTSC	Cathepsin C	0.99	1.08			
NM_004083	DDIT3	DNA-damage-inducible transcript 3	0.74		0.50	1.44	0.58
NM_001343	DAB2	Disabled homolog 2 mitogen-responsive phosphoprotein			0.78		0.59
NM_004093	EFNB2	Ephrin-B2	0.80	1.07		0.87	
NM_004438	EPHA4	EPH receptor A4			0.87	0.81	0.46
NM_004440	EPHA7	EPH receptor A7			-0.51	-0.79	-0.48
NM_001924	GADD45A	Growth arrest and DNA-damage-inducible alpha			0.41	0.66	
NM_201612	IKIP	IKK interacting protein transcript variant 2	0.53		0.68	0.61	0.41
NR_002819	MALAT1	Metastasis associated lung adenocarcinoma transcript 1	1.19		0.65		
NM_006879	MDM2	Mdm2 transformed 3T3 cell double minute 2	1.77	1.53	1.23	1.85	1.13
NM_006533	MIA	Melanoma inhibitory activity	0.94	0.97	0.43	0.66	0.62

CR613982	MIA3	Melanoma inhibitory activity protein 3			0.43		
NM_004739	MTA2	Metastasis associated 1 family member 2					-0.52
NM_001077493	NFKB2	Nuclear factor of kappa light polypeptide gene enhancer in B-cells 2				0.55	
NM_020529	NFKBIA/IκBα	Nuclear factor of kappa light polypeptide gene enhancer in B-cells inhibitor alpha	1.36		0.96	1.27	0.74
NM_001031689	PLAA	Phospholipase A2-activating protein					-0.40
NM_000314	PTEN	Phosphatase and tensin homolog				0.72	
NM_006509	RELB	v-Rel reticuloendotheliosis viral oncogene homolog B	0.79	0.68	0.77	1.06	0.74
NM_152756	RICTOR	Rapamycin-insensitive companion of mTOR				-1.04	
NM_003942	RPS6KA4	Ribosomal protein S6 kinase 90kDa polypeptide 4			-0.38	-0.39	-0.64
U46752	SQSTM1	Human phosphotyrosine independent ligand	0.77	0.76	0.98	0.52	
ENST00000366930	TGFB2	Transforming growth factor beta-2 precursor TGF-beta-2					0.42
NM_001024847	TGFBR2	Transforming growth factor beta receptor II			0.87		0.56
NM_014452	TNFRSF21	Tumor necrosis factor receptor superfamily member 21			0.50		
NM_033285	TP53INP1	Tumor protein p53 inducible nuclear protein 1	1.16	0.74	1.18	0.74	0.99
NM_016058	TPRKB	TP53RK binding protein				-0.54	
NM_003295	TPT1	Tumor protein translationally-controlled 1			0.42		0.40
NM_021643	TRIB2	Tribbles homolog 2	0.80	0.68		0.79	
NM_000548	TSC2	Tuberous sclerosis 2	0.61	0.74	0.45	0.60	
NM_001025366	VEGFA	Vascular endothelial growth factor Atranscript variant 1			0.35		0.38
NM_001025370	VEGFA	Vascular endothelial growth factor A transcript variant 6			-0.38		
NM_003377	VEGFB	Vascular endothelial growth factor B					-0.47
NM_031477	YPEL3	Yippee-like 3	0.79		0.61		
NM_145008	YPEL4	Yippee-like 4	1.71	1.71	1.50	2.27	1.12
Cell cycle and DNA repair							
NM_004336	BUB1	BUB1 budding uninhibited by benzimidazoles 1 homolog	-1.03				-0.75
NM_001211	BUB1B	BUB1 budding uninhibited by benzimidazoles 1 homolog beta	-0.75	-0.95		-0.53	
NM_001237	CCNA2	Cyclin A2	-0.91	-1.00		-0.69	
NM_031966	CCNB1	Cyclin B1	-0.69	-1.17			
NM_004701	CCNB2	Cyclin B2	-1.11	-1.07		-0.66	
NM_053056	CCND1	Cyclin D1	-0.88		-0.38		

NM_003858	CCNK	Cyclin K		-0.89	-0.47	-1.02	
NM_020307	CCNL1	Cyclin L1					0.39
NM_020739	CCPG1	Cell cycle progression 1					-0.54
NM_001786	CDC2	Cell division cycle 2 G1 to S and G2 to M	-1.3	-1.45	-0.91	-1.24	-0.84
NM_001255	CDC20	Cell division cycle 20 homolog	-0.72	-0.99		-0.5	
NM_033487	CDC2L1	Cell division cycle 2-like 1			-0.69	-0.82	
NM_003718	CDC2L5	Cell division cycle 2-like 5				-0.54	
NM_044472	CDC42	Cell division cycle 42 transcript variant 2					0.39
NM_005851	CDK2AP2	CDK2-associated protein 2					-0.43
NM_001261	CDK9	Cyclin-dependent kinase 9				0.83	
NM_001800	CDKN2D	Cyclin-dependent kinase inhibitor 2D	-0.82				
NM_030928	CDT1	Chromatin licensing and DNA replication factor 1	-0.88	-0.88	-0.52	-0.96	-0.56
NM_001810	CENPB	Centromere protein B 80kda					-0.52
NM_001813	CENPE	Centromere protein E 312kda	-1.03	-0.63			
NM_018451	CENPJ	Centromere protein J	-0.88	-0.66	-0.5		
NM_033319	CENPL	Centromere protein L	-0.95	-0.72			-0.36
NM_018455	CENPN	Centromere protein N		-0.72			
NM_025082	CENPT	Centromere protein T	-0.92				
NM_018131	CEP55	Centrosomal protein 55kda		-1.09			
NM_014679	CEP57	Centrosomal protein 57kda	-0.9			-0.62	
NM_004365	CETN3	Centrin EF-hand protein 3				-0.69	
NM_001826	CKS1B	CDC28 protein kinase regulatory subunit 1B	-0.72	-1.04		-0.63	
NM_199077	CNNM2	Cyclin M2			-1.31		
NM_020184	CNNM4	Cyclin M4					
BC111740	DNA2L	DNA2 DNA replication helicase 2-like		-0.714			
NM_004947	DOCK3	Dedicator of cytokinesis 3			0.49		
NM_014705	DOCK4	Dedicator of cytokinesis 4	-0.67				
NM_012291	ESPL1	Extra spindle pole bodies homolog 1	-1.30	-0.99		-0.57	
NM_018063	HELLS	Helicase lymphoid-specific	-0.99	-0.60			-0.52
NM_005733	KIF20A	Kinesin family member 20A	-0.67			-0.50	-0.67
NM_007317	KIF22	Kinesin family member 22	-0.73	-0.77			
NM_017576	KIF27	Kinesin family member 27					-0.78

NM_007054	KIF3A	Kinesin family member 3A			-0.46		
NM_004798	KIF3B	Kinesin family member 3B			0.40		
NM_012310	KIF4A	Kinesin family member 4A	-0.95	-0.84		-0.51	
NM_002263	KIFC1	Kinesin family member C1	-0.95	-1.02		-0.75	
NM_006101	KNTC2	Kinetochore associated 2	-0.78	-0.95			-0.43
NM_005572	LMNA	Lamin A/C transcript variant 2					-0.48
NM_005573	LMNB1	Lamin B1	-0.88	-1.60	-0.98	-1.64	-1.02
NM_032737	LMNB2	Lamin B2	-0.95	-0.66			
NM_002358	MAD2L1	MAD2 mitotic arrest deficient-like 1	-0.87	-1.05		-0.59	-0.48
NM_006341	MAD2L2	MAD2 mitotic arrest deficient-like 2	-0.91		-0.38		-0.41
NM_006739	MCM5	MCM5 minichromosome maintenance deficient 5 cell division cycle 46	-0.86	-0.77	-0.57	-0.89	-0.55
NM_198175	NME1	Non-metastatic cells 1 protein transcript variant 1			0.37		0.37
NM_145697	NUF2	NUF2 NDC80 kinetochore complex component homolog	-0.73	-1.20		-0.84	
NM_016359	NUSAP1	Nucleolar and spindle associated protein 1	-0.98	-0.87	-0.53		-0.71
NM_004153	ORC1L	Origin recognition complex subunit 1-like	-1.45	-0.91	-0.86	-1.23	-0.99
NM_002553	ORC5L	Origin recognition complex subunit 5-like	-0.91				-0.40
NM_002577	PAK2	p21 -activated kinase 2			-0.51	-0.78	
NM_002592	PCNA	Proliferating cell nuclear antigen	-1.11	-1.05	-0.51	-1.10	-0.51
NM_002648	PIM1	Pim-1 oncogene					0.87
NM_005030	PLK1	Polo-like kinase 1		-0.93			
NM_006622	PLK2	Polo-like kinase 2	0.95	0.96	0.96	1.23	0.99
NM_014264	PLK4	Polo-like kinase 4	-0.91	-0.70			
NM_005053	RAD23A	RAD23 homolog A					-0.47
NM_002874	RAD23B	RAD23 homolog B			-0.51	-0.77	
NM_005732	RAD50	RAD50 homolog	-0.62		-0.50		-0.58
NM_012415	RAD54B	RAD54 homolog B					1.64
NM_003579	RAD54L	RAD54-like	-0.85	-0.89			
NM_001034836	RDM1	RAD52 motif 1	-0.61	-0.87		-0.66	
NM_004260	RECQL4	RECQ protein-like 4		-0.98	-0.42	-0.59	
NM_002913	RFC1	Replication factor C 1			-1.10		-0.86
NM_181471	RFC2	Replication factor C 2	-0.78			-0.54	-0.59

NM_002916	RFC4	Replication factor C 4	-0.77	-0.76		-0.62	
NM_006306	SMC1A	Structural maintenance of chromosomes 1A	-0.90	-0.99	-0.66	-0.65	-0.60
NM_001042550	SMC2	Structural maintenance of chromosomes 2	-1.22	-1.07		-0.83	-0.51
NM_005445	SMC3	Structural maintenance of chromosomes 3			-0.38		-0.57
NM_024624	SMC6	Structural maintenance of chromosomes 6					-0.47
NM_020675	SPBC25	Spindle pole body component 25 homolog	-0.92	-1.09	-0.75	-0.69	-0.55
NM_203401	STMN1	Stathmin 1/oncoprotein 18		-0.77	-0.33	-0.80	
NM_030795	STMN4	Stathmin-like 4					0.98
NM_003286	TOP1	Topoisomerase 1					-0.41
NM_007027	TOPBP1	Topoisomerase	-0.87				-0.61
Oxidative stress related							
NM_002032	FTH1	Ferritin heavy polypeptide 1			0.53	0.65	0.42
NM_002083	GPX2	Glutathione peroxidase 2			-0.49		-0.62
NM_000846	GSTA2	Glutathione S-transferase A2					0.59
NM_014685	HERPUD1	Homocysteine-inducible endoplasmic reticulum stress-inducible ubiquitin-like domain 1	0.80	0.78		1.12	
NM_002133	HMOX1	Heme oxygenase 1	0.59	0.74	0.77	1.15	0.95
NM_145791	MGST1	Microsomal glutathione S-transferase 1 transcript variant 1c	-0.76	-0.93		-0.9	
NM_000625	NOS2A	Nitric oxide synthase 2A				0.75	0.36
NM_004337	OSGIN2	Oxidative stress induced growth inhibitor family member 2				-0.5	
NM_005109	OXSR1	Oxidative-stress responsive 1			-0.47		-0.57
NM_002574	PRDX1	Peroxiredoxin 1 transcript variant 1					-0.43
NM_005809	PRDX2	Peroxiredoxin 2 nuclear gene encoding mitochondrial protein			0.44		
NM_006793	PRDX3	Peroxiredoxin 3				-1.06	
NM_002970	SAT1/SSAT	Spermidine/spermine N1-acetyltransferase 1	0.61		0.8	0.81	0.68
NM_175839	SMOX	Spermine oxidase	0.64	0.81		0.91	
NM_001024465	SOD2	Superoxide dismutase 2		0.86		1.1	
NM_006819	STIP1	Stress-induced-phosphoprotein 1	-0.52		-0.58		-0.47
NM_005783	TXNDC9	Thioredoxin domain containing 9			-0.39		
NM_004786	TXNL1	Thioredoxin-like 1			-0.37		

Phosphatases							
NM_001008392	CTDSPL	Carboxy-terminal domain small phosphatase-like protein					-0.77
NM_004417	DUSP1	Dual specificity phosphatase 1	1.16	1.29	1.97	2.05	1.33
NM_001007271	DUSP13	Dual specificity phosphatase 13				0.76	
NM_080611	DUSP15	Dual specificity phosphatase 15				0.86	
NM_004418	DUSP2	Dual specificity phosphatase 2		0.71		1.62	
NM_003713	PPAP2B	Phosphatidic acid phosphatase type 2B	0.9	0.92		1.43	
NM_177983	PPM1G	Protein phosphatase 1G magnesium-dependent gamma isoform	-0.54		-0.51		
NM_002710	PPP1CC	Protein phosphatase 1 catalytic subunit gamma isoform	-0.58	-0.61	-0.47		
NM_032105	PPP1R12B	Protein phosphatase 1 regulatory subunit 12B			0.82	0.81	
NM_033256	PPP1R14A	Protein phosphatase 1 regulatory subunit 14A			0.53		
NM_138689	PPP1R14B	Protein phosphatase 1 regulatory subunit 14B			-0.53		
NM_002720	PPP4C	Protein phosphatase 4 catalytic subunit				0.62	-0.44
NM_174907	PPP4R2	Protein phosphatase 4 regulatory subunit 2			-0.45		-0.44
NM_000314	PTEN	Phosphatase and tensin homolog				0.74	
NM_003463	PTP4A1	Protein tyrosine phosphatase type IVA			0.69	0.7	0.45
NM_080391	PTP4A2	Protein tyrosine phosphatase type IVA member 2					-0.64
NM_016395	PTPLAD1	Protein tyrosine phosphatase-like A domain containing 1			-0.39		
NM_080685	PTPN13	Protein tyrosine phosphatase non-receptor type 13				0.69	
NM_005401	PTPN14	Protein tyrosine phosphatase non-receptor type 14			-0.92		-0.82
NM_002829	PTPN3	Protein tyrosine phosphatase non-receptor type 3			0.45		
NM_002830	PTPN4	Protein tyrosine phosphatase non-receptor type 4					-0.42
NM_006504	PTPRE	Protein tyrosine phosphatase receptor type E			0.56		-0.5
NM_002840	PTPRF	Protein tyrosine phosphatase receptor type F	0.6			0.94	0.63
NM_002843	PTPRJ	Protein tyrosine phosphatase receptor type J		0.99		0.9	
NM_002844	PTPRK	Protein tyrosine phosphatase receptor type K				1.3	
NM_002845	PTPRM	Protein tyrosine phosphatase receptor type M			2.35		
NM_030791	SGPP1	Sphingosine-1-phosphate phosphatase 1				-0.92	-0.51
Kinases							
NM_152221	CSNK1E	Casein kinase 1 epsilon			-0.97		-0.63

NM_201444	DGKA	Diacylglycerol kinase alpha 80kda	0.66	0.77	0.67	0.52	0.44
NM_003646	DGKZ	Diacylglycerol kinase zeta 104kda				-0.49	-0.45
NM_001004023	DYRK3	dual-specificity tyrosine--phosphorylation regulated kinase 3				0.79	0.43
NM_002031	FRK	Fyn-related kinase	0.98	1.15	0.72	1.57	
NM_001005910	IHPK2	Inositol hexaphosphate kinase 2		0.79	0.35		
NM_002227	JAK1	Janus kinase 1			-0.97		-1.05
NM_145109	MAP2K3	Mitogen-activated protein kinase kinase 3				0.57	
NM_002758	MAP2K6	Mitogen-activated protein kinase kinase 6					-0.64
ENST00000264777	MAP3K1	Mitogen-activated protein kinase kinase kinase 1					-0.44
NM_004721	MAP3K13	Mitogen-activated protein kinase kinase kinase 13					-0.49
NM_004672	MAP3K6	Mitogen-activated protein kinase kinase kinase 6					-0.45
NM_003618	MAP4K3	Mitogen-activated protein kinase kinase kinase kinase 3					-0.52
NM_138957	MAPK1	Mitogen-activated protein kinase 1					-0.44
ENST00000374189	MAPK8/JNK1	Mitogen-activated protein kinase 8					0.43
NM_014791	MELK	Maternal embryonic leucine zipper kinase	-1.21	-1.10		-1.09	-0.67
NM_017572	MKNK2	MAP kinase interacting serine/threonine kinase 2	1.1	0.88		0.79	
NM_053025	MYLK	Myosin light chain kinase	-0.49		-0.64	-0.8	-0.66
NM_014840	NUAK1	NUAK family SNF1-like kinase 1			0.45		0.49
NM_022731	NUCKS1	Nuclear casein kinase and cyclin-dependent kinase substrate 1			-1.06	-1.2	-0.69
NM_152835	PDIK1L	PDLIM1 interacting kinase 1 like	-0.61			-0.82	
NM_006823	PKIA	Protein kinase transcript variant 6			0.36		0.42
NM_182687	PKMYT1	Protein kinase membrane associated tyrosine/threonine 1 transcript variant 2	-0.95	-0.64			
NM_006622	PLK2	Polo-like kinase 2	0.95	0.96	0.96	1.23	0.99
NM_014264	PLK4	Polo-like kinase 4	-0.91	-0.69			
NM_016203	PRKAG2	Protein kinase AMP-activated gamma 2 non-catalytic subunit		0.64	0.54		
NM_004157	PRKAR2A	Protein kinase cam*P*-dependent regulatory type II alpha		-0.63		-0.6	
NM_002737	PRKCA	Protein kinase C alpha			0.36		
NM_012408	PRKCBP1	Protein kinase C binding protein 1 transcript variant 2			-0.47		
NM_145906	RIOK3	RIO kinase 3		0.75	0.6	0.69	0.4
NM_004586	RPS6KA3	Ribosomal protein S6 kinase 90kDa polypeptide 3			-0.87	-0.84	-0.57
NM_005627	SGK	Serum/glucocorticoid regulated kinase				-0.75	-1.16

NM_000455	STK11	Serine/threonine kinase 11			-0.38	1.06	
NM_001032296	STK24	Serine/threonine kinase 24			0.5		
NM_015000	STK38L	Serine/threonine kinase 38 like			1.03	0.64	
NM_006282	STK4	Serine/threonine kinase 4				-0.71	
NM_032017	STK40	Serine/threonine kinase 40			0.82	1	0.56
NM_020791	TAOK1	TAO kinase 1				0.7	
NM_016281	TAOK3	TAO kinase 3			0.37		
NM_005781	TNK2	Tyrosine kinase non-receptor 2				-0.65	-0.41
NM_003318	TTK	TTK protein kinase	-0.88	-0.79			
Epigenetics-related and chromatin modifications							
NM_014577	BRD1	Bromodomain containing 1				0.57	
NM_005104	BRD2	Bromodomain containing 2			-0.41		
NM_176812	CHMP4B	Chromatin modifying protein 4B		-1.41			
NM_014473	DIMT1L	DIM1 dimethyladenosine transferase 1-like	-0.57				
NM_001379	DNMT1	DNA methyl transferase 1	-0.8	-0.58	-0.45	-0.58	-0.64
NM_013369	DNMT3L	DNA -methyltransferase 3-like			0.49		0.54
NM_032482	DOT1L	DOT1-like histone H3 methyltransferase			0.42		
NM_004456	EZH2	Enhancer of zeste homolog 2	-0.5				
NM_006026	H1FX	H1 histone family member X	-0.79			-0.66	-0.66
NM_012412	H2AFV	H2A histone family member V					0.39
NM_002106	H2AFZ	H2A histone family member Z	-0.61	-1.02	-0.36	-1.05	
NM_002107	H3F3A	H3 histone family 3A			-0.92		
NM_005324	H3F3B	H3 histone family 3B					0.36
NM_003642	HAT1	Histone acetyltransferase 1	-0.68	-0.88	-0.4	-1.12	-0.36
NM_018486	HDAC8	Histone deacetylase 8			-0.69		-0.55
NM_178423	HDAC9	Histone deacetylase				-0.72	
NM_005321	HIST1H1E	Histone cluster 1 H1e	-0.89		-1.21	-1.4	-0.84
NM_170745	HIST1H2AA	Histone cluster 1 h2aa				-0.71	
NM_003513	HIST1H2AB	Histone cluster 1 h2ab			-0.35		
NM_021065	HIST1H2AD	Histone cluster 1 h2ad	0.82			0.57	
NM_021052	HIST1H2AE	Histone cluster 1 h2ae			-0.71		

NM_021064	HIST1H2AG	Histone cluster 1 h2ag			-0.4		
NM_080596	HIST1H2AH	Histone cluster 1 h2ah			-0.44		
NM_021066	HIST1H2AJ	Histone cluster 1 h2aj	-0.61		-0.82	-0.92	
NM_003510	HIST1H2AK	Histone cluster 1 h2ak	0.59				
NM_003514	HIST1H2AM	Histone cluster 1 h2am			-0.47		-0.5
NM_021062	HIST1H2BB	Histone cluster 1 h2bb		0.74	0.77		
BQ683489	HIST1H2BD	Histone cluster 1 h2bd	-0.86	-1.30	-1.29	-1.98	-0.59
NM_003523	HIST1H2BE	Histone cluster 1 h2be					
NM_003522	HIST1H2BF	Histone cluster 1 h2bf	0.67		0.66		
NM_003524	HIST1H2BH	Histone cluster 1 h2bh	0.97	0.69	0.69		
NM_003525	HIST1H2BI	Histone cluster 1 h2bi	1	0.61	0.72		0.53
BC014312	HIST1H2BJ	Histone cluster 1 h2bj					1.04
NM_003519	HIST1H2BL	Histone cluster 1 h2bl	0.92	0.66	0.65		
NM_003521	HIST1H2BM	Histone cluster 1 h2bm	0.96		0.67	0.63	0.42
NM_003527	HIST1H2BO	Histone cluster 1 h2bo	0.99	0.82	0.7	0.61	
NM_003529	HIST1H3A	Histone cluster 1 H3a			-0.6		
NM_003537	HIST1H3B	Histone cluster 1 H3b	-0.86	-1.39	-1.19	-1.56	-0.97
NM_003530	HIST1H3D	Histone cluster 1 h3d		-0.56	-0.5	-0.67	
NM_021018	HIST1H3F	Histone cluster 1 H3f			-0.56	-0.85	
NM_003534	HIST1H3G	Histone cluster 1 H3g	-0.85	-1.30	-0.67	-1.61	-0.48
NM_003536	HIST1H3H	Histone cluster 1 H3h			-0.49		
NM_003535	HIST1H3J	Histone cluster 1 H3j			-0.81		
NM_003544	HIST1H4B	Histone cluster 1 H4b				-0.72	
NM_003543	HIST1H4H	Histone cluster 1 H4h				-0.61	
NM_003495	HIST1H4I	Histone cluster 1 H4i				-0.87	
NM_021968	HIST1H4J	Histone cluster 1 H4j			-0.57	-1.03	
NM_001040874	HIST2H2AA4	Histone cluster 2 h2aa4	0.8		0.78	0.79	0.62
NM_175065	HIST2H2AB	Histone cluster 2 h2ab	-0.79	-0.78	-0.37	-1.02	-0.45
NM_003517	HIST2H2AC	Histone cluster 2 h2ac	-1.06	-1.47	-1.62	-1.68	-0.94
NM_003528	HIST2H2BE	Histone cluster 2 h2be			0.35		
NM_001005464	HIST2H3A	Histone cluster 2 h3a		-0.68	-0.91		-0.52
NM_001025303	HIST2H3PS2	Histone cluster 2 H3 pseudogene 2	-1.01	-1.44	-0.95	-1.78	-0.59

NM_001034077	HIST2H4B	Histone cluster 2 H4b				-0.73	
DB010344	HIST3H2BB	Histone cluster 3 h2bb	-0.82	-1.35	-1.57	-2.16	-0.75
NM_003493	HIST3H3	Histone cluster 3 H3			-0.35		
NM_172164	NASP	Nuclear autoantigenic sperm protein	-0.81	-0.75	-0.46	-0.64	-0.44
NM_006315	PCGF3	Polycomb group ring finger 3				0.75	
NM_032373	PCGF5	Polycomb group ring finger 5			-0.58		
NM_198319	PRMT1	Protein arginine methyltransferase 1			-0.58	-0.52	-0.46
NM_206962	PRMT2	Protein arginine methyltransferase			0.53		
NM_015355	SUZ12	Suppressor of zeste 12 homolog			-0.7	-0.94	-0.65
NM_182931	MLL5	Myeloid/lymphoid or mixed-lineage leukemia 5			-0.84		-0.77
Structural							
NM_004411	DYNC1I1	Dynein cytoplasmic 1 intermediate chain 1		0.72	0.46	0.84	0.53
NM_019063	EML4	Echinoderm microtubule associated protein like 4			-1.54	-0.80	-0.81
NM_080386	H2-ALPHA	Alpha-tubulin isotype H2-alpha	-0.51		-0.86		-0.80
NM_002374	MAP2	Microtubule-associated protein 2 transcript variant 1			0.51		
NM_003980	MAP7	Microtubule-associated protein 7			-0.60		-0.41
NM_015471	NSL1	NSL1 kinetochore complex component 1	-0.83	-0.80			
NM_145697	NUF2	NUF2 NDC80 kinetochore complex component	-0.72	-1.20		-0.84	
NM_016359	NUSAP1	Nucleolar and spindle associated protein 1	-0.97	-0.87	-0.53		-0.71
NM_006306	SMC1A	Structural maintenance of chromosomes 1A	-0.9	-0.99	-0.66	-0.66	-0.60
NM_079836	TUBA2	Tubulin alpha 2 transcript variant 2	-0.66		-1.11	-0.56	-1.11
NM_006009	TUBA3	Tubulin alpha 3	-0.47		-1.15		-1.02
NM_032704	TUBA6	Tubulin alpha 6	-0.55		-1.34		
NM_018943	TUBA8	Tubulin alpha 8			-0.62		-0.68
NM_178014	TUBB	Tubulin beta	-0.52		-1.07		-0.92
NM_001069	TUBB2A	Tubulin beta 2A			-0.47		-0.68
NM_006088	TUBB2C	Tubulin beta 2C	-1.07	-0.78	-1.32	-0.80	-1.09
NM_006086	TUBB3	Tubulin beta 3			-1.27	-0.66	-1.25
NM_006087	TUBB4	Tubulin beta 4			-0.80		-0.53
NM_032525	TUBB6	Tubulin beta 6			-0.67		-0.59
NM_177987	TUBB8	Tubulin beta 8			-1.03		-0.69

NM_001070	TUBG1	Tubulin gamma 1			-0.58		-0.44
Regulation of Transcription							
NM_005194	CEBPB	CCAAT/enhancer binding protein beta	0.83	0.77		1.30	
NM_006079	CITED2	Cbp/p300-interacting transactivator with Glu/As*P*-rich carboxy-terminal domain 2	0.72	1.10	0.85	0.84	
NM_133467	CITED4	Cbp/p300-interacting transactivator with Glu/As*P*-rich carboxy-terminal domain 4	-0.64				
NM_182898	CREB5	Camp responsive element binding protein 5 transcript variant 1			0.47	0.71	0.52
NM_017779	DEPDC1	DEP domain containing 1	-0.75	-1.01			
NM_004405	DLX2	Distal-less homeobox 2			-0.64	-1.03	-0.90
NM_005225	E2F1	E2F transcription factor 1	-0.63	-0.60			
NM_024680	E2F8	E2F transcription factor 8	-1.40	-1.12	-0.75		
NM_001964	EGR1	Early growth response 1	0.80	0.63		1.21	
NM_005252	FOS	V-fos FBJ murine osteosarcoma viral oncogene homolog	0.83	1.38		1.23	
NM_181054	HIF1A	Hypoxia-inducible factor 1 alpha subunit transcript variant 2	0.45			0.86	0.42
NM_145904	HMGA1	High mobility group AT-hook 1 transcript variant 6	-0.49	-0.59	-0.58		
NM_003483	HMGA2	High mobility group AT-hook 2	-0.51	-0.62	-0.39	-0.53	
NM_002128	HMGB1	High-mobility group box 1	-0.55	-0.68	-0.67	-0.70	-0.75
NM_002129	HMGB2	High-mobility group box 2	-0.70	-0.87			
NM_000600	IL6	Interleukin 6	2.44	2.34	1.68	3.66	1.93
NM_198219	ING1	Inhibitor of growth family member 1	-0.61	-0.68	-0.47	-0.61	
NM_002192	INHBA	Inhibin beta A	1.20	1.14		1.47	
NM_004973	JARID2	Jumonji AT rich interactive domain 2	0.72		0.63	0.82	0.65
NM_002228	JUN	Jun oncogene	0.76				
NM_016269	LEF1	Lymphoid enhancer-binding factor 1	0.72	0.57	0.66	0.93	0.54
NM_006879	MDM2	Mdm2 transformed 3T3 cell double minute	1.77	1.53	1.23	1.85	1.13
NM_031300	MXD3	MAX dimerization protein 3	-0.73	-0.89		-0.71	-0.39
NM_006454	MXD4	MAX dimerization protein 4	0.76	0.73			
X66087	MYBL1	v-Myb myeloblastosis viral oncogene homolog (avian)-like 1	-1.13	-0.97	-0.70	-1.03	-0.94
NM_005595	NFIA	Nuclear factor I/A			-0.75	-0.72	-0.96
NM_005450	NOG	Noggin	-0.80			-0.58	

NM_021005	NR2F2	Nuclear receptor subfamily 2 group F member 2	-0.67	-0.97	-0.91	-1.33	-0.77
NM_006191	PA2G4	Proliferation-associated 2G4 38kda	-0.72	-0.70	-0.53	-0.60	-0.54
NM_002691	POLD1	Polymerase delta 1 catalytic subunit 125kda	-0.64			-0.55	-0.62
NM_021144	PSIP1	PC4 and SFRS1 interacting protein 1 transcript variant 1	-0.78		-0.69	-0.98	-0.53
NM_006325	RAN	RAN member RAS oncogene family	-0.49	-0.73	-0.76		
NM_001012761	RGMB	RGM domain family member B transcript variant 1			0.78	0.90	0.65
NM_012249	RHOQ	Ras homolog gene family member Q			0.57	0.91	0.47
NM_017420	SIX4	Sine oculis homeobox homolog 4			-0.34	-0.56	-0.36
NM_022739	SMURF2	SMAD specific E3 ubiquitin protein ligase 2		0.75	0.49		
NM_003107	SOX4	SRY -box 4	0.89		0.55	1.92	0.42
U46752	SQSTM1	Human phosphotyrosine independent ligand	0.77		0.98	0.52	
NM_001005291	SREBF1	Sterol regulatory element binding transcription factor	-0.52		-0.35		-0.64
NM_003168	SUPT4H1	Suppressor of Ty 4 homolog 1	0.98	0.99	0.81	0.94	0.83
NM_139215	TAF15	TAF15 RNA polymerase II		-1.27	-0.63	-1.41	
NM_003221	TFAP2B	Transcription factor AP-2 beta	-0.66	-0.55			0.47
NM_194259	UBE2I	Ubiquitin-conjugating enzyme E2I transcript variant 2		-0.61		-0.53	
NM_013282	UHRF1	Ubiquitin-like containing PHD and RING finger domains	-1.11	-1.39	-0.99	-1.59	-1.06
NM_003400	XPO1	Exportin 1	-0.52		-0.58		
Translation							
NM_001280	CIRBP	Cold inducible RNA binding protein	0.47			0.61	
NM_001950	E2F4	E2F transcription factor 4 p107/p130-binding			-0.45		
NM_032378	EEF1D	Eukaryotic translation elongation factor 1 delta transcript variant 1			-0.34		
NM_014239	EIF2B2	Eukaryotic translation initiation factor 2B subunit 2 beta 39kda					-0.41
NM_003907	EIF2B5	Eukaryotic translation initiation factor 2B subunit 5 epsilon 82kda					-0.45
NM_004094	EIF2S1	Eukaryotic translation initiation factor 2 subunit 1 alpha 35kda				0.67	
NM_003755	EIF3S4	Eukaryotic translation initiation factor 3 subunit 4 delta 44kda			-0.34		
NM_001568	EIF3S6	Eukaryotic translation initiation factor 3 subunit 6 48kda				-0.84	
NM_003753	EIF3S7	Eukaryotic translation initiation factor 3 subunit 7 zeta 66/67kda			-0.39		-0.41
NM_001037808	EIF3S8	Eukaryotic translation initiation factor 3 subunit 8 110kda					-0.45
NM_001416	EIF4A1	Eukaryotic translation initiation factor 4A isoform 1			-0.48		-0.55
NM_001967	EIF4A2	Eukaryotic translation initiation factor 4A isoform 2				0.67	

NM_001417	EIF4B	Eukaryotic translation initiation factor 4B			-0.42	0.71	
NM_001968	EIF4E	Eukaryotic translation initiation factor 4E	-0.72	-0.79	-0.38	-1.01	
NM_182917	EIF4G1	Eukaryotic translation initiation factor 4 gamma 1					-0.38
NM_006532	ELL	Elongation factor RNA polymerase II			0.50		
NM_012081	ELL2	RNA polymerase II elongation factor ELL2.			0.66	0.63	
NM_017572	MKNK2	MAP kinase interacting serine/threonine kinase 2	1.10	0.89	0.79		
NM_006191	PA2G4	Proliferation-associated 2G4 38kda	-0.72	-0.70	-0.53	-0.60	-0.54
NM_002568	PABPC1	Polybinding protein cytoplasmic 1			-0.63		-0.51
NM_002691	POLD1	Polymerase delta 1 catalytic subunit 125kda				-0.55	
NM_017443	POLE3	Polymerase epsilon 3					-0.41
NM_003246	THBS1	Thrombospondin 1	0.53	1.02	0.47	1.14	0.50
NM_001033930	UBA52	Ubiquitin A-52 residue ribosomal protein fusion product 1			0.34		
Ras-related							
NM_015576	ERC2	ELKS/RAB6-interacting/CAST family member 2					0.86
BC034222	HRASLS5	HRAS-like suppressor family member 5			0.56		
NM_012219	MRAS	Muscle RAS oncogene homolog			-0.73		-0.78
NM_016131	RAB10	RAB10 member RAS oncogene family					-0.44
NM_014904	RAB11FIP2	RAB11 family interacting protein 2			-0.52	-0.91	-0.68
NM_001025300	RAB12	RAB12 member RAS oncogene family				0.83	
NM_016322	RAB14	RAB14 member RAS oncogene family					-0.36
NM_198686	RAB15	RAB15 member RAS onocogene family			-0.46		
NM_014999	RAB21	RAB21 member RAS oncogene family				0.85	
NM_001031677	RAB24	RAB24 member RAS oncogene family					0.36
NM_004794	RAB33A	RAB33A member RAS oncogene family	-0.81	-1.01	-0.72	-0.95	
NM_004162	RAB5A	RAB5A member RAS oncogene family				0.59	
NM_005370	RAB8A	RAB8A member RAS oncogene family			-0.52	-0.68	-0.48
NM_004703	RABEP1	Rabaptin RAB gtpase binding effector protein 1			1.59		
NM_014857	RABGAP1L	RAB gtpase activating protein 1-like				0.56	
NM_014504	RABGEF1	RAB guanine nucleotide exchange factor			0.5	0.68	
NM_004582	RABGGTB	Rab geranylgeranyltransferase beta subunit					0.42
NM_002871	RABIF	RAB interacting factor			0.57		

NM_173825	RABL3	RAB member of RAS oncogene family-like 3				-0.52	
NM_006860	RABL4	RAB member of RAS oncogene family-like 4				-0.62	
NM_013277	RACGAP1	Rac GTPase activating protein 1	-0.76	-0.98			
NM_006325	RAN	RAN member RAS oncogene family	-0.49	-0.727		-0.76	
NM_006989	RASA4	RAS p21 protein activator 4				0.62	
NM_032023	RASSF4	Ras association domain family 4	0.72				-0.57
NM_032023	RASSF4	Ras association domain family 4					
NM_007211	RASSF8	Ras association domain family 8			0.65		
NM_000539	RHO	Rhodopsin					0.6
NM_004040	RHOB	Ras homolog gene family member B			0.45		
NM_175744	RHOC	Ras homolog gene family member C				0.77	
NM_012249	RHOQ	Ras homolog gene family member Q			0.72	0.91	0.39
NM_005168	RND3	Rho family gtpase 3				0.85	-0.63
NM_004165	RRAD	Ras-related associated with diabetes		0.883	1.38	0.56	0.69
NM_006270	RRAS	Related RAS viral			0.53		
NM_012250	RRAS2	Related RAS viral oncogene homolog 2	0.53	0.86	0.48	1.15	
Extracellular matrix							
NM_001110	ADAM10	ADAM metallopeptidase domain 10				0.48	
NM_001005845	ADAM9	ADAM metallopeptidase domain 9 transcript variant 2			0.56	1.21	
NM_014243	ADAMTS3	ADAM metallopeptidase with thrombospondin type 1 motif 3		0.62	0.39	0.85	
NM_014272	ADAMTS7	ADAM metallopeptidase with thrombospondin type 1 motif 7			-0.52	0.67	
NM_014272	ADAMTS7	ADAM metallopeptidase with thrombospondin type 1 motif 7					
NM_001792	CDH2	Cadherin 2 type 1 N-cadherin				0.70	
NM_022478	CDH24	Cadherin-like 24 transcript variant 1			-0.91		
NM_006383	CIB2	Calcium and integrin binding family member 2			0.55		0.39
NM_054113	CIB3	Calcium and integrin binding family member 3			0.41	0.50	
NM_001903	CTNNA1	Catenin alpha 1 102kda				0.55	
NM_001904	CTNNB1	Catenin beta 1 88kda				0.68	
ENST00000320216	ENST00000320216	Integrin beta-2 precursor	1.14				
NM_003862	FGF18	Fibroblast growth factor 18			0.94		
NM_212482	FN1	Fibronectin 1 transcript variant 1			0.61		

NM_005114	HS3ST1	Heparan sulfate 3-O-sulfotransferase 1	1.07	1.15	-0.72	1.04	0.87
NM_006043	HS3ST2	Heparan sulfate 3-O-sulfotransferase 2			0.38		
NM_006040	HS3ST4	Heparan sulfate 3-O-sulfotransferase 4				0.99	
NM_001077188	HS6ST2	Heparan sulfate 6-O-sulfotransferase 2 transcript variant L				0.62	
NM_030790	ITFG1	Integrin alpha FG-GAP repeat containing 1			0.43		
NM_002205	ITGA5	Integrin alpha 5					-0.40
NM_002210	ITGAV	Integrin alpha V					-1.83
NM_133376	ITGB1	Integrin beta 1 transcript variant 1E			0.41	0.71	
NM_014288	ITGB3BP	Integrin beta 3 binding protein		-0.72		-0.76	
NM_002213	ITGB5	Integrin beta 5				-0.65	
NM_002214	ITGB8	Integrin beta 8					-0.50
NM_002421	MMP1	Matrix metallopeptidase 1			1.93		
NM_002427	MMP13	Matrix metallopeptidase 13				0.57	0.73
NM_016155	MMP17	Matrix metallopeptidase 17			-0.41	0.64	
NM_002429	MMP19	Matrix metallopeptidase 19	0.60			0.82	
NM_004994	MMP9	Matrix metallopeptidase 9		0.56		0.53	
NM_004994	MMP9	Matrix metallopeptidase 9				0.55	
NM_005947	MT1B	Metallothionein 1B	0.80		0.77	0.66	0.38
NM_175617	MT1E	Metallothionein 1E	0.79		0.78	0.68	
NM_005950	MT1G	Metallothionein 1G			0.60		
NM_005951	MT1H	Metallothionein 1H	0.85		0.78	0.59	
NM_005952	MT1X	Metallothionein 1X	0.88		0.81	0.60	
NM_198883	MTX1	Metaxin 1			-0.33		
NM_003255	TIMP2	TIMP metallopeptidase inhibitor 2	1.05	1.16	1.38	1.18	0.40
Protein folding							
AY956764	HSP90AB3P	Heat shock protein 90Bc			-1.14		-0.59
NM_006819	STIP1/HOP	Stress-induced-phosphoprotein 1	-0.52		-0.58		-0.47
ENST00000378770	ENST00000378770	Heat shock protein 90Ad.				-0.86	
NM_001040141	HSP90AA2	Heat shock protein 90kda alpha , class A member 2			-0.65	-0.74	-0.69
NM_001540	HSPB1	Heat shock 27kda protein 1			0.49		
NM_002155	HSPA6	Heat shock 70kda protein 6			1.50		

NM_003299	HSP90B1	Heat shock protein 90kda beta member 1			-1.54		-1.34
NM_005347	HSPA5	Heat shock 70kDa protein 5	0.53	0.68		1.07	
NM_005348	HSP90AA1	Heat shock protein 90kDa alpha (, class A member 1	-0.51				-0.92
NM_007034	DNAJB4	DnaJ homolog, subfamily B, member B4			0.51		
NM_007355	HSP90AB1	heat shock protein 90kDa alpha class B member 1			-1.35		-0.80
NM_013238	DNAJC15	DnaJ homolog, subfamily C, member 15			0.43		
NM_014280	DNAJC8	DnaJ homolog, subfamily C, member 8			-0.48		
NM_014787	DNAJC6	DnaJ homolog, subfamily C, member 6			0.64	0.63	
NM_015268	DNAJC13	DnaJ homolog, subfamily C, member 13					-0.43
NM_017626	DNAJB12	DnaJ homolog, subfamily B, member 12				-0.67	
NM_018981	DNAJC10	DnaJ homolog, subfamily C, member 10					-0.47
NM_021800	DNAJC12	DnaJ homolog, subfamily C, member 12					-0.41
NM_021979	HSPA2	Heat shock 70kDa protein 2			-0.43		-0.67
NM_152686	DNAJC18	DnaJ homolog, subfamily C, member 18			0.49	0.56	
NM_173650	DNAJC5G	DnaJ homolog, subfamily C, member 5G			0.45		

Reverse transcription quantitative polymerase chain reaction

Analysis of mRNA levels via reverse transcription quantitative polymerase chain reaction(RTq-PCR) was carried out with SABiosciences' (Maryland, USA) Human RT^2 profiler Arrays for apoptosis- and cell cycle-related genes. RTq-PCR is a good method to validate data from microarray results and more sensitive than microarrays and are able to lift out false negatives from microarray data(222). In order to validate microarray data, mRNA levels for apoptosis-associate genes were tested for ESE-16-exposed (200 nM) MCF-7, MDA-MB-231 and MCF-12A cells for 24 h. For cell cycle-related genes mRNA levels were tested for ESE-16 exposed (200 nM) for 12 h. The reason for testing mRNA expression after for MCF-7 and MDA-MB-231 cells after 12 h exposure to ESE-16 is that cells in G_2/M phase of the cell cycle reached a maximum after 12 h exposure and maintained a plateau until 24 h, before going into apoptosis (Table 3.15, Table 3.16).

Bcl2-associated X protein transcript variant beta (BAX) verified to be differentially expressed in MCF-12A cells after 24 h exposure (Table 3.20). It was also the case in MCF-7 and MDA-MB-231-exposed cells, indicating that the gene is most likely up regulated in all cell lines (Table 3.20). Growth arrest and DNA-damage-inducible alpha (GADD45A) and Bcl2-like 11 (BCL2L11) were verified to be differentially expressed in MDA-MB-231 cells after 24 h exposure (Table 3.20). GADD45A was also confirmed to be differentially expressed in MCF-7 cells (Table 3.20). BAX and GADD45A were also differentially expressed after 12 h exposure in MCF-7 and MDA-MB-231 cells, indicating a common response to the exposure of ESE-16 (Table 3.21).

Table 3.20: Statistically significantly ($P< 0.05$) differentially expressed apoptosis-associate genes as determined by RTq-PCR in MCF-7, MDA-MB-231 and MCF12A cells exposed to ESE-16for 24 h.

RefSeq number	Gene Name	Description	Log fold change		
			MCF-7	MDA-MB-231	MCF-12A
NM_001160	APAF1	Apoptotic peptidase activating factor 1	3.95	1.47	2.11
NM_004874	BAG4	BCL2-associated athanogene 4			2.69
NM_004324	BAX	BCL2-associated X protein transcript variant beta	9.67	2.91	2.25
NM_006538	BCL2L11	BCL2-like 11 (apoptosis facilitator)		1.31	
NM_014739	BCLAF1	BCL2-associated transcription factor 1 transcript variant 1			-0.62
NM_016561	BFAR	Bifunctional apoptosis regulator	4.73		
NM_004330	BNIP2	BCL2/adenovirus E1B 19kda interacting protein 2			2.46
NM_004331	BNIP3L	BCL2/adenovirus E1B 19kda interacting protein 3-like	7.46	2.01	
NM_004333	BRAF	V-raf murine sarcoma viral oncogene homolog B1	5.70	2.42	2.72
NM_001924	GADD45A	Growth arrest and DNA-damage-inducible alpha	2.86	1.46	
NM_000875	IGF1R	Insulin-like growth factor 1 receptor	5.12	4.98	
NM_001167	XIAP/BIRC4	Baculoviral IAP repeat-containing 4		-2.02	-0.54

Table 3.21:Statistically significantly ($P< 0.05$) differentially expressed cell-cycle-associate genes as determined by RTq-PCR in MCF-7 and MDA-MB-231 cells exposed to ESE-16for 12 h.

RefSeq number	Gene Name	Description	Log fold change	
			MCF-7	MDA-MB-231
NM_013366	ANAPC2	Anaphase-promoting complex subunit 2	-0.60	-0.62
NM_013367	ANAPC4	Anaphase-promoting complex subunit 4	1.58	2.11
NM_138764	BAX	Bcl-2-associated X protein	2.05	2.69
NM_031966	CCNB1	Cyclin B1	1.68	2.27
NM_001759	CCND2	Cyclin D2	-0.59	-0.62
NM_058241	CCNT2	Cyclin T2	-1.60	-0.54
NM_003903	CDC16	Cell division cycle 16 homolog	1.31	1.81
NM_004359	CDC34	Cell division cycle 34 homolog	1.95	2.46
NM_001786	CDK1/CDC2	Cell division cycle 2 G1 to S and G2 to M	1.12	1.53
NM_004064	CDKN1B	Cyclin-dependent kinase inhibitor 1B (p27 Kip1)		1.05
NM_005192	CDKN3	Cyclin-dependent kinase inhibitor 3		1.56
NM_001827	CKS2	CDC28 protein kinase regulatory subunit 2	1.52	2.05
NM_003591	CUL2	Cullin 2	2.03	2.73
NM_001924	GADD45A	Growth arrest and DNA-damage-inducible, alpha		1.14
NM_014708	KNTC1	Kinetochore associated 1	1.30	1.82
NM_006739	MCM5	MCM5 minichromosome maintenance deficient 5 cell division cycle 46	-0.65	-0.70
NM_002431	MNAT1	Menage a trois homolog 1 cyclin H assembly factor	2.30	2.84
NM_183404	RBL1	Retinoblastoma-like 1		1.15
NM_002947	RPA3	Replication protein A3	0.89	1.34
NM_001005781	SUMO1	SMT3 suppressor of MIF two 3 homolog 1	-0.60	-0.63

Protein expression analysis

Protein microarray

However, gene expression does not necessarily correlate with protein expression or activity. Therefore, antibody microarrays, a common analytical tool to measure protein expression levels in whole cell extracts, was used to determine protein expression changes in response to ESE-16 treatment after 24 h exposure (223). After analysis, 44 proteins were considered differentially expressed in MCF-7 cells and 48 proteins were considered differentially expressed in MDA-MB-231 cells after 24 h exposure to 200 nM of ESE-16. Of these proteins, 33 were differentially expressed in both cell lines indicating a shared proteomic response to ESE-16 exposure in both MCF-7 and MDA-MB-231 cells (Figure 3.40, Table 3.22).

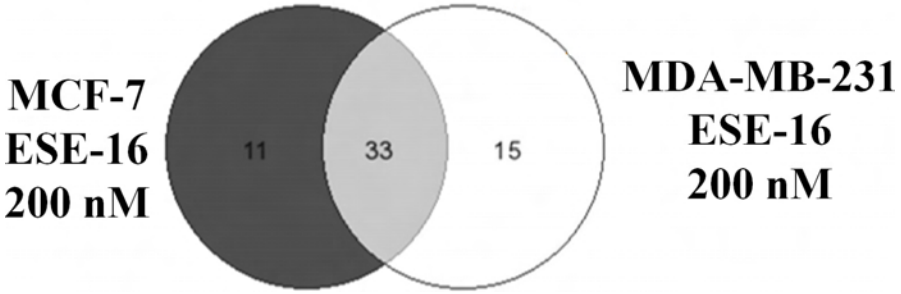

Figure 3.40: GeneVenn diagram showing common proteins affected in MCF-7 and MDA-MB-231 cells exposed to ESE-16 for 24 h.

Table 3.22: Expression of proteins deemed statistically significantly(standard deviation of less than 5% of *Average Log M* or has an *Average M* of greater than ±0.2) differentially expressed proteins as determined by antibody array analyses in MCF-7 and MDA-MB-231 cells exposed to ESE-16(200 nM) for 24 h.

RefSeq RNA	Gene ID	Protein ID	Description	MCF-7		MDA-MB-231	
				Average	STDEV	Average	STDEV
Cell death							
BAX	581	Q07814	BCL2-associated X protein			**0.23**	0.067
DAP3	7818	P51398	Death associated protein 3			**0.43**	0.1
EPB49	2039	Q08495	Erythrocyte membrane protein band 4.9 (dematin)	**0.77**	<0.001	**0.63**	0.115
BIRC4	331	P98170	Baculoviral IAP repeat-containing 4	**-0.27**	0.013		
CASP4	837	P49662	Caspase 4, apoptosis-related cysteine protease			**0.32**	0.001
CASP7	840	P55210	Caspase 7, apoptosis-related cysteine protease			**0.23**	0.06
ARRB1	408	P49407	Arrestin, beta 1			**0.71**	0.002
STAT3	6774	P40763	Signal transducer and activator of transcription 3	**0.23**	0.062	**0.46**	0.071

DAB2	1601	P98082	Disabled homolog 2, mitogen-responsive phosphoprotein (Drosophila)	**0.47**	0.022		
DFF45	1676	O00273	DNA fragmentation factor (ICAD)			**0.27**	0.033
Cell cycle							
GSPT2	23708	Q9NY44	G1 to S phase transition 2	**-0.32**	0.057	**-0.56**	0.029
CCNB1	891	P14635	Cyclin B1			**0.15**	0.001
BUB3	9184	O43684	BUB3 budding uninhibited by benzimidazoles 3 homolog (yeast)			**0.34**	0.144
CDK7	1022	P50613	Cyclin-dependent kinase 7	**0.26**	0.016		
KIF3B	9371	O15066	Kinesin family member 3B	**-0.19**	0.04	**-0.56**	0.007
SKP1	6500	P34991	S-phase kinase-associated protein 1A (p19a)	**-0.28**	0.09	**-0.35**	0.223
Protein folding							
HSP60	3329	P10809	Heat shock 60kDa protein 1 (chaperonin)	**0.2**	0.05		
HDJ-2	3301	P31689	DnaJ (Hsp40) homolog, subfamily A, member 1	**0.31**	0.05	**-0.24**	0.04
HSPA1A	3303	P08107	Heat shock 70kda protein 1A			**0.32**	0.053
Ras-related							
CSK	1445	P41240	c-Src tyrosine kinase	**0.27**	0.004	**0.19**	0.017
ARHGEF7	8874	Q14155	Rho guanine nucleotide exchange factor (GEF) 7	**-0.29**	0.035	**-0.21**	0.073
ARHGDIB	397	P52566	Rho GDP dissociation inhibitor (GDI) beta	**0.24**	0.008		
ROK alpha	9475	Q62868	Rho-associated, coiled-coil containing protein kinase 2			**0.26**	0.019
RASA2	5922	Q15283	RAS p21 protein activator 2			**0.27**	0.062
RAC1	5879	P15154	Ras-related C3 botulinum toxin substrate 1			**-0.44**	0.062
RAF1	5894	P04049	V-raf-1 murine leukemia viral oncogene homolog 1	**-0.33**	0.005		
DIAPH1	1729	O60610	Diaphanous homolog 1 (Drosophila)			**0.51**	0.167
RAB4A	5867	P20338	RAB4A, member RAS oncogene family			**0.24**	0.001
Ras-GAP	5921	P20936	RAS p21 protein activator (GTPase activating protein) 1			**0.2**	0.12

Transcription and translation							
TCERG1	10915	O14776	Transcription elongation regulator 1 (CA150)	**0.28**	0.013	**0.29**	0.019
NASP	4678	P49321	Nuclear autoantigenic sperm protein (histone-binding)	**-0.27**	0.013	**-0.58**	0.025
RPS6KB1	6198	P23443	Ribosomal protein S6 kinase, 70kda, polypeptide 1			**-0.12**	0.011
NR3C1	2908	P04150	Nuclear receptor subfamily 3, group C, member 1 (glucocorticoid receptor)	**-0.3**	0.002	**-0.15**	0.006
NCOR2	9612	Q9Y618	Nuclear receptor co-repressor 2	**-1.11**	0.127		

Caspase 3 and caspase 7 expression

Executioner caspases 3, 6 and 7 are responsible completing apoptotic cell death by destroying key components of cellular infrastructure and activate factors which damage the cell, and ultimately resulting in the morphological characteristics of apoptosis (231).Dylight™ 488-conjugated secondary antibodies were used to bind to active caspase 3 and active caspase 7 primary antibodies that were fixed to vehicle-treated control, ESE-16-treated (200 nM) andActinomycin D-treated (0.2 µg/mL) MCF-7, MDA-M-231 and MCF-12A cells after 24 h exposure. Actinomycin D was used as a possible control for apoptosis induction. Flow cytometry was employed to monitor fluorescence changes.

No difference in caspase 3 expression was observed in MCF-7 cells exposed to either Actinomycin D or ESE-16 treatment (Figure 3.41). Caspase 3 protein expression was elevated in both ESE-16 and Actinomycin D-treated MDA-MB-231 and MCF-12A cells (Figure 3.41). Caspase 7 protein expression was elevated in both ESE-16 and Actinomycin D-treated MCF-7, MDA-MB-231 and MCF-12A cells (Figure 3.42). Together this data suggest that both caspase 3 and caspase 7 play a role in inducing apoptosis in ESE-16-treated cells. Caspase 3 does not appear to be expressed in MCF-7 cells, explaining why only caspase 7 is expressed in ESE-16-treated MCF-7 cells(229).

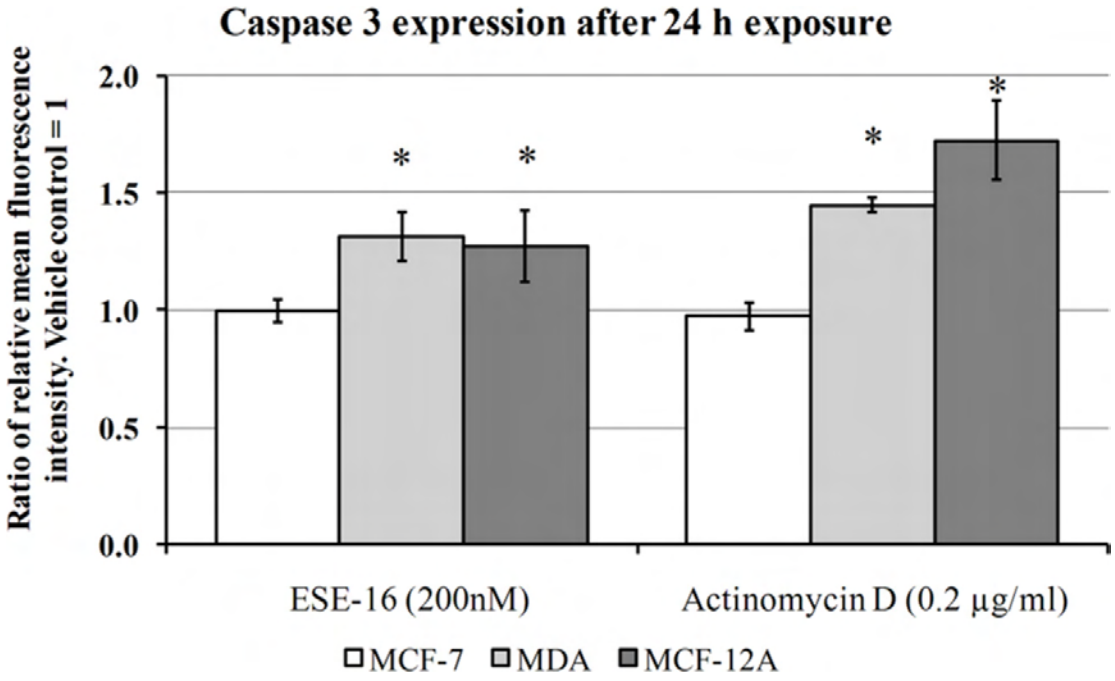

Figure 3.41: Relative fluorescence intensity for Dylight™ 488-conjugated secondary antibodies bound to caspase 3 primary antibodies (FL1 log).

*indicates a *P*-value < 0.05 between vehicle-treated cells and ESE-16-treated cells

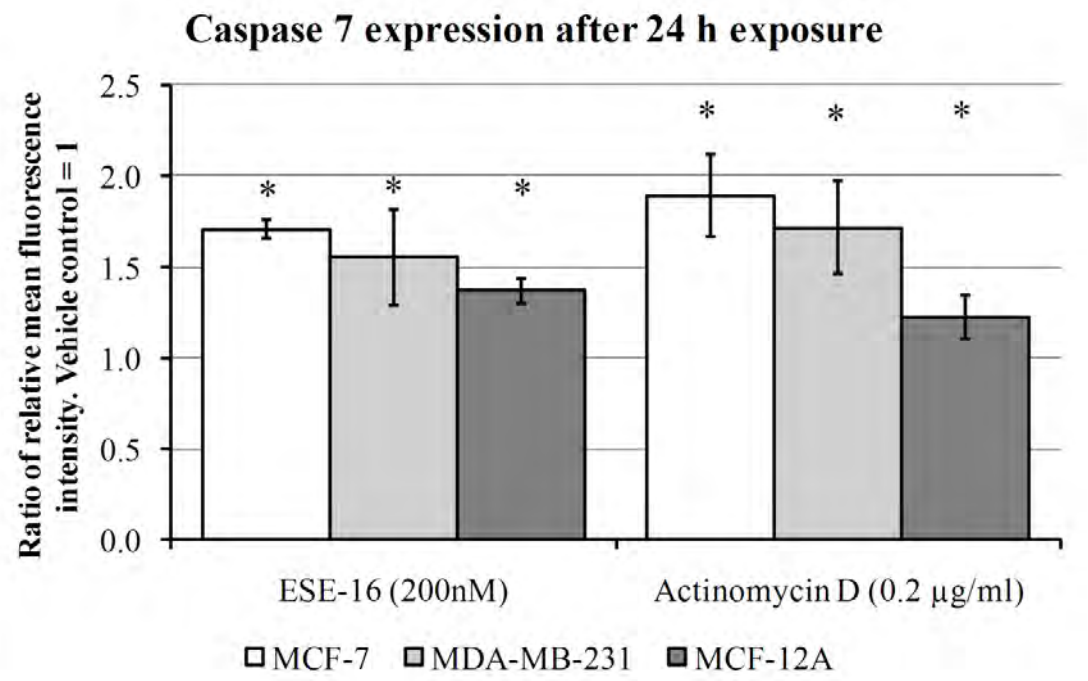

Figure 3.42: Relative fluorescence intensity for Dylight™ 488-conjugated secondary antibodies bound to caspase 7 primary antibodies (FL1 log).

*indicates a *P*-value < 0.05 between vehicle-treated cells and ESE-16-treated cells

Phosphorylation of Bcl-2 at Serine 70

Flow cytometry was employed to study the phosphorylation status of Bcl-2 at Ser 70 (pBcl-2 (ser70)) in the MCF-7, MDA-MB-231 and MCF-12A cell lines after 24 h exposure to ESE-16 (200 nM) compared to the vehicle-treated control. The expression levels of pBcl-2 (ser70) was also monitored in ESE-15-ol-treated (50 nM) MDA-MB-231 cells. The FlowCellect Bcl-2 Activation Dual Detection Kit (Millipore) uses two antibodies to measure the abundance of Bcl-2 protein expression generally and the abundance of Bcl-2 phosphorylated at Ser 70 specifically (FL3 Log).

No statistically significant effects on total Bcl-2 expression were observed when comparing exposed to ESE-15-ol-treated samples. ESE-16 exposure, however, resulted in a decrease in the total amount of Bcl-2 protein when compared to the vehicle-treated cells (Figure 3.44 and Figure 3.45). The fluorescence intensity (FI) unit range of 7.51-75 corresponds to the phosphorylation status of pBcl-2 (ser70)for >90% of cells in the vehicle-treated samples in all cell lines (Table 3.23). From this, it was concluded that an increase in the number of cells with an FI unit range greater than 75 would constitute an example of a population of cells with increased pBcl-2 (ser70) expression when compared to the vehicle-treated control. Also, an increase in the number of cells with an FI unit range less than 7.5 would constitute an example of a population of cells with decreased pBcl-2 (ser70) expression when compared to the vehicle-treated control.

The FI unit range of 7.51-75 statistically significantly decreased in all cell lines treated with ESE-15-ol and ESE-16 (Table 3.23, Figure 3.43, Figure 3.44, Figure 3.46, Figure 3.47,Figure 3.47 and Figure 3.48). In ESE-16-treated cells, the FI unit rangeof 7.51-75 decreased the least in MCF-12A cells (94.5% to 45.1%) when compared to the MCF-7 (91.3% to 19.7%) and MDA-MB-231 cells (96.3% to 23.7%) (91.3% to 19.7%) (Table 3.23, Figure 3.49). The decreases in the FI unit rangeof 7.51-100 resulted in increases in both the FI unit rangeof 0-7.5 and 75.1-1000 (Table 3.23, Figure 3.43, Figure 3.44, Figure 3.46, Figure 3.47,Figure 3.47 and Figure 3.48). In MCF-12A cells the number of cells in the FI unit rangeof 0-7.5 increased from 1.9% in the vehicle-treated control to 29.9% for ESE-16-treated cells (Table 3.23, Figure 3.49). This was statistically significantly less than MCF-7 cells (5.1% to 46.2%) and MDA-MB-231 cells (2.7%

to 51.5%) (Table 3.23, Figure 3.49). The number of cells in the FI unit rangeof 75.1-1000 increased in MCF-7 cells (5.1% to 31.3%), MDA-MB-231 (3% to 24%) and MCF-12A (3.9% to 27.8%) (Table 3.23, Figure 3.49).

Further analyses of the dot-plot data indicated that ESE-15-ol-treated cells with increased Bcl-2 phosphorylation tended to have a higher side-scatter (SS Lin) signal (Figure 3.43). Side scatter depends on the inner complexity of the particle. For example, an increase in the amount of DNA in a cell would correlate to an increased side-scatter signal. The data suggests that ESE-15-ol-treated cells with increased inner complexity also have an increase in Bcl2-2[p70]. A similar effect was observed in MCF-7, MDA-MB-231 and MCF-12A cells exposed to ESE-16 after 24 h (Figure 3.50, Figure 3.51 and Figure 3.52).

The effects of inhibiting the p38α and JNK1/2/3 kinases in modulating the expression of Bcl2-2[p] were also investigated in ESE-16-treated cells. SB239063 (15 µM) and SP600125 (25µM) were used to inhibit the p38α and JNK1/2/3 kinases respectively by incubating them with ESE-16 for 24 h. Inhibition of the p38α and JNK1/2/3 kinases in conjunction with exposure to ESE-16 altered the Bcl2-2[p70] dynamics differently in each cell line (Table 3.23, Figure 3.44, Figure 3.46, Figure 3.47 and Figure 3.48).

In MCF-7 and MDA-MB-231 cells, treatment with the JNK inhibitor and p38α inhibitor resulted in an increase in the number of cells in the FI unit range of 7.51-75 when compared to the ESE-16-treated cells (Table 3.23, Figure 3.46 and Figure 3.47). This effect was statistically significantly more in the ESE-16/JNK inhibitor-treated cells when compared to the ESE-16/p38α inhibitor-treated cells (Table 3.23, Figure 3.46). Both ESE-16/JNK inhibitor-treated cells and ESE-16/p38α inhibitor-treated cells resulted in a decrease in the number of cells in the FI unit range of 0-7.5 when compared to the ESE-16-treated cells (Table 3.23, Figure 3.46 and Figure 3.47). In the MDA-MB-231 cells, this effect was more pronounced in the ESE-16/JNK inhibitor-treated cells when compared to the ESE-16/p38α inhibitor-treated cells (Table 3.23, Figure 3.47). While ESE-16/JNK inhibitor-treated MCF-7 cells resulted in a decrease in the amount of cells in the FI unit range of 75.1-1000, ESE-16/p38α inhibitor-treated cells resulted in an increase (Table 3.23, Figure 3.46).

In MCF-12A, treatment with the JNK inhibitor and p38α inhibitor did not result in any differences in the number of cells in the FI unit range of 7.51-75 when compared to the ESE-16-treated cells (Table 3.23, Figure 3.48). ESE-16/JNK inhibitor-treated cells resulted in a decrease in the amount of cells in the FI unit range of 75.1-1000 when compared to ESE-16-treated cells (Table 3.23, Figure 3.48).ESE-16/p38α inhibitor-treated cells resulted in an increase in the amount of cells in the FI unit range of 75.1-1000 when compared to the ESE-16-treated cells (Table 3.23, Figure 3.48). Also, ESE-16/p38α inhibitor-treated cellsresulted in a decrease in the number of cells in the FI unit range of 0-7.5 when compared to the ESE-16-treated cells (Table 3.23, Figure 3.48). These results suggest that ESE-15-ol and ESE-16are able to abrogate the balance of Bcl-2 phospohorylation in a manner that promotes apoptosis via intrinsic pathways. Furthermore, JNK and p38α inhibition affects the Bcl-2 phospohorylation differently in each cell line.

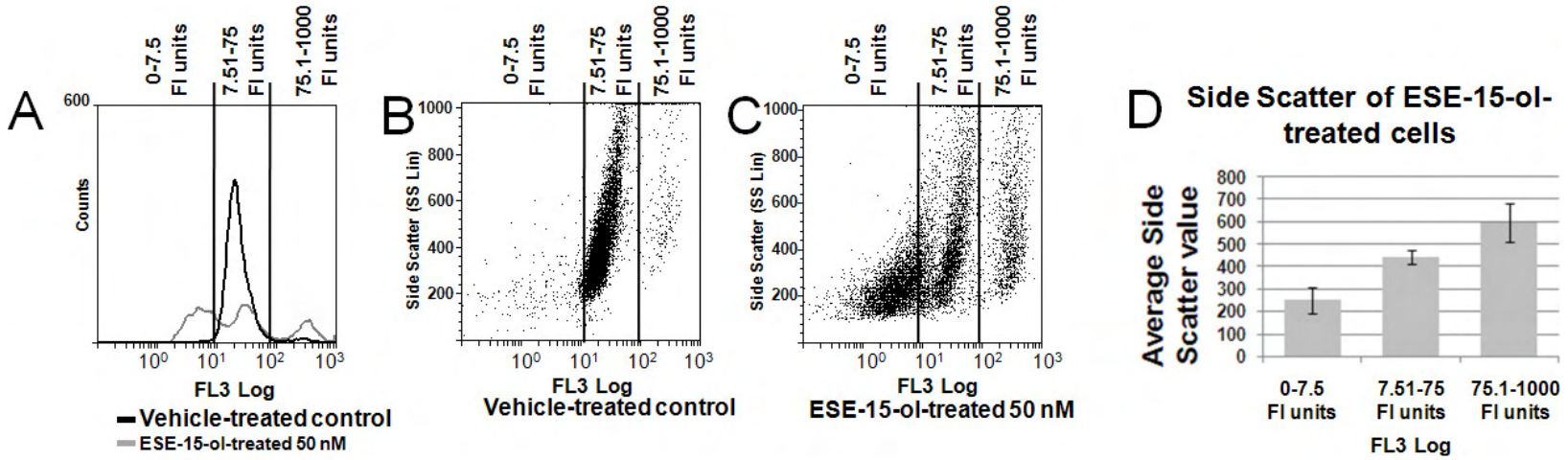

Figure 3.43: Flow cytometry histogram, dot-plots of Bcl-2 (Ser 70) relative quantity (FL3-log) in vehicle-treated and ESE-15-ol-treated (50 nM) MDA-MB-231 cells after 24 h exposure.Flow cytometry histogram (A) of Bcl-2 (Ser 70) relative quantity (FL3-log). Flow cytometry dot-plot of Bcl-2 (Ser 70) (FL3-log) relative quantity vs relative cellular complexity (SS lin) in (B) vehicle-treated or (C) ESE-15-ol-treated MDA-MB-231 cells. D) Bar-chart demonstrating the differences in cell size with different amounts of Bcl-2 (Ser 70) per cell. Means of three biological replicates are presented in bar charts. No differences in the overall Bcl-2 expression was observed (data not shown). [a] The fluorescence intensity of the FL3 filter is indicated by "FI units". [b] Values are presented as the average ± SD.

Table 3.23: Percentage of cells in the FI unit ranges of 0-7.5, 7.51-75 and 75.1-1000 as an indication of the quantity of Bcl-2 (Ser 70) phosphorylation per cell.

Cell line	Description	FI units (7.51-75)		FI units (0-7.5)		FI units (75.1-1000)	
		Average	STDEV	Average	STDEV	Average	STDEV
MCF-7	Vehicle-treated	91.26	2.9	2.51	0.9	6.27	2.1
	ESE-16-treated control	19.67	3.4	46.85	3.7	33.43	2.3
	ESE-16 + SP600125 (JNKi)-treated	58.59	7.3	21.79	5.3	19.64	4.0
	ESE-16 + SB239063 (p38i)-treated	30.13	4.3	29.50	6.1	39.70	2.9
MDA-MB-231	Vehicle-treated	96.26	0.5	2.59	0.2	1.14	0.3
	ESE-15-ol-treated control	49.57	8.8	36.85	9.8	13.57	1.5
	ESE-16-treated control	23.69	1.8	51.42	3.0	24.87	1.5
	ESE-16 + SP600125 (JNKi)-treated	78.76	3.9	16.00	5.1	5.24	2.6
	ESE-16 + SB239063 (p38i)-treated	36.26	2.1	37.87	2.0	25.87	0.9
MCF-12A	Vehicle-treated	94.54	1.3	1.26	0.7	4.20	1.6
	ESE-16-treated control	45.10	3.4	24.95	7.5	29.94	4.6
	ESE-16 + SP600125 (JNKi)-treated	52.65	8.8	27.64	8.3	19.61	0.8
	ESE-16 + SB239063 (p38i)-treated	39.05	1.4	15.49	0.9	45.44	1.6

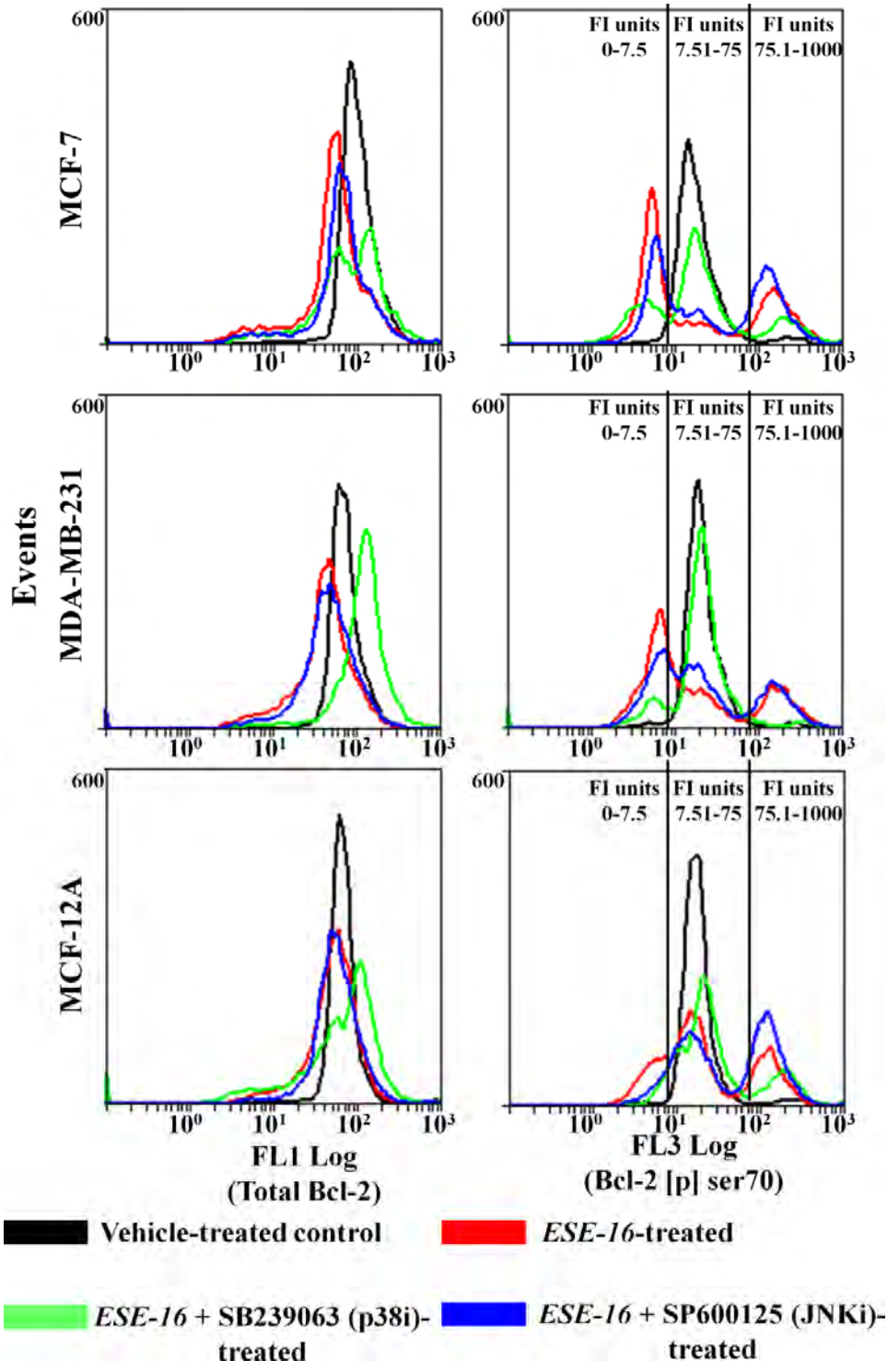

Figure 3.44: Flow cytometry histograms of total Bcl-2 content (FL1 Log) and Bcl-2 phosphorylated at Ser70 (FL3log) in MCF-7, MDA-MB-231 and MCF-12A cells after 24 h exposure.Fluorescence Intensity units = FI units.

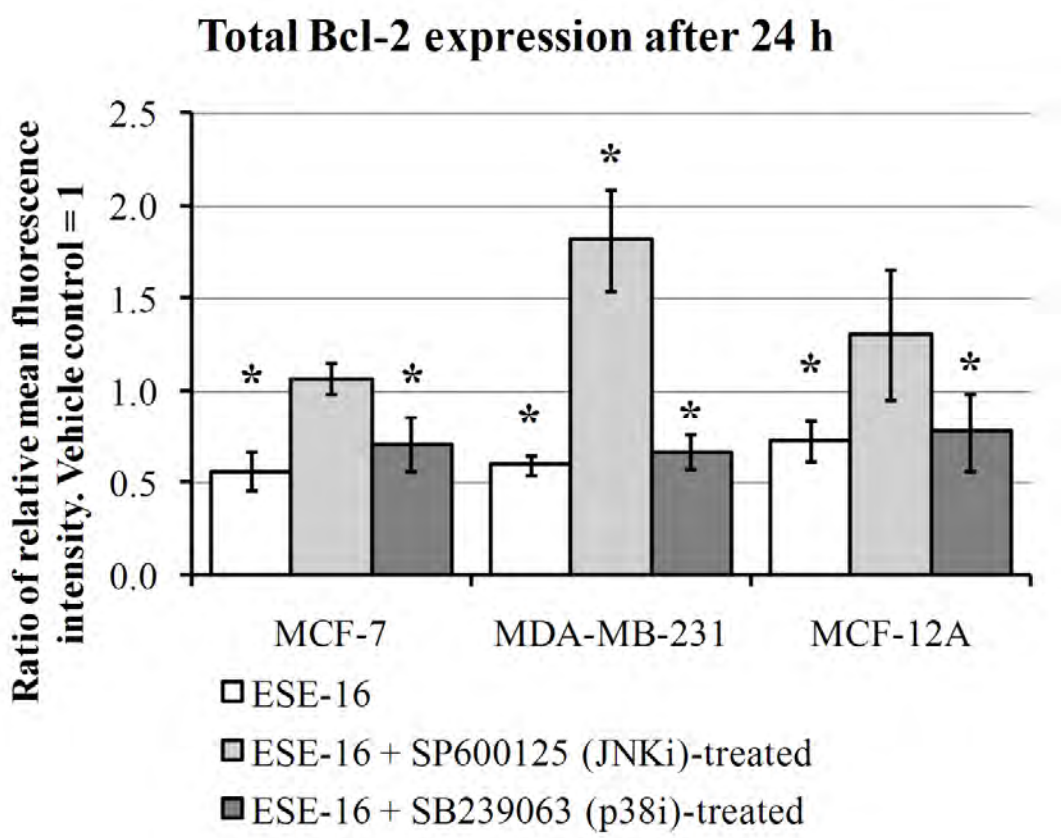

Figure 3.45: Total Bcl-2 expression after 24 h for MCF-7, MDA-MB-231 and MCF-12A cells.

*indicates a *P*-value < 0.05 between vehicle-treated cells and treated cells exposed to various experimental conditions

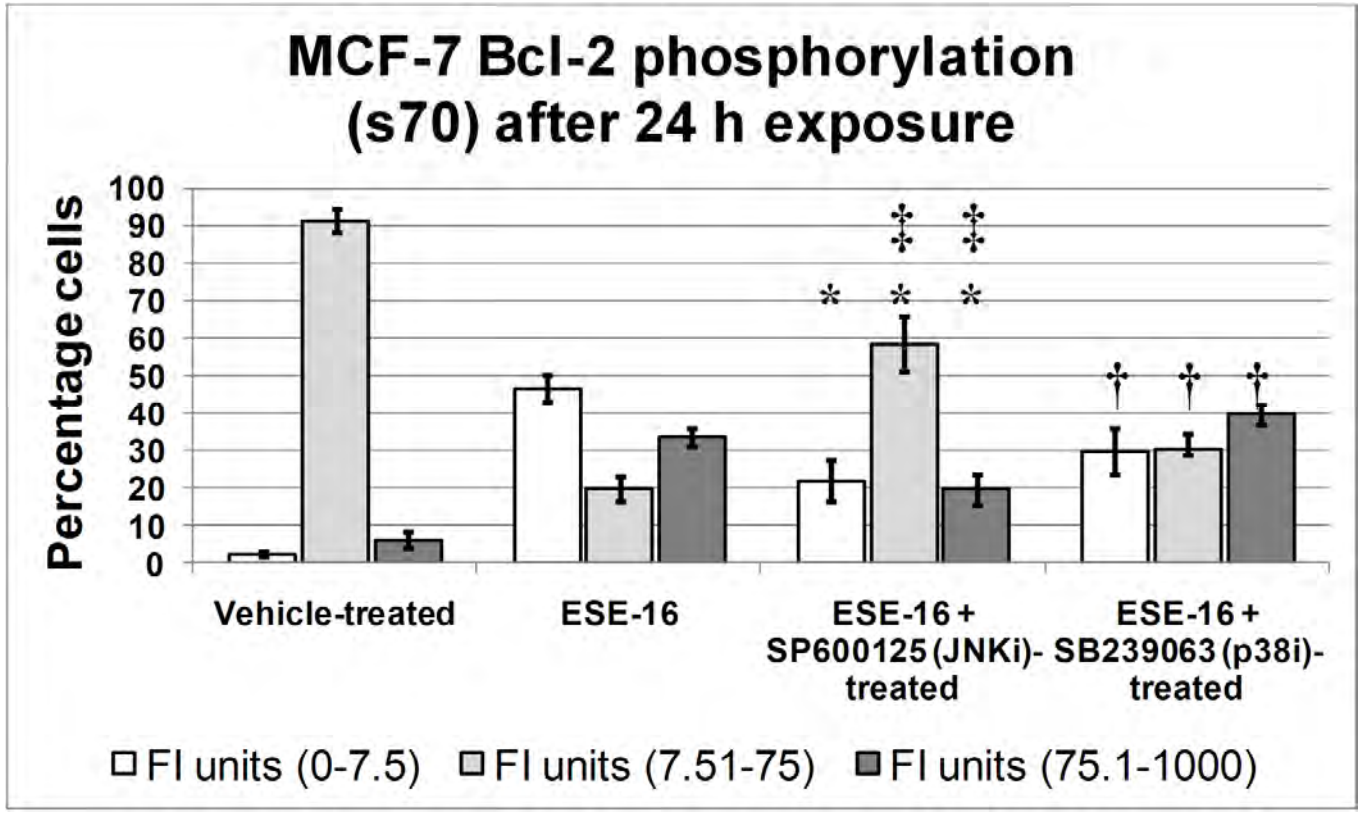

Figure 3.46: Bar-chart demonstrating the distribution of fluorescence intensity (FI) units of Bcl-2 (Ser 70) (FL3 Log) labeled MCF-7, cells after 24 h exposure to ESE-16 (200 nM).

*indicates a *P*-value < 0.05 between cells treated with ESE-16 and the JNK inhibitor and ESE-16-treated cells

†indicates a *P*-value < 0.05 between cells treated with ESE-16 and the p38α inhibitor and ESE-16-treated cells

‡indicates a *P*-value < 0.05 between cells treated with ESE-16 and the JNK inhibitor and cells treated with ESE-16 and the p38α inhibitor

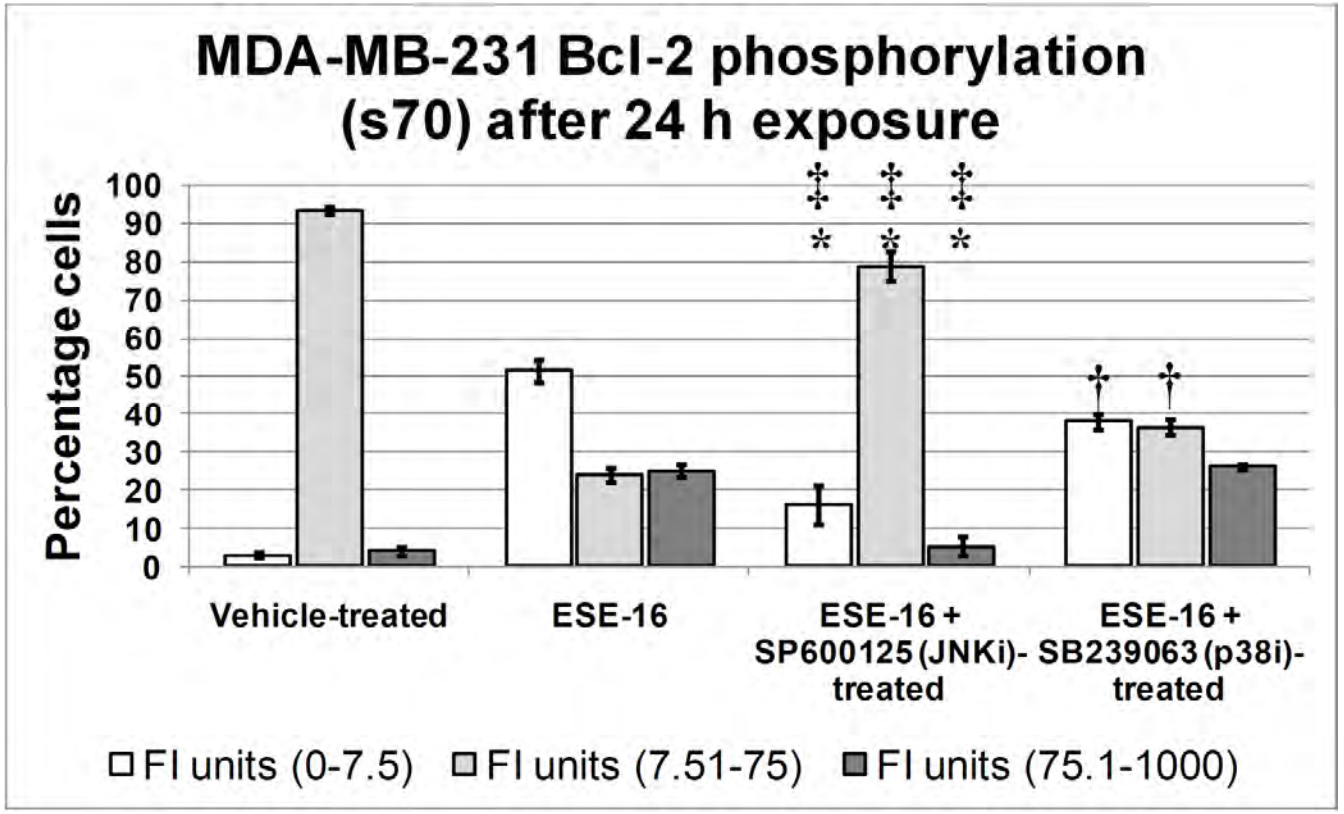

Figure 3.47: Bar-chart demonstrating the distribution of fluorescence intensity (FI) units of Bcl-2 (Ser 70) (FL3 Log) labeled MDA-MB-231, cells after 24 h exposure to ESE-16 (200 nM).

*indicates a *P*-value < 0.05 between cells treated with ESE-16 and the JNK inhibitor and ESE-16-treated cells

†indicates a *P*-value < 0.05 between cells treated with ESE-16 and the p38α inhibitor and ESE-16-treated cells

‡indicates a *P*-value < 0.05 between cells treated with ESE-16 and the JNK inhibitor and cells treated with ESE-16 and the p38α inhibitor

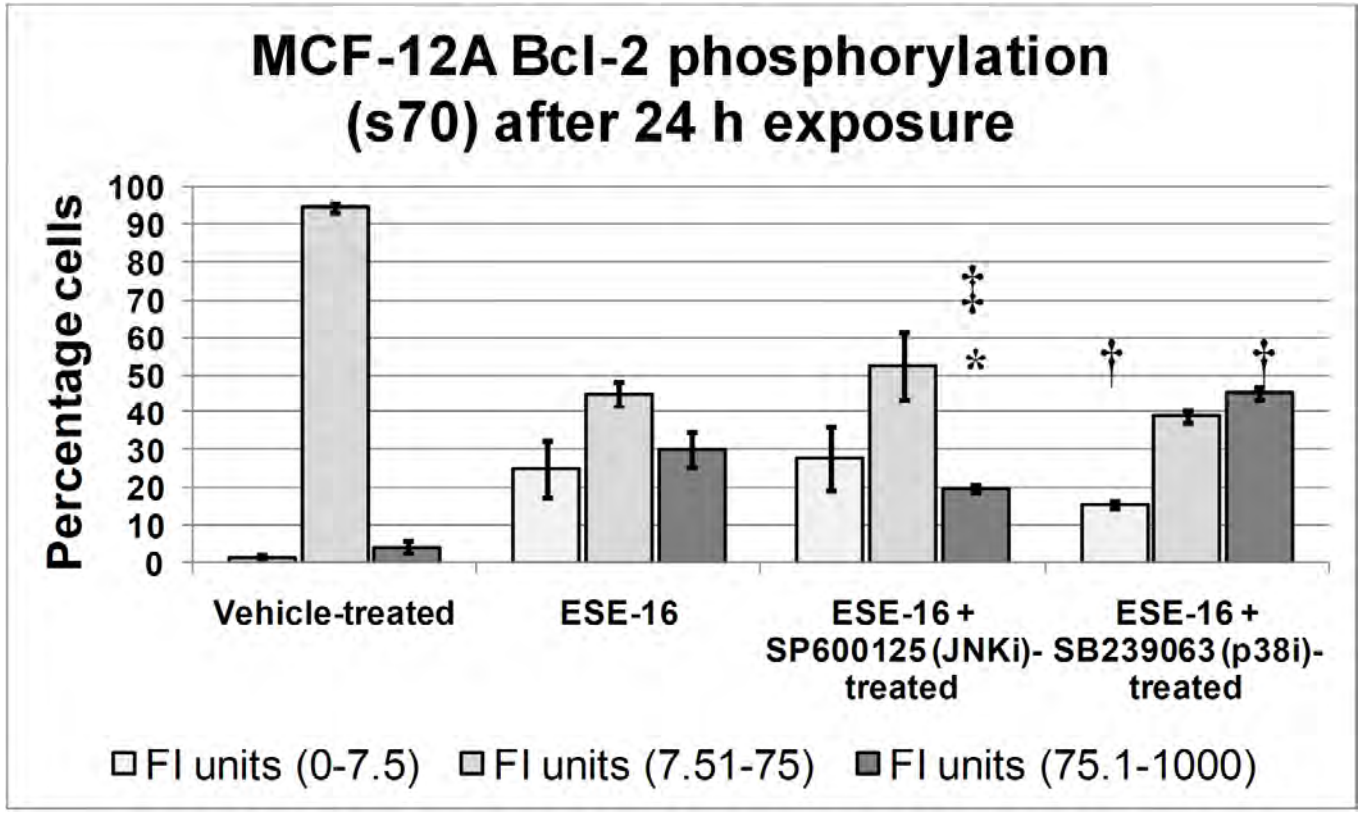

Figure 3.48: Bar-chart demonstrating the distribution of fluorescence intensity (FI) units of Bcl-2 (Ser 70) (FL3 Log) labeled MCF-12A, cells after 24 h exposure to ESE-16 (200 nM).

*indicates a *P*-value < 0.05 between cells treated with ESE-16 and the JNK inhibitor and ESE-16-treated cells

†indicates a *P*-value < 0.05 between cells treated with ESE-16 and the p38α inhibitor and ESE-16-treated cells

‡indicates a *P*-value < 0.05 between cells treated with ESE-16 and the JNK inhibitor and cells treated with ESE-16 and the p38α inhibitor

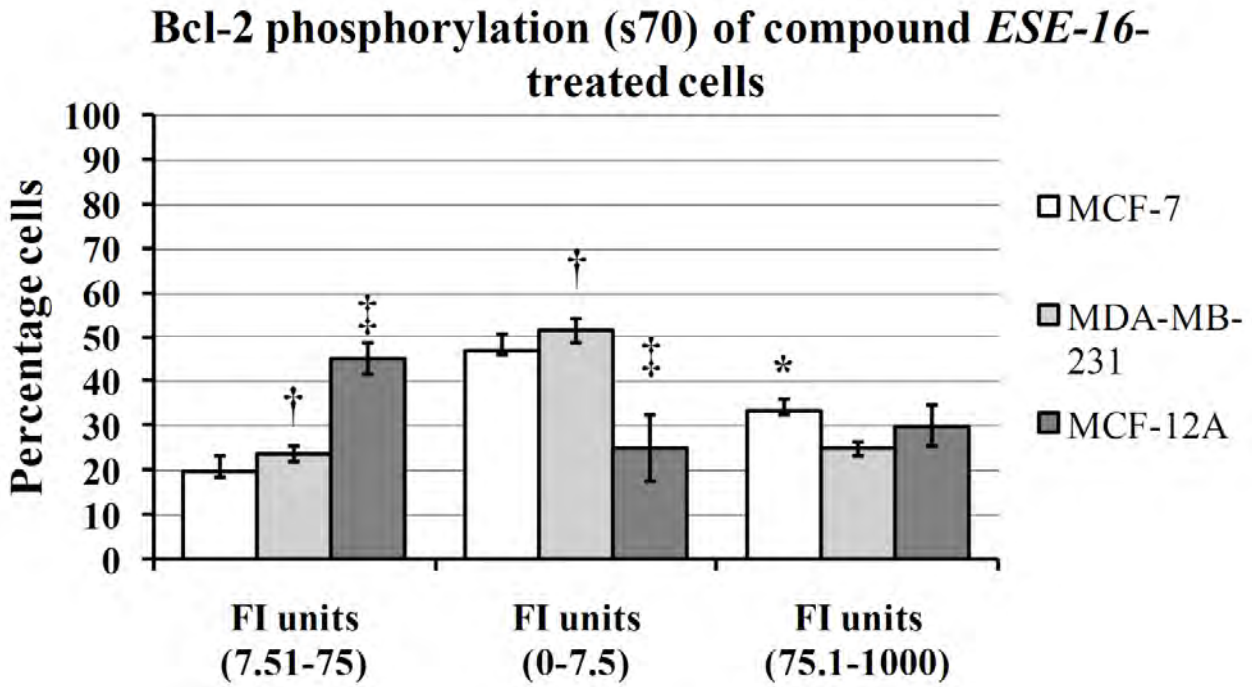

Figure 3.49: Comparison of differences in distribution of fluorescence intensity (FI) units of Bcl-2 (Ser 70) (FL3 Log) labeled MCF-7, MDA-MB-231 and MCF-12A cells after 24 h exposure to ESE-16 (200 nM).

*indicates a *P*-value < 0.05 between MCF-7-treated cells and MDA-MB-231-treated cells

†indicates a *P*-value < 0.05 between MDA-MB-231-treated cells and MCF-12A-treated cells

‡ indicates a *P*-value < 0.05 between MCF-12A-treated cells and MCF-7-treated cells

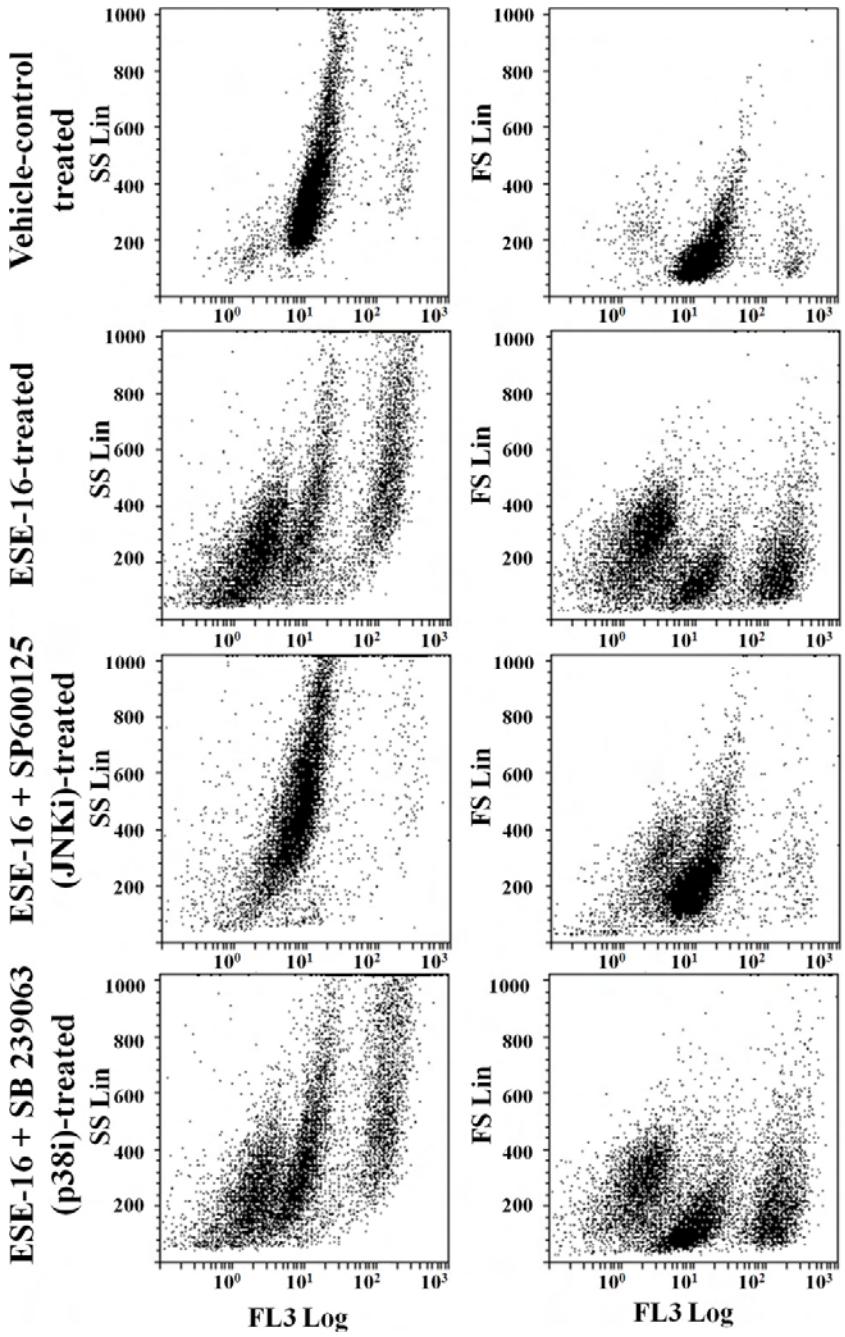

Figure 3.50: Flow cytometry dot-plot of Bcl-2 (Ser 70) (FL3-log) relative quantity vs relative cellular complexity (SS lin) in MCF-7 cells.Cells with increased FL3 fluorescence appear to have increased complexity and decreased cell size.

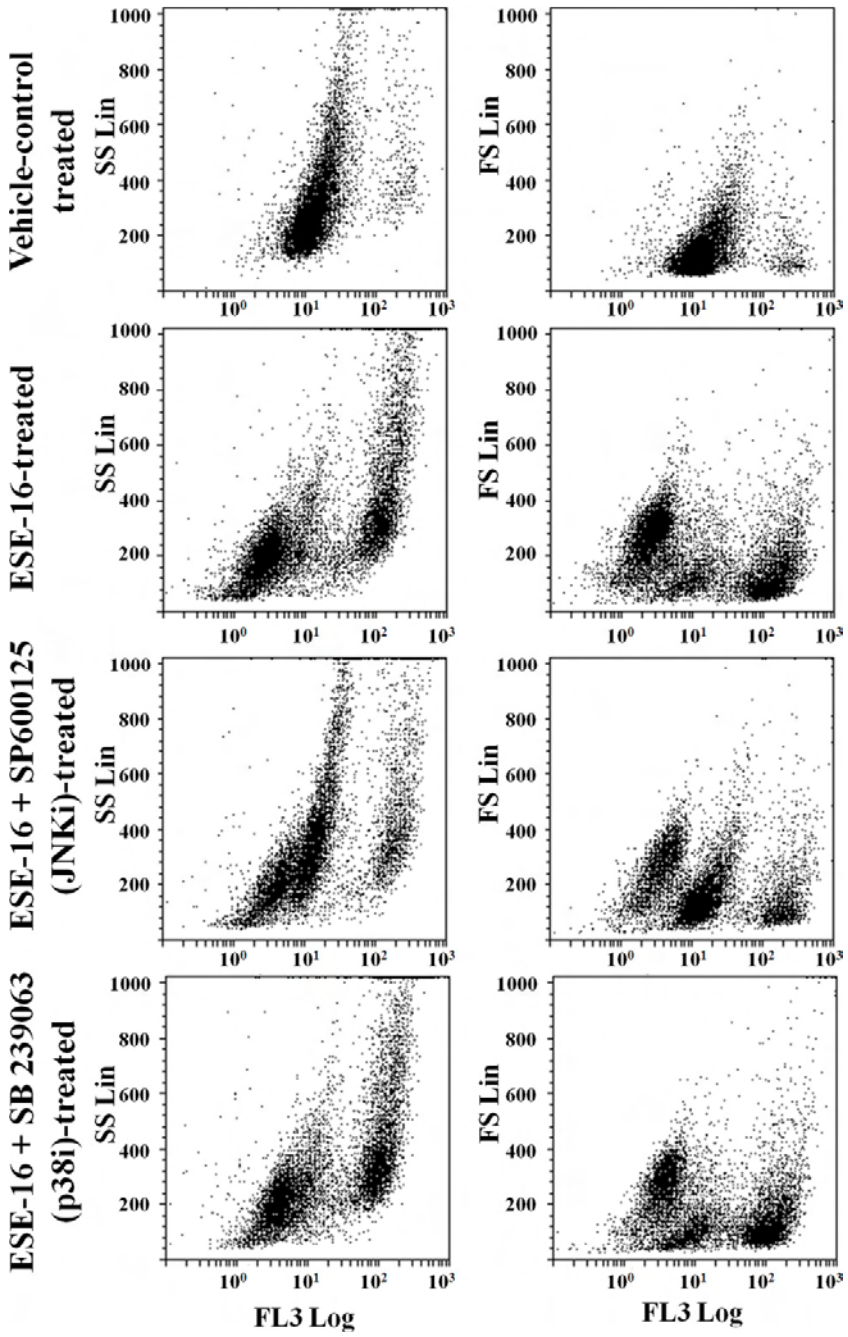

Figure 3.51: Flow cytometry dot-plot of Bcl-2 (Ser 70) (FL3-log) relative quantity vs relative cellular complexity (SS lin) in MDA-MB-231 cells.Cells with increased FL3 fluorescence appear to have increased complexity and decreased cell size.

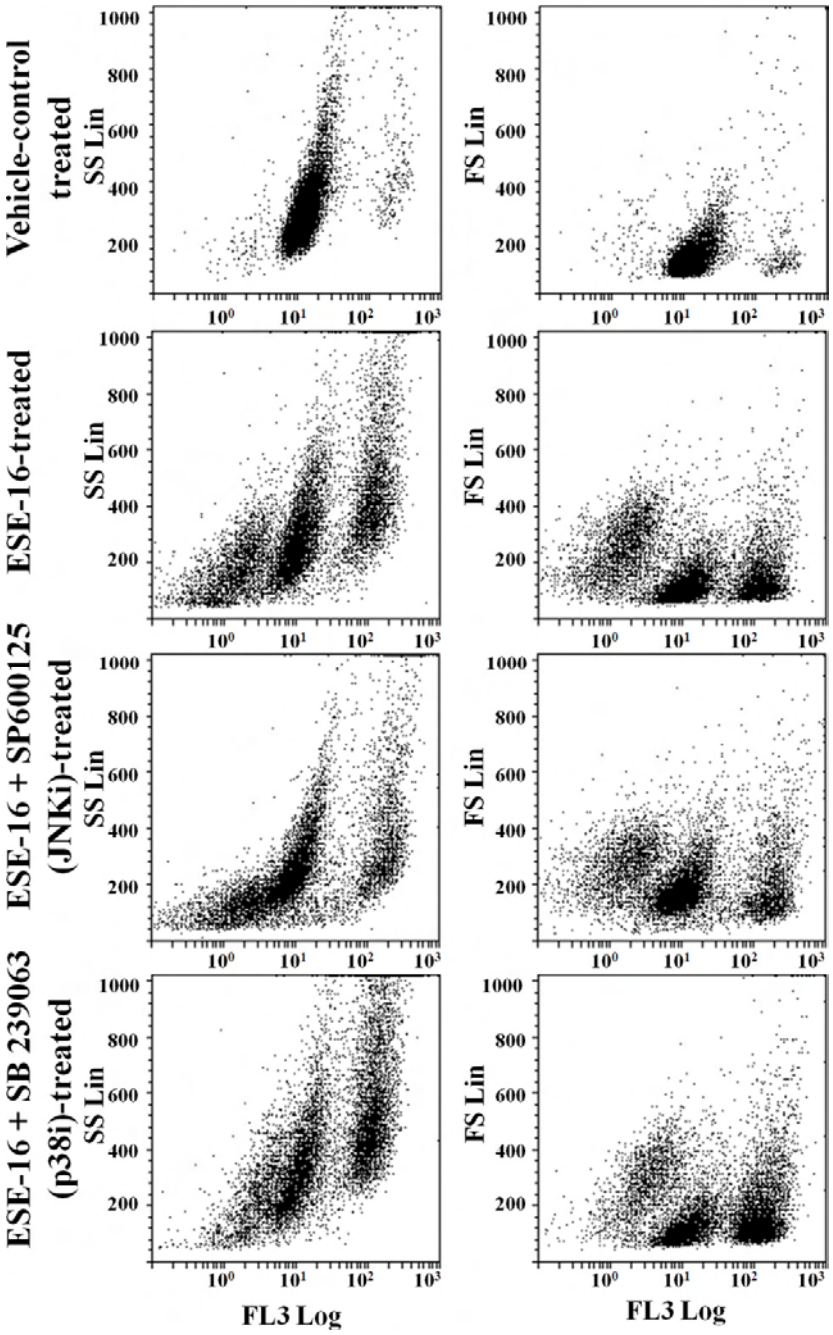

Figure 3.52: Flow cytometry dot-plot of Bcl-2 (Ser 70) (FL3-log) relative quantity vs relative cellular complexity (SS lin) in MCF-12A cells.Cells with increased FL3 fluorescence appear to have increased complexity and decreased cell size.

Carbonic Anhydrase IX and II kinetics

The inhibition of the catalyzed exchange of ^{18}O between CO_2 and water as measured by membrane-inlet mass spectrometry was used to determine the inhibition constants (K_i) of ESE-15-one, ESE-15-ol, 14-16 (from Figure 3.5) and ESE-16 (from Figure 3.5) on CAIX and a CAIX mimic (233).

Kinetics data indicated that ESE-15-ol has an almost 2-fold higher affinity for the CAIX mimic (K_i = 89 ± 23 nM) when compared to the wild-type CAII (K_i = 167 ± 19 nM) (Table 3.24). ESE-16 also inhibited the CAIX mimic (K_i = 453 ± 43 nM) at a lower concentration when compared to the wild-type CAII (K_i = 569 ± 61 nM) (Table 3.24). ESE-15-one was more than three time more selective towards inhibiting the activity of the wild-type CAII (K_i = 167 ± 19 nM) when compared to the CAIX mimic (K_i = 453 ± 43 nM) (Table 3.24). Therefore, of the novel compounds ESE-15-ol and ESE-16 were the compounds that were selective towards theCAIX mimic and were chosen to be used in subsequent mechanistic studies.

This selectivity of ESE-15-ol was surprising since it is a desaturated D-ring derivative of 2-ethylestradiol sulfamate (2EE). 2EE is reported to have a 12-fold reduction in affinity for the CAIX mimic when compared to CAII Table 3.24(194). In order to analyze the possible binding position of ESE-15-ol, an ensemble docking study was performed by docking ESE-15-ol and 2EE into the CAII (2gd8, 3bet, 3d8w, 3d9z, 3daz, 3dd0, 3oim, 3oku, 3x7t), wild-type CAIX (3iai, chains A-D) and the CAIX mimic (3dbu, 3dc3, 3dcc, 3dcs, 3dcw, 3oik, 3oil, 3okv) receptors. The lowest energy conformation was selected and the RMSD for 2EE was calculated with the crystal poses of 3EE bound to CAII (3oim) and CAIX mimic (3oil).2EE was docked with Autodock Vina into the various The lowest energy score for 2EE was obtained in 3oku (CAII, -9 kcal/mol) and 3dcs (CAIX mimic, -8.2 kcal/mol) with root means squared deviation (RMSD) values of 1.332 and 1.42 respectively compared to the crystal pose (Figure 3.53). This indicated that the docking software was able to reproduce the crystal poses and relative binding energies reasonably well and would be useful in determining the possible binding mode and pose of ESE-15-ol into CAII, the wild-type CAIX and the CAIX mimic. Chain C of the wild-type CAIX (3iaia_C) yielded the lowest dock energy for 2EE (-9 kcal/mol). The 3oil crystal structure

with 2EE bound to the CAIX mimic was superimposed onto 3iai_C (RMSD = 0.32) and the RMSD of 2EE docked into 3aia_C was 1.61 when compared to the crystal structure of 2EE in 3oil (Figure 3.53). This indicates that the docking pose of 2EE into the wild-type CAIX is probably similar to that of 2EE into the CAIX mimic.

The lowest energy score for ESE-15-ol was when it was docked into 2oku (-9 kcal/mol), 3okv (-8.3 kcal/mol) and 3aia_C (-9.3 kcal/mol) for CAII, the CAIX mimic and the wild-type CAIX respectively. The docking pose of ESE-15-ol into CAII was similar to that of the docking pose of 2EE into CAII (Figure 3.53). Sippel *et al.* (2011) reported that the inhibition constant (K_i) for 2EE in CAII is 180 ± 10 nM(194). The present study reports that the K_i of ESE-15-ol in CAII is 167 ± nM (Figure 3.54), indicating that the binding modes of 2EE and ESE-15-ol into CAII are likely very similar. However, when we look at the binding pose of ESE-15-ol into the CAIX mimic and the wild-type CAIX we observe different interactions (Figure 3.53 and Figure 3.54). Sippel *et al.* (2011) reported that 2EE has a hydrophobic interaction with ASN 62 at the D-ring and that the O17 hydroxyl form a weak hydrogen bond with a water that interacts with Gln 67(194). ESE-15-ol, however, appears to have very different interactions at the D-ring. In the CAIX mimic, the double bond of ESE-15-ol at C15 and C16 acts as a nucleophile and is able to interact with the electrophylic hydrogen of His 61 (Figure 2). This position also allows ESE-15-ol to have van der Waals interactions with Trp 2 as well as Asn 59. ESE-15-ol also engages in hydrophobic van der Waals contacts with Val 118, Leu 194 and Phe 127. In the wild-type CAIX, the His 1 residue is closer to the O17 hydroxyl group and can form a hydrogen bond while retaining the the nucleophylic-electrophylic interaction between His 61 and the C15-C16double bond of ESE-15-ol (Figure 3.54). Together these interactions may explain the isoform specificity of ESE-15-ol towards the CAIX mimic over CAII and also suggest that it may even be more specific towards the wild-type CAIX due to the potential His 1-O17 hydrogen bond interaction.

Table 3.24: Carbonic anhydrase II and IX mimic inhibitory activity of estradiol analogues. ESE-15-ol, 2-Ethylestradiol bisulfamate and ESE-16 are more selective towards the CAIX mimic than the wild-type CAII.

Compound	Carbonic anhydrase II		Carbonic anhydrase IX mimic		Selectivity towards CAIX mimic compared to CAII
	Inhibition constant nM(Ki)	Standard error	Inhibition constant nM(Ki)	Standard error	
ESE-15-one	228	30	715	103	0.32
ESE-15-ol	167	19	89	23	1.88
2-Ethylestradiol bisulfamate	875	65	678	42	1.29
2-Ethylestradone sulfamate	437	46	585	26	0.75
2-Ethylestradiol sulfamate	177	9	2089	215	0.08
ESE-16	659	61	453	43	1.45

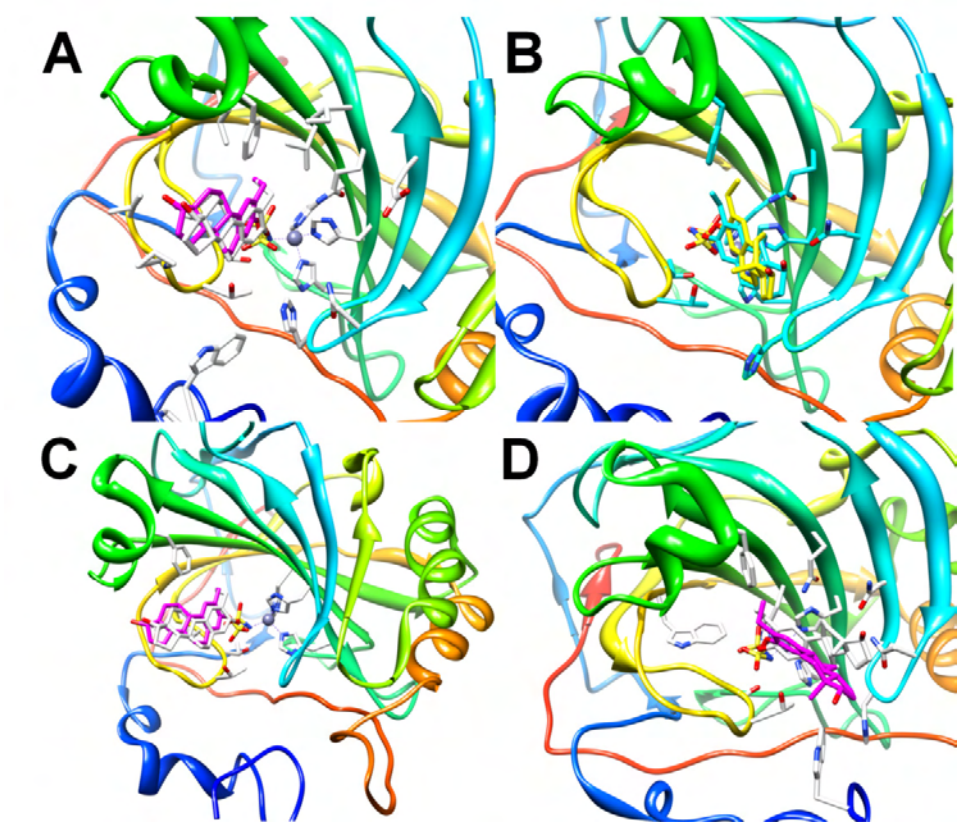

Figure 3.53:Crystal structures and redocked poses of 2-ethylestradiol sulfamate (2EE) positioned in CAII and the CAIX mimic2EE (white in A, C and D and cyan in B) positioned in CAII (A and C) and the CAIX mimic (B and D). The docking poses of 2EE into CAII (A, pink ligand) and into the CAIX mimic (B, yellow ligand) have an RMSD value of 1.332 and 1.42 respectively compared to the crystal pose. ESE-15-ol docked into CAII (C, pink ligand) shows a close fit compared to the crystal pose of 2EE in CAII. The docking pose of ESE-15-ol into the CAIX mimic diverges from 2EE, allowing an interaction between the nucleophilic double bond at C15 and C16 and the electrophylic hydrogen of His 61(D).

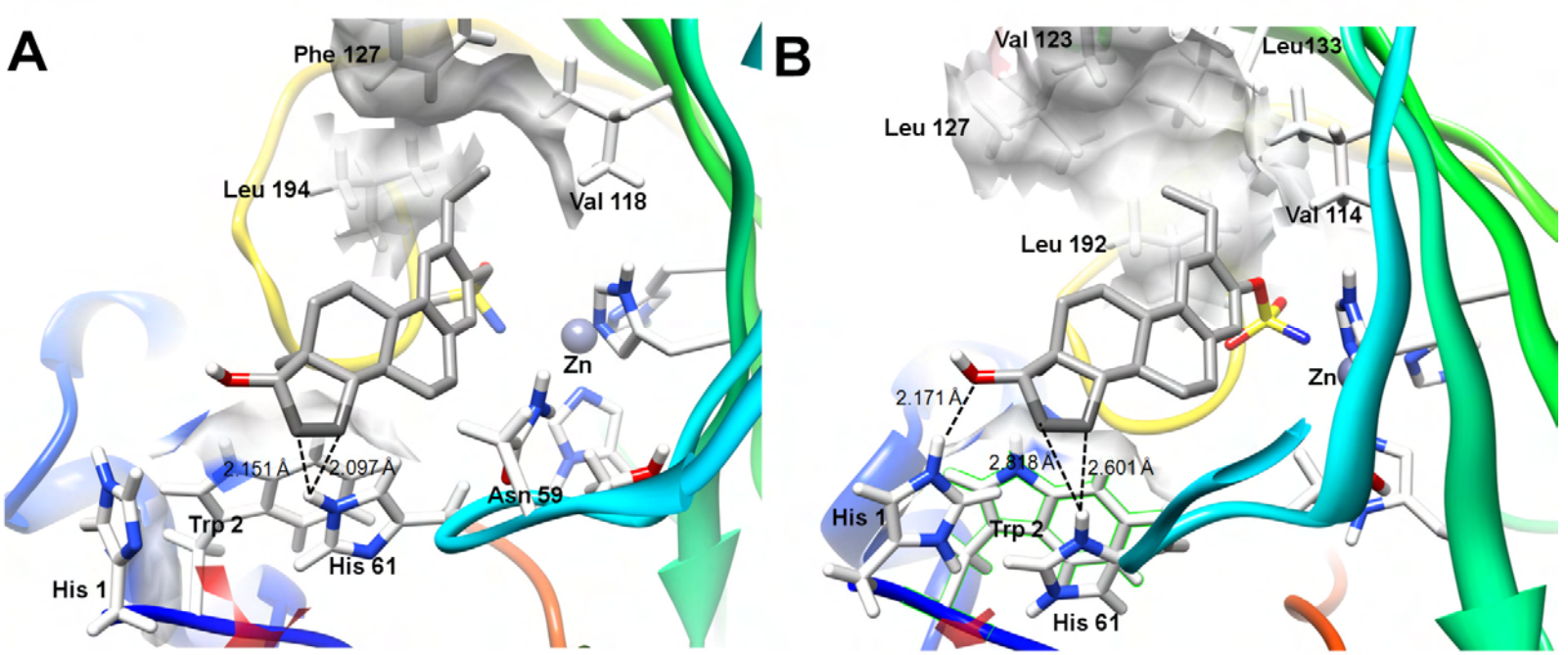

Figure 3.54: Docking and kinetics data of ESE-15-ol.Docking of ESE-15-ol into a mimic of CAIX (A) and the wild-type isoform of CAIX (B) revealed that the double bond of ESE-15-ol at carbon 15 and carbon 16 (dark grey) may act as a nucleophile and interact with the electrophylic hydrogen of His 61. This interaction is posited to be specific of ESE-15-ol over 2EE and explain the isoform specificity of ESE-15-ol towards the CAIX mimic over CAII. Kinetics data (C) demonstrates that ESE-15-ol has an almost 2-fold higher affinity for the CAIX mimic when compared to the wild-type CAII.